

Deposit & Copying of Dissertation Declaration



UNIVERSITY OF
CAMBRIDGE

Board of Graduate Studies

Please note that you will also need to bind a copy of this Declaration into your final, hardbound copy of thesis - this has to be the very first page of the hardbound thesis.

1	Surname (Family Name)	Forenames(s)	Title
	Howett	David Michael Victor	Mr.
2	Title of Dissertation as approved by the Degree Committee		
	The function and structure of the entorhinal cortex in mild cognitive impairment		

In accordance with the University Regulations in *Statutes and Ordinances* for the PhD, MSc and MLitt Degrees, I agree to deposit one print copy of my dissertation entitled above and one print copy of the summary with the Secretary of the Board of Graduate Studies who shall deposit the dissertation and summary in the University Library under the following terms and conditions:

1. Dissertation Author Declaration

I am the author of this dissertation and hereby give the University the right to make my dissertation available in print form as described in 2. below.

My dissertation is my original work and a product of my own research endeavours and includes nothing which is the outcome of work done in collaboration with others except as declared in the Preface and specified in the text. I hereby assert my moral right to be identified as the author of the dissertation.

The deposit and dissemination of my dissertation by the University does not constitute a breach of any other agreement, publishing or otherwise, including any confidentiality or publication restriction provisions in sponsorship or collaboration agreements governing my research or work at the University or elsewhere.

2. Access to Dissertation

I understand that one print copy of my dissertation will be deposited in the University Library for archival and preservation purposes, and that, unless upon my application restricted access to my dissertation for a specified period of time has been granted by the Board of Graduate Studies prior to this deposit, the dissertation will be made available by the University Library for consultation by readers in accordance with University Library Regulations and copies of my dissertation may be provided to readers in accordance with applicable legislation.

3	Signature	Date
		11/12/2016

Corresponding Regulation

Before being admitted to a degree, a student shall deposit with the Secretary of the Board one copy of his or her hard- bound dissertation and one copy of the summary (bearing student's name and thesis title), both the dissertation and the summary in a form approved by the Board. The Secretary shall deposit the copy of the dissertation together with the copy of the summary in the University Library where, subject to restricted access to the dissertation for a specified period of time having been granted by the Board of Graduate Studies, they shall be made available for consultation by readers in accordance with University Library Regulations and copies of the dissertation provided to readers in accordance with applicable legislation.

*The function and structure of the entorhinal
cortex in mild cognitive impairment*



David Michael Victor Howett

Darwin College
University of Cambridge

A thesis submitted for the degree of Doctor of
Philosophy

November 2019

Declaration

I declare that except where specific reference is made to the work of others, the contents of this dissertation are original and have not been submitted in whole or in part for any other degree, diploma or qualification at the University of Cambridge or any other universities. This thesis is the result of my own work except where specifically indicated in the text, and has been carried out at the University of Cambridge between October 2015 and May 2019 under the supervision of Dr Dennis Chan and Professor Rik Henson.

The quantitative chapters 2, 3 and 4 are my own work. However, this work would not have been possible without key collaborators and contributors. Zoe Adler assisted with the data collection and neuropsychological testing outlined in chapters 2 and 3. Emma Bird and Katarzyna Krzywicka assisted in the recruitment and testing of the data presented in chapter 2, this was submitted as part of Ms. Krzywicka's M.Phil, July 2017. Jim Dickinson assisted with testing healthy controls used in chapter 2 which was presented as part of his part II project (April 2017) and Deepti Marchment assisted with neuropsychological testing these healthy controls. Elizabeth Harding and Adrienne Lee (UCL) assisted with pilot data collection of chapter 3 and Coco Newton and I manually assessed all data for 'swap' errors.

Katarzyna Krzywicka was instrumental to designing and adapting the manual segmentation protocol outlined in chapter 4. Whilst I performed the majority of these segmentations, Johanna Hagman's segmentations were used in the final analysis. MRIs were collected by myself or were collected as part of a research protocol following routine diagnostic MRI scanning in patients.

Both immersive virtual reality tasks were designed and built by Andrea Castegnaro (UCL), however I contributed in adapting both tasks (chapters 2 and 3) for use in older participants and patients with cognitive impairment through iterative piloting. Andrea Castegnaro was primarily responsible for the collection

of the young control data used in chapters 2 and 3 as supported by Daniel Bush, Elizabeth Harding and Adrienne Lee (UCL).

The research questions were developed in collaboration with Professor Neil Burgess, Dr John King, Dr Dennis Chan and Andrea Castegnaro. The work outlined in chapter 2 was published: Howett *et al.*, *Brain* (2019). The length of this thesis does not exceed the 60,000-word limit set by the Degree Committee for the faculties of Clinical Medicine and Clinical Veterinary Medicine.

Signed: 
Date: 01/06/2019

Executive Summary

The function and structure of the entorhinal cortex in mild cognitive impairment

David Howett

Background:

The entorhinal cortex (EC) is the first brain region to exhibit neurodegeneration in Alzheimer's disease (AD). As such, tests of EC function may help aid detection of the disease in its earliest stages. Animal and human studies indicate that the posteromedial (pmEC) and anterolateral (alEC) subdivisions of the EC are involved respectively in navigation and object-location memory. The advent of immersive VR (iVR) technology provides an opportunity to determine whether tests of pmEC and alEC function has value in the detection of AD prior to dementia onset.

Aim:

To test the hypotheses that measures of pmEC and alEC function and structure differentiate i) patients with mild cognitive impairment (MCI) from age-matched healthy controls and ii) MCI patients at high and low risk of developing AD dementia.

Methodology:

Participants underwent testing of EC function using novel iVR paradigms of path integration and object-location memory. Total EC, pm-EC and al-EC volumes were segmented from high resolution MRI. A proportion of MCI patients underwent CSF testing for AD biomarkers to separate into biomarker-positive and negative groups (MCI+ and MCI-). The ability of the VR tests to classify pre-dementia AD (i.e. MCI+ patients) was compared with that of a battery of comparator cognitive tests used in current clinical and research practice.

Results:

Performance on the path integration task was not only impaired in MCI but importantly differentiated MCI+ from MCI- with greater classification accuracy than comparator cognitive tasks. Task performance correlated with pm-EC volume. For the object-location task MCI patients demonstrated larger distance errors than controls, with performance associated with both anterolateral EC volume and total hippocampal volume. However, no difference between MCI+ and MCI- was observed.

Conclusion

This work demonstrates that iVR-based testing of EC function may improve diagnosis of early AD above and beyond current cognitive tests. The basis of such tests on single cell physiology and their comparability with behavioural tasks used in animal models of disease, confers additional advantages for translational research aimed at understanding the mechanisms linking pathological spread, disruption of cell physiology and behavioural alterations in early AD.

Table of Contents

DECLARATION	5
EXECUTIVE SUMMARY	7
TABLE OF CONTENTS	9
CONTENTS OF FIGURES	12
CONTENTS OF TABLES	13
LIST OF ABBREVIATIONS	14
ACKNOWLEDGEMENTS	16
CHAPTER 1 - INTRODUCTION	17
1. CHAPTER OVERVIEW.....	17
1.2. ALZHEIMER'S DISEASE	17
1.2.1. <i>Clinical characterisation of mild cognitive impairment and predementia AD</i>	18
1.2.2. <i>AD Pathophysiology</i>	20
1.2.3. <i>Amyloid beta and the amyloid cascade hypothesis</i>	20
1.2.4. <i>Tau</i>	23
1.3. NEUROIMAGING IN ALZHEIMER'S DISEASE	24
1.3.1. <i>Structural MRI</i>	24
1.3.2. <i>Diffusion Tensor Imaging</i>	25
1.3.3. <i>Resting-state functional MRI</i>	26
1.3.4. <i>Ligand-positron emission tomography</i>	27
1.4. COGNITIVE IMPAIRMENT IN ALZHEIMER'S DISEASE	27
1.4.1. <i>Global cognitive tests</i>	28
1.4.2. <i>Episodic memory</i>	28
1.4.3. <i>Other memory domains</i>	29
1.4.4. <i>Neuropsychiatric symptoms</i>	29
1.5. LIMITATIONS OF TRADITIONAL NEUROPSYCHOLOGICAL TEST PARADIGMS.....	29
1.6. SPATIAL COGNITION	31
1.6.1. <i>Neural correlates of spatial cognition</i>	31
1.6.2. <i>Spatial cognition in Alzheimer's disease</i>	35
1.7. SUMMARY OF STUDY RATIONALE.....	38
CHAPTER 2 - PATH INTEGRATION	41
2.1. INTRODUCTION	42
2.2. METHODOLOGY.....	44

2.2.1. Participants.....	44
2.2.2. Comparator neuropsychological tests.....	46
2.2.3. Immersive virtual reality.....	47
2.2.4. The path integration task.....	48
2.2.5. Calculation of outcome measures.....	50
2.2.6. Statistical Analysis.....	53
2.3. RESULTS.....	55
2.3.1. Demographics and neuropsychological testing.....	55
2.3.2. Immersive VR path integration task.....	55
2.3.3. Absolute distance error.....	58
2.3.4. Proportional Angular Error.....	60
2.3.5. Proportional Linear Error.....	61
2.3.6. Effect of return condition.....	63
2.3.7. ROC curves and classification accuracy.....	66
2.4. DISCUSSION.....	68
CHAPTER 3 - OBJECT-LOCATION TASK.....	73
3.1. INTRODUCTION.....	73
3.2. METHODOLOGY.....	78
3.2.1. Participants.....	78
3.2.2. Object-replacement subtask.....	78
3.2.3. Object-recognition subtask.....	84
3.2.4. Object-environment association subtask.....	84
3.2.5. Data processing and Statistics.....	84
3.3. RESULTS.....	88
3.3.1. Demographics and neuropsychological testing.....	88
3.3.2. Object-replacement subtask.....	88
3.3.3. Object-recognition subtask.....	89
3.3.4. Object-environment association subtask.....	91
3.3.5. Classification accuracy of the object-location task.....	92
3.3.6. A posteriori hypothesis.....	93
3.4 DISCUSSION.....	96
CHAPTER 4 - MRI MEASURES OF ENTORHINAL CORTEX STRUCTURE AND THEIR RELATIONSHIP TO SPATIAL COGNITION.....	103
4.1. INTRODUCTION.....	103
4.2. METHODS.....	106

4.2.1. Participants.....	106
4.2.2. MRI acquisition parameters:.....	106
4.2.3. Voxel-based morphometry preprocessing.....	106
4.2.4. Manual Segmentation of the Parahippocampal gyrus	107
4.2.5. Statistics.....	109
4.3. RESULTS.....	112
4.3.1. Demographic differences.....	112
4.3.2. Reliability of segmentation protocol	112
4.3.3. Between group differences in volumetry and morphometry.....	113
4.3.4. Association between ROI volumetry and path integration performance.....	117
4.3.5. Association between ROI volumetry and object-location task performance.....	120
4.3.6. Classification Accuracy	121
4.4. DISCUSSION	124
CHAPTER 5 - DISCUSSION	131
REFERENCES.....	136

Contents of Figures

FIGURE 1.1. ALZHEIMER'S DISEASE STAGING.	18
FIGURE 1.2. SPATIOTEMPORAL DISTRIBUTION OF KEY PATHOLOGICAL HALLMARKS.	22
FIGURE 1.3. ILLUSTRATION OF SPATIALLY MODULATED CELLS IN THE MEDIAL TEMPORAL LOBE.	34
FIGURE 1.4. SCHEMATIC SUMMARY OF THE SPATIAL NETWORK, ITS FUNCTION AND OVERLAP WITH THE SPATIOTEMPORAL PROPAGATION OF AD PATHOLOGY.....	38
FIGURE 2.1. PATH INTEGRATION TASK.	50
FIGURE 2.2. ILLUSTRATIONS OF OUTCOME MEASURES FOR THE PATH INTEGRATION TASK.	52
FIGURE 2.3. PROPORTION OF DATA EXCLUDED DUE TO REACHING THE 'OUT OF BOUNDS' SUBDIVIDED BY PARTICIPANT GROUP AND RETURN CONDITION.....	56
FIGURE 2.4. EFFECTS OF AGEING ON PATH INTEGRATION PERFORMANCE.	58
FIGURE 2.5. GRAPH SUMMARISING THE BETWEEN GROUP DIFFERENCES IN PATH INTEGRATION PERFORMANCE.....	59
FIGURE 2.6. ASSOCIATION BETWEEN ABSOLUTE DISTANCE ERROR AND CSF MEASURES.	60
FIGURE 2.7. GRAPH SUMMARISING BETWEEN GROUP DIFFERENCES IN PROPORTIONAL ERRORS.	62
FIGURE 2.8. WITHIN GROUP EFFECTS ON RETURN CONDITION.	64
FIGURE 2.9. DISTRIBUTION OF GOAL LOCATION BY GROUP.	65
FIGURE 2.10. RECEIVER OPERATING CHARACTERISTIC PLOT.....	67
FIGURE 3.1. ILLUSTRATION OF OBJECT-LOCATION TASK.	80
FIGURE 3.2. ILLUSTRATION OF ABSOLUTE DISTANCE ERROR.	81
FIGURE 3.3. PARTICIPANT DATA ILLUSTRATING SWAP SCENARIOS.....	83
FIGURE 3.4. BETWEEN GROUP DIFFERENCES IN PERFORMANCE.....	89
FIGURE 3.5. DISCRIMINATION OF OBJECT FAMILIARITY BETWEEN GROUPS.....	90
FIGURE 3.6. CORRECT DISCRIMINATION OF OBJECT-ENVIRONMENT ASSOCIATION.....	92
FIGURE 3.7. RECEIVER OPERATING CHARACTERISTIC PLOT.	93
FIGURE 3.8. DISTRIBUTION OF SWAP ERRORS.....	94
FIGURE 4.1. ILLUSTRATION OF ENTORHINAL SUBDIVISIONS AND BA35 SEGMENTATION.....	108
FIGURE 4.2. BETWEEN GROUP DIFFERENCES IN ROI VOLUMES.	113
FIGURE 4.3. BETWEEN GROUP DIFFERENCES IN ROI VOLUMES ACROSS MCI+ AND MCI-.	114
FIGURE 4.4. ASSOCIATION BETWEEN PATH INTEGRATION OUTCOME MEASURES AND ROIS.....	117
FIGURE 4.5. GREY MATTER REGIONS ASSOCIATED WITH IVR PERFORMANCE.....	120
FIGURE 4.6. ASSOCIATIONS BETWEEN OBJECT LOCATION PERFORMANCE AND ROIS.	121
FIGURE 4.7. RECEIVER OPERATING CHARACTERISTIC CURVE FOR IVR TASKS COMBINED WITH ROI VOLUMETRY.	123

Contents of Tables

TABLE 2.1 BETWEEN GROUP DIFFERENCES IN NEUROPSYCHOLOGICAL TEST PERFORMANCE.	57
TABLE 3.1. BETWEEN GROUP DIFFERENCES IN DEMOGRAPHICS AND NEUROPSYCHOLOGICAL TEST PERFORMANCE.....	87
TABLE 3.2. RAW NUMBERS USED FOR SIGNAL DETECTION IN OBJECT RECOGNITION TASK.	90
TABLE 3.3. OBJECT-ENVIRONMENT ASSOCIATION PERFORMANCE AS INDICATED BY HIT RATES.	91
TABLE 4.1 DEMOGRAPHIC TABLE SUMMARY FOR VBM AND MANUAL SEGMENTATION ANALYSES.	111
TABLE 4.2 DICE SIMILARITY COEFFICIENT WAS COMPUTED FOR BOTH INTRA- AND INTER-RATER RELIABILITY.	112
TABLE 4.3. BETWEEN GROUP DIFFERENCES ACROSS EC, ALEC, PMEC AND BA35.	114
TABLE 4.4 VBM DIFFERENCES BETWEEN GROUPS AND ASSOCIATED WITH PIT AND OLT PERFORMANCE.	116
TABLE 4.5. UNIVARIATE STATISTICS SUMMARY OF ROIS AND PIT/OLT PERFORMANCE.....	119
TABLE 4.6. CLASSIFICATION ACCURACY OF REGIONS OF INTEREST ACROSS GROUP.	122

List of abbreviations

Abbreviations:

4MT = Four Mountains Task

A β = Amyloid beta

ACE-R = Addenbrookes Cognitive Examination – Revised

AD = Alzheimer’s Disease

alEC = anterolateral Entorhinal Cortex

AUC = Area Under the Curve

BA35 = Brodmann’s Area 35

CDR = Clinical Dementia Rating

CSF = CerebroSpinal Fluid

CS = Collateral Sulcus

EC = Entorhinal Cortex

DST = Digit Symbol Substitution Test

FCSRT = Free and Cued Selective Remind Test

HCs = Healthy Controls

iVR = immersive Virtual Reality

IEC = lateral Entorhinal Cortex

(G)LME = (Generalized) Linear Mixed Effect Model

JDR = Join Dementia Research

mEC = medial Entorhinal Cortex

MTL = Medial Temporal Lobe

MCI = Mild Cognitive Impairment

MCI+ = Mild Cognitive Impairment with CSF evidence of underlying Alzheimer’s disease.

MCI- = Mild Cognitive Impairment without CSF evidence of underlying Alzheimer’s disease.

MMSE = Mini-Mental State Examination

(f)MRI = (functional) Magnetic Resonance Imaging

NART = National Adult Reading Test

OLT = Object Location Task

PIT = Path Integration Task

PCC = Posterior Cingulate Cortex

PET = Positron Emission Tomography

PI = Path Integration

pmEC = posteromedial Entorhinal Cortex

RSc = RetroSplenial cortex

RFR = Rey-Osterrieth Figure Recall Test

ROC = Receiver Operating Characteristic

ROI = Region of Interest

TMTB = Trail Making Test B

VBM = Voxel Based Morphometry

YCs = Young Controls

Acknowledgements

My thanks must be extended to the patients and participants who gave up their time and energy to support this research. I would also like to thank the staff of the Department of Clinical Neurosciences, Cognitive and Brain Sciences Unit, Wolfson Brain Imaging Centre and Darwin College for supporting this research. Special thanks to Merete Bergmann who always encouraged me and found time for my odd requests, no matter how busy she was. I would also like to thank Zoe Adler, Coco Newton, Kat Krzywicka, Andrea Castegnaro, Johanna Hagman, Ilse Geraedts, Adrienne Lee and Liz Harding for their help, input and support.

I am grateful to my supervisors for their continued support and guidance throughout that shaped me both as a researcher and as a person. From our first meeting Dennis taught me how to see and evaluate the big picture and, despite his perpetual sleep deprivation, never failed me as a mentor. Rik has a talent for making the complex comprehensible, it is therefore fitting that he described Hofstadter's law to me of which this thesis is a definite example. I am very grateful to Rik for taking up the mantle at the eleventh hour.

I would also like to thank my family and friends whose unwavering support, despite my inability to get a 'proper job', kept me motivated through the difficult times. Thank you to my parents: Mum, Dad, Steve, Ali, Ai Choo and Martin, you gave me strength and determination (or a kick in the butt) when I needed it most. I couldn't ask for better role models. Thank you to my wonderful sisters Tanya and Carly who are a constant source of inspiration, your friendship, empathy and wisdom are never misguided, as much as it pains me to say it. Thank you to my beautiful nieces Jess, Chloe, Emily and Sophie for always bringing a smile to my face, you're awesome, and make me very proud. Thanks to Matt, Ugi, Ian and Jon who never failed to make me laugh over a beer or 6.

To Holly, you are astonishing and I am indescribably lucky. Thank you for your love and support throughout this adventure and the many more to come.

Chapter 1 - Introduction

1. Chapter Overview

The purpose of this chapter is to provide a background on mild cognitive impairment (MCI), Alzheimer's disease (AD) and spatial cognition focusing on the role of the medial temporal lobe, particularly the entorhinal cortex and hippocampus.

This introduction provides an overview of:

- i) The clinical definition, pathology, neuroimaging and cognitive deficits observed in MCI and AD dementia
- ii) The cellular and anatomical basis of spatial cognition and its deficits in MCI and AD dementia.
- iii) Thesis rationale.
- iv) Aims and objectives.

1.2. Alzheimer's Disease

AD is the leading cause of dementia accounting for an estimated 60-70% of all dementia cases. It is estimated that in 2017 over 50 million people were affected by dementia worldwide, accounting for more than 1% of global gross domestic product, and is forecasted to increase to 152 million by 2050 (Association, 2015). Given that the prevalence of AD dementia has been shown to double every 5 years after the age of 65 (Qiu *et al.*, 2009) and that the number of over 65 year olds is projected to reach 1.5 billion by 2050, the World Health Organisation has recognised AD as a public health priority (World Health Organization, 2015).

AD is a chronic neurodegenerative condition characterised by a systematic decline in cognitive function, particularly in short-term memory, that invariably results in dementia. There is now a consensus that AD's multifaceted pathological cascade is present decades before clinical presentation and significant cognitive decline. However the inability to identify the disease during its prodromal period before substantial and irreversible neuronal-loss has occurred, is the primary source of failure in developing disease-modifying therapies; interventions are administered

too late. Correspondingly, no disease-modifying therapeutics for the treatment of AD currently exists and licenced pharmaceuticals are only efficacious for enhancing cognition in mild dementia.

1.2.1. Clinical characterisation of mild cognitive impairment and predementia AD

The nosological entity of MCI has its origins in ‘benign senescent forgetfulness’ (KRAL, 1962) but the concept has evolved to encompass individuals who exhibit objective cognitive decline more severe than would be expected by ageing alone with preserved functional activities (Petersen, 2004). MCI has a prevalence of between 16-20% which in turn confers a rate of progression to dementia of between 10-15% after two years, with higher rates being predicted by hippocampal volume loss, neuropsychological test performance, vascular and neuropsychiatric comorbidity (Petersen *et al.*, 2018). However, not all MCI patients progress to dementia; approximately 20% of MCI patients will revert back to ‘normal’ cognition, although are at a heightened risk of subsequent ‘relapse’, whereas approximately 50% remain stable in their MCI diagnosis (Roberts R, 2013). MCI is common to a host of aetiologies encompassing neurodegenerative (e.g. fronto-temporal, Lewy-body, and vascular dementia) and neuropsychiatric conditions (e.g. anxiety or depression). Given this heterogeneity, MCI has been broadly subcategorised into amnestic and non-amnestic subtypes

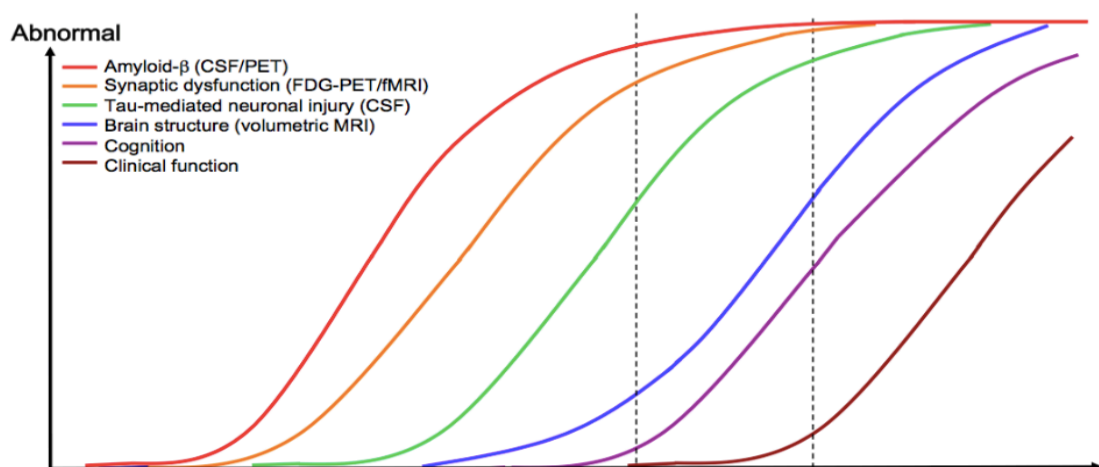


Figure 1.1. Alzheimer's Disease staging (x-axis) and biomarker abnormality (y-axis). The detection threshold for the two key indicators used to stage the disease is approximated for each biomarker (black dotted line). Adapted from Jack *et al* (2013).

with the extent of cognitive deficits either being single or multi-domain. Amnesic MCI is more associated with AD, whereas non-amnesic MCI is associated with non-AD dementias, and multi-domain MCI denotes a greater extent of the disease conferring a greater risk of progression to dementia than single-domain MCI (Palmer *et al.*, 2008).

The disparate pathological origins of MCI combined with the overlapping cognitive deficits have significant implications not only for clinical management of patients, but also for the targeted development of interventions aimed at delaying progression from MCI to dementia. The differentiation of MCI due to AD (i.e. prodromal AD, Dubois *et al.*, 2010) from MCI of non-AD origin requires evidence of abnormal $a\beta$ and either abnormal tau or imaging evidence of hippocampal atrophy and/or cerebral hypometabolism (Petersen, 2016). Decreased cerebrospinal fluid (CSF) concentrations of $a\beta$ 1-42 combined with increased concentration of either total tau and/or phosphorylated tau are the most common pathological diagnostic marker of prodromal AD (Dubois *et al.*, 2014) due to their high sensitivity and specificity (Olsson *et al.*, 2016). Recently however, an emerging concept of preclinical AD has become apparent that broadly describes individuals who have evidence of AD pathology but do not yet exhibit substantial cognitive decline, although this field is in its infancy (Dubois *et al.*, 2016).

Preclinical AD is characterised by *in vivo* evidence of AD pathology using biological or molecular biomarkers, with changes in both CSF tau and amyloid being present more than 15 years prior to clinical presentation (Fagan *et al.*, 2014). Consequently a timeline for biomarker sensitivity to preclinical AD has been proposed (Figure 1.1, Jack *et al.*, 2013; Dubois *et al.*, 2016). Preclinical AD was originally defined as an asymptomatic stage of AD where no cognitive symptoms were manifest, more recently however there is mounting evidence that there are distinct cognitive changes in preclinical AD (Mortamais *et al.*, 2017), notably in spatial cognition (Allison *et al.*, 2016; Coughlan. *et al.*, 2018; Ritchie *et al.*, 2018) owing to its dependency on structures that degenerate early in AD pathology.

1.2.2. AD Pathophysiology

Macroscopic changes

At post-mortem the AD brain exhibits gross cortical atrophy typically in the entorhinal cortex (EC), and hippocampus as well as parietal, frontal and cingulate cortices, whereas motor, sensory and visual cortices are relatively spared. Neocortical thinning gives rise to widening of the cortical sulci and dilation of the lateral ventricles, particularly the temporal horns (Perl, 2010). Cerebrovascular disease is frequently comorbid with AD pathology whereby small vessel disease, demyelination of the periventricular white matter or micro and lacunar infarcts may be present (De La Torre, 2004). Macroscopic changes to anatomy are further discussed in 1.2.3

Microscopic changes

AD is a protein misfolding disease with a unique proteopathic profile involving two major aggregating proteins; amyloid beta ($a\beta$) and tau (Figure 1.2). Conformational changes in these proteins structure enable their aggregation, accumulation and eventual spread that culminate in the degeneration of both neurons and glial cells. Macroscopic changes observed in the AD brain are the result of a synergistic toxicity between proteinopathies and neuroinflammation, however the primary cause and precise mechanism of AD remains elusive and contentious (Perl, 2010). The emergent role of neuroinflammation in AD's pathological cascade is vital. However, capturing the inherent complexity of cell signalling pathways, mechanics of glia-mediated neurodegeneration and role of genetics is beyond the scope of this summary.

1.2.3. Amyloid beta and the amyloid cascade hypothesis

Extracellular deposits of $a\beta$ plaques are a pathological hallmark of the AD brain. Monomeric $a\beta$ is a proteolytic by-product of amyloid-precursor protein (APP) cleavage that is physiologically implicated in neuronal growth and repair. However, when the concentration of monomeric amyloid is sufficiently high it undergoes a conformational change that results in its oligomerisation and the

formation of amyloid fibrils. Neuropathological studies characterise neuritic plaques into two categories: diffuse and dense-core, the latter is heavily implicated in AD pathology having a deleterious effect on synapses and neurons, whereas diffuse plaques are found in cognitively healthy elderly adults (Murphy and Iii, 2010).

According to the amyloid cascade hypothesis, $A\beta$ plaques exert their neurotoxic effect through disrupting calcium (Ca^{2+}) homeostasis and inducing apoptosis (Selkoe and Hardy, 2016). However, the severity of amyloid plaque burden is not correlated with the severity of cognitive impairment or duration of dementia (Morris *et al.*, 2014). Whereas more recent evidence found that non-fibrillar oligomeric $A\beta$ is capable of forming membrane ion channels that disrupt Ca^{2+}

homeostasis, correspondingly inhibition of $A\beta$ fibrillisation has been linked to improved cognition (Nelson P. T. et al, 2013).

Whilst the spatiotemporal progression of $A\beta$ is relatively inconsistent, there have been many attempts to stage its spread (Braak and Braak, 1991; Thal *et al.*, 2002). Whilst the link between amyloid burden and cognitive impairment is not reliable,

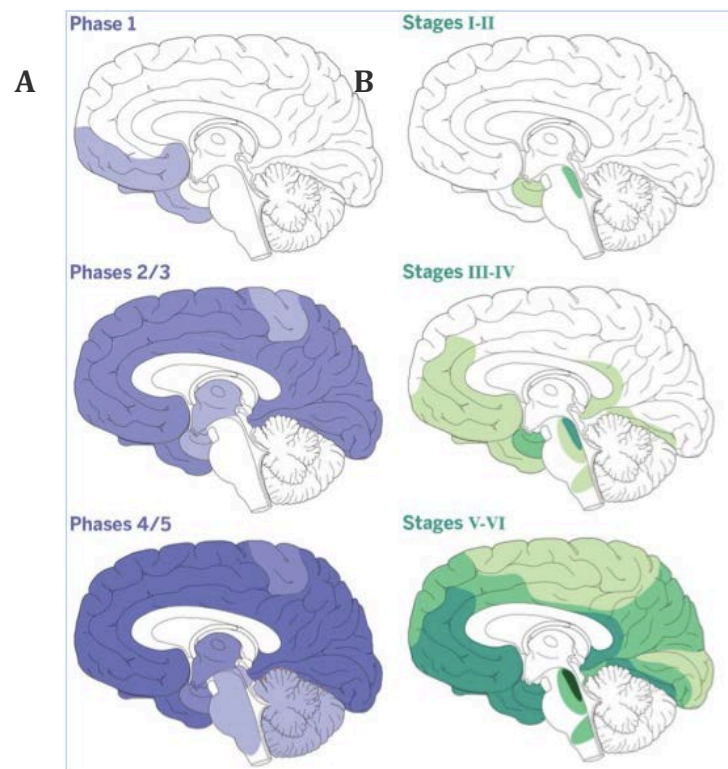


Figure 1.2. Spatiotemporal distribution of key pathological hallmarks. A, Blue) $A\beta$ plaques develop first in the basal temporal and orbitofrontal neocortex (phase 1), spreading throughout the neocortex, hippocampus, amygdala, diencephalon, and basal ganglia (phases 2 and 3). In severe cases of AD, $A\beta$ plaques are also found in mesencephalon, lower brainstem, and cerebellar cortex (phases 4 and 5). B, Green) Tau inclusions develop in the in the transentorhinal and entorhinal cortex, along with the locus coeruleus (stages I and II) subsequently spreading to the hippocampus and some parts of the neocortex (stages III and IV). Later stages are characterised by large deposits in the neocortex (stages V and VI). Adapted from Goedert (2015).

experimental evidence illustrates a trans-synaptic progression of $A\beta$ from the EC to the hippocampus that induces spatial learning and memory deficits (Harris *et al.*, 2011) that likely occur through synaptic dysfunction in the perforant path (Hyman *et al.*, 1984). However tau deposition is more predictive of cognitive decline than $A\beta$ pathology.

1.2.4. Tau

In its physiological state tau is an intracellular soluble microtubule-associated protein, however in AD tau becomes misfolded, insoluble and aberrantly hyperphosphorylated resulting in its self-assembly and the formation of filamentous tangles (Avila *et al.*, 2004). Hyperphosphorylated tau aggregates into neurofibrillary tangles (NFTs) eliciting nucleus displacement and abnormal dendritic processes that ultimately culminate in synaptic dysfunction and cell death (Di *et al.*, 2016). Unlike amyloid, the spatiotemporal staging of tau propagation is relatively consistent between laminar and neuroanatomical structures (Figure 1.2). The transentorhinal and entorhinal cortices (EC) are the primary sites of tau pathology primarily affecting stellate neurons of layer ii (Braak and Del Tredici, 2015; Kaufman *et al.*, 2018). Tau subsequently spreads to layer iii and iv (stage i - preclinical AD) of the EC before infiltrating the hippocampus, specifically CA1 (stage ii - preclinical AD) and subiculum (stage iii - approximately early MCI), thereby impairing the perforant path via deficits in axonal trafficking (Hyman *et al.*, 1984; Thal *et al.*, 2000). In stage iv the amygdala (MCI), thalamus and claustrum are affected ahead of the wider neocortex (stage v - approximately late MCI/early AD dementia) and finally the primary sensory, motor and visual areas (stage vi - AD dementia, Braak and Braak, 1995). Whilst the 'prion-like' spread of tau remains controversial (Mudher *et al.*, 2017), there is substantial evidence indicating that the progressive spread of tau pathology occurs transneuronally propagating through connectivity, and not proximity (Ahmed *et al.*, 2014).

In further contrast to amyloid, the quantity and distribution of NFTs positively correlates with the severity of cognitive impairment (Nelson P. T. *et al.*, 2013), and is reflected in the sequential neuropsychological deficits observed in AD dementia. Given the role of the transentorhinal and entorhinal cortices in spatial behaviours it is anticipated that tau-induced neurodegeneration may primarily manifest as deficits in spatial cognition. Importantly, layer ii (Braak stage i) of the EC contains the highest density of spatially-modulated grid cells anywhere in the brain

(Hafting *et al.*, 2005), and the presence and degree of tau pathology has been shown to elicit impairments in grid cell function that is predictive of impaired performance in spatial tasks (Fu *et al.*, 2017). Subsequently, the spatiotemporal propagation of tau pathology is associated with domain-specific cognitive impairments in episodic (hippocampus) and semantic memory (left anterior temporal lobe, supramarginal gyrus), as well as dysfunction in visuospatial (occipitotemporal), executive (frontoparietal) and language (left posteriosuperior temporal lobe and supramarginal gyrus) processing (Bejanin *et al.*, 2017).

The putative link between tau propagation, cellular dysfunction and cognitive impairment indicates that the development of cognitive assays sensitive to tau-induced dysfunction may aid in the detection of prodromal AD. Given the increasingly understood link between spatial behaviours and cell physiology, it is postulated that tau-induced neuronal dysfunction in the EC may primarily manifest as spatial deficits.

1.3. Neuroimaging in Alzheimer's disease

1.3.1. Structural MRI

AD-associated atrophy occurs throughout the medial temporal lobe (MTL) coinciding with the spread of NFTs (Chan *et al.*, 2001). Within the MTL numerous MRI studies report a specific reduction in hippocampal (Jack *et al.*, 1997; Schuff *et al.*, 2009; Shi *et al.*, 2009) and EC (de Toledo-Morrell *et al.*, 2000; Jessen *et al.*, 2006; Devanand *et al.*, 2012) volume in MCI and AD dementia. As such hippocampal atrophy is a common biomarker of AD (Albert *et al.*, 2011; McKhann *et al.*, 2011) with the rate of atrophy accelerated in individuals with Apo ϵ 4 polymorphism (Li *et al.*, 2016), occurring up to three times faster in AD than in healthy ageing (Barnes *et al.*, 2009). The commonly deployed visual rating scale of MTL atrophy yields between 50-75% sensitivity for predicting conversion from MCI to AD dementia (Dubois *et al.*, 2007; Yuan *et al.*, 2009) and up to 80% when combined with cognitive tests (Korolev *et al.*, 2016). Hippocampal degeneration does not occur uniformly throughout hippocampal subfields (see de Flores *et al.*, 2015 for

review), the precise patterning of degeneration is confounded by differing boundary definitions, although international collaborations are attempting to resolve this (Wisse *et al.*, 2017). Studies of global hippocampal degeneration in early-onset AD dementia have produced more mixed results (Fox and Freeborough, 1997; Apostolova *et al.*, 2011), reflecting the limited specificity to AD pathology. Hippocampal atrophy is observed in Parkinson's disease (Camicioli *et al.*, 2003), recurrent major depression (Sheline *et al.*, 1996; Bremner *et al.*, 2000), Lewy Body and vascular dementia (Barber *et al.*, 2000).

The structure of the EC exhibits significant atrophy in dementia (Juottonen *et al.*, 1998) and is predictive of episodic memory impairment (Di Paola *et al.*, 2007; Dickerson and Wolk, 2013). In MCI, smaller EC volumes at baseline were predictive of disease severity and subsequent conversion to AD dementia (Dickerson *et al.*, 2001) and exhibited greater disease specificity than hippocampal atrophy (Killiany *et al.*, 2002; DeToledo-Morrell *et al.*, 2004; Pennanen *et al.*, 2004; Devanand *et al.*, 2007, 2012). Critically, EC atrophy is predictive of memory decline, and the EC is more resistant to age-related degeneration than the hippocampus, which atrophies with age and is less predictive of cognitive decline (Raz *et al.*, 2004). The patterning of EC atrophy appears to occur in a lateral-medial gradient and is discussed further below and in chapter 4.

1.3.2. Diffusion Tensor Imaging.

Increasing emphasis is being placed upon pathological white matter changes in individuals with MCI and AD dementia, microstructural damage is revealed by examining the diffusion of water across a fibre. Such pathological changes in white matter are primarily observed in regions that are myelinated later in neurodevelopment, typically with smaller diameter axons and lower oligodendrocyte-to-axon ratio, such as the MTL (Bartzokis, 2004). This 'retrogenesis' is molecularly characterised by a reduction in myelin density (Sjöbeck *et al.*, 2005), myelin basic protein (Wang *et al.*, 2004) and

oligodendrocytes (Sjöbeck *et al.*, 2006). Increases in mean diffusivity has been observed in the frontal, parietal and medial temporal lobes, including regions of interest such as the hippocampus and EC, of patients with MCI and AD dementia (Fellgiebel *et al.*, 2004; Rose *et al.*, 2006; Stahl *et al.*, 2007). Furthermore, decreased fractional anisotropy, a measure of diffusion directionality and isotropy indicative of white matter damage, is reported in the MTL of MCI patients (Fellgiebel *et al.*, 2004; Rose *et al.*, 2006; Zhou *et al.*, 2008; Choo *et al.*, 2010; Salat *et al.*, 2010).

1.3.3. Resting-state functional MRI

Functional MRI (fMRI) measures brain activity by detecting blood oxygen level dependent (BOLD) changes as a surrogate of neuronal activity either at rest or in response to a specific task, but its currently not accepted as a clinical biomarker for the detection of AD (Sperling, 2011). However the increasing concordance of findings indicating aberrant functional connectivity associated with prodromal AD may result in rs-fMRI being included as biomarker for prodromal AD (Badhwar *et al.*, 2017; de Vos *et al.*, 2018).

AD-induced deficits in resting-state functional connectivity have been observed in hippocampal synchrony as well as the default-mode network. Such deficits differentiate AD dementia patients from healthy controls with high sensitivity and specificity (72–85%) (Li *et al.*, 2002; Greicius *et al.*, 2004; Supekar *et al.*, 2008). These deficits in inter- and intra- network functional connectivity are additionally observed in MCI (Wang *et al.*, 2015), and are predictive of conversion to AD dementia at 24-month follow up (Li *et al.*, 2016). Critically, MCI is associated with disrupted connectivity in the dorsal ‘where’ pathway (Goodale and Milner, 1992), with disconnection observed between parahippocampal gyrus and hippocampus (Chen *et al.*, 2016). Disrupted functional connectivity of the perirhinal cortex may be a sensitive biomarker for preclinical AD, aberrant connectivity of the perirhinal cortex was associated with $\text{a}\beta$ deposition in cognitively normal adults, (Song *et al.*, 2015).

Whilst the targeted evaluation of functional and effective connectivity using resting state fMRI measures may offer high specificity for incipient AD, these methods are currently limited by differences in pre-processing pipelines (Cusack *et al.*, 2015) and may require prospective motion-correction to be more reliable (Vemuri *et al.*, 2012; Huang *et al.*, 2018).

1.3.4. Ligand-positron emission tomography

Positron emission tomography (PET) ligands binding filamentous tau recapitulates the broad topographical distribution of histopathological tau *in vivo* and correlates with cognitive decline (Small *et al.*, 2006; Schwarz *et al.*, 2016). The localisation of neurofibrillary (Okamura *et al.*, 2014) and paired helical filamentous tau (Chien *et al.*, 2014; Shcherbinin *et al.*, 2016) correlates with the clinical and neuroanatomic variability of AD (Ossenkoppele *et al.*, 2016). The binding of $a\beta$ ligands spatially overlaps with patterns of hypometabolism as well as histopathological distribution observed in AD. Whilst approximately 50% of MCI patients have heightened binding retention compared to controls (Pike *et al.*, 2007; Okello *et al.*, 2009; Wolk *et al.*, 2009; Vandenberghe *et al.*, 2010), the diagnostic specificity of $a\beta$ PET is no more effective than CSF biomarkers in differentiating between AD staging (Morris *et al.*, 2016). However the associated cost, logistical considerations, invasiveness and the short half-life of PET ligands limits their clinical viability (Bateman, 2012).

1.4. Cognitive impairment in Alzheimer's disease

Given that AD is defined clinically by its cognitive symptoms, and the relative low cost of cognitive testing, there is considerable value in developing cognitive tests that are sensitive and specific to prodromal AD. The ability of global and domain-specific cognitive tests to detect and differentiate AD from other neurodegenerative pathologies is discussed, as well as their limitations in aiding the detection of prodromal and preclinical AD.

1.4.1. Global cognitive tests

Brief tests of global cognition are used to capture a snapshot of deficits in specific cognitive domains to inform diagnosis of dementia or MCI. These tests are brief, efficient and have high sensitivity and specificity for the detection of dementia (Mitchell, 2009; Velayudhan *et al.*, 2014). However these tests are not anatomically specific or sensitive to the underlying pathology (Hutchinson and Mathias, 2007; Mathias and Burke, 2009) limiting their accuracy in classifying MCI (Carvalho *et al.*, 2013; KF *et al.*, 2015) and preclinical AD (Mortamais *et al.*, 2017; Papp *et al.*, 2017).

1.4.2. Episodic memory

Functional anatomy of episodic memory

Ever since the profound anterograde amnesia observed in patient H.M following temporal lobectomy (Scoville and Milner, 1957) there has been consensus that the hippocampus is critical for declarative short-term memory, particularly CA1 (Rempel-Clower *et al.*, 1996; Cipolotti *et al.*, 2006). The profound episodic memory deficits observed in MCI and AD dementia have been thoroughly reviewed elsewhere (Bäckman *et al.*, 2001; Gold and Budson, 2008; Gallagher and Koh, 2011; Tromp *et al.*, 2015). Theoretical models of hippocampal function implicate the hippocampus as an integration site binding items and contexts (BIC model), or objects and scenes via connectivity with lateral and medial EC networks, respectively (Ranganath, 2010). The “PMAT” model extends the BIC model to extra-MTL networks that converge on the EC prior to the hippocampus. The posteromedial (PM) network (including thalamus, retrosplenial and posterior parietal cortices) converges on the medial EC encoding spatial and temporal representations. Whereas anterior-temporal (AT) networks include the orbitofrontal, amygdala, and perirhinal cortices that converge on the lateral EC and is thought to encode semantic and perceptual information (Ranganath and Ritchey, 2012). Given the central role of the EC in these models concomitant with the spatiotemporal deposition of tau pathology in early AD it is anticipated that

deficits in scene and object processing may be detectable ahead of holistic episodic memory impairment (Maass *et al.*, 2019).

1.4.3. Other memory domains

Autobiographical memory is impaired in both MCI and AD dementia (Leyhe *et al.*, 2009; Irish *et al.*, 2011) and is associated with hippocampal atrophy (Philippi *et al.*, 2012) reflecting the hippocampus' role in the integration of contextual information. This may culminate in compromised representations of self and/or increase the frequency of de-contextualised memories commonly expressed as “*déjà vu*”. AD is also associated with deficits in semantic memory (Hodges and Patterson, 1995; Joubert *et al.*, 2008). However, semantic memory deficits are not specific to AD and is far more sensitive to semantic dementia localised to a left-lateralised temporal lobe network (Lambon Ralph and Patterson, 2008; Binder *et al.*, 2009). Implicit memory is preserved in MCI and AD dementia as evidenced by priming tasks requiring perceptual, but not conceptual, processing (Meiran and Jelicic, 1995), although maybe be confounded in severe AD by concomitant apraxia and agnosia that approximately coincides with neocortical and cerebellar spread of AD pathology (Machado *et al.*, 2009).

1.4.4 Neuropsychiatric symptoms

The prevalence of neuropsychiatric symptoms in patients with cognitive impairment and AD is greater than in the general population, and the presence of depression or apathy is associated with an increased risk of conversion to dementia in MCI patients (Taragano *et al.*, 2009). As the disease progresses agitation, sleep disorders, delusions and hallucinations are also more frequently reported (Lyketsos *et al.*, 2011).

1.5. Limitations of traditional neuropsychological test paradigms

Both global and domain-specific neuropsychological tests have demonstrated varying degrees of efficacy in aiding the detection of MCI and AD dementia, with

some exhibiting greater sensitivity and specificity to prodromal AD (e.g. episodic memory) than others (e.g. semantic memory). However, given the importance of identifying AD in its infancy (see Petersen (2018) for a summary), a paradigm shift away from 'typical' pen-and-paper neuropsychological tasks is important for 4 reasons:

1) Target sites of early pathology. Given the importance of identifying the disease in its infancy, ideally before hippocampal infiltration, neuropsychological tests that target brain areas compromised in the earliest stages of AD is required. A substantial proportion of current 'traditional' neuropsychological tasks are not predicated on brain-behaviour relationships.

2) Translation. All tests created to probe the aforementioned neuropsychological domains are not translatable to animal models, for example the inability to generate a rodent equivalent of verbal memory tests used widely in clinical studies. Given the wide use of spatial memory tasks such as the Morris water maze in preclinical AD trials, it makes heuristic sense to develop comparable outcome measures that enable across species comparison. Such links would simultaneously benefit both diagnosis and the development of translatable outcome measures for use in both preclinical and human anti-AD trials.

3) Cellular basis of behaviour. Given AD pathology's influence on the function and physiology of neurons, neuropsychological tests should seek to target behaviours and cognitive processes that are increasingly understood at the level of cell physiology. It is currently unclear how episodic memory, processing speed or executive function are represented at the cellular level. Such an approach would permit the translation of causal manipulations at the level of single cell physiology to animal, and subsequently human, behaviours that may aid in the detection of preclinical AD.

4) Ecological validity; pen-and-paper tasks have limited ecological validity and are rarely representative of impaired daily functioning e.g. Rey figure recall or trail-making test. There is an increasing demand for direct behavioural observations

that are more ecologically valid (e.g. Pflueger *et al.*, 2018; Serino and Repetto, 2018).

1.6. Spatial Cognition

Evolutionarily spatial navigation and spatial memory are critical for survival. MTL regions are heavily involved in supporting these phylogenetically conserved behaviours, with spatially modulated cells in the hippocampus and EC implicated in the formation and updating of a ‘cognitive map’ of an environment. Critically, the anatomical localisation of these spatially modulated cells overlaps considerably with brain regions that exhibit dysfunction and degeneration in early AD.

1.6.1. Neural correlates of spatial cognition

Nearly half a century ago, O’Keefe and Dostrovsky (1971) discovered that neurons in the rat hippocampus had spatially receptive fields, with the depolarisation of these cells corresponding to an animal’s location within its environment and were correspondingly named ‘place’ cells (Figure 1.3A). The spatial selectivity of hippocampal neurons meant that position within an environment could be inferred from a small sample of neurons. Seven years later O’Keefe and Nadel (1978) published their seminal work positing that hippocampal place cells are the neural instantiation of the cognitive map that underpins allocentric landmark navigation. However, navigation requires a neural representation of heading direction and space that is independent of environmental landmarks. Correspondingly, the Mosers (2004) began to look upstream of the hippocampus to the EC and discovered grid cells in the medial EC (mEC). Unlike place cells, mEC grid cells exhibit multiple firing fields forming a hexagonal grid (Figure 1.3B) that spans the entire environment and are independent of environmental landmarks, travel speed or direction. By some estimates up to 95% of the cells in the mEC are grid cells (Diehl *et al.*, 2017) and they are thought to encode a neural representation of Euclidean space as well as being integral to the dynamic computation of current position (Hafting *et al.*, 2005). Head-direction cells found in the presubiculum, thalamus and EC are tuned to a specific cardinal direction

reliant upon idiothetic cues and an allocentric representation of space (Figure 1.3C, Taube *et al.*, 1990). In the deeper layers of the EC conjunctive head direction x grid cells (cells firing in a grid like pattern tuned to a specific direction) are thought to be critical for navigation by path integration, i.e. the ability to keep track of, and return to, a previously visited location using only idiothetic cues (McNaughton *et al.*, 2006). Object cells in the lateral EC (IEC) are thought to encode a representation of objects, or the 'content' of a specific environment, their activity is localised around the position of a given object (Figure 1.3D, top), whereas object-trace cells fire at the location of the object when the object has been removed (Figure 1.3D, bottom, Tsao *et al.* (2013)). Homologous trace cells have recently been demonstrated in the human EC with remapping highly related to memory demands during an object-location task (Qasim *et al.*, 2018). Recently, object-vector cells have been reported in the mEC whose activity corresponds to a specific distance and direction from a given object and is consistent despite the object's translocation (Figure 1.3E). These cells are postulated to provide a positional map that is relative to local landmarks that can be used for landmark navigation (Høydal *et al.*, 2019). Object-responsive and place-responsive neurons indicate a pivotal role of the IEC in the formation of associations between objects and contexts upstream of the hippocampus (Deshmukh and Knierim, 2011). A plethora of other spatially modulated cells are also emerging throughout the MTL including boundary cells (Lever *et al.*, 2009), speed cells (Kropff *et al.*, 2015) and time cells (Mankin *et al.*, 2012), however these are beyond the scope of this thesis.

Spatially-modulated place (Ekstrom *et al.*, 2003; Miller *et al.*, 2013), trace and grid (Jacobs *et al.*, 2013; Nadasdy *et al.*, 2017) cells have also been directly observed in humans using intracranial EEG. Grid cell-like 6 fold symmetric activity has also been indirectly observed in the EC using fMRI (Doeller *et al.*, 2010), this approach revealed increased grid cell-like representations during virtual and imagined navigation (Horner *et al.*, 2016) and is predictive of performance in spatial tasks (Kunz *et al.*, 2015; Stangl *et al.*, 2018a). Intracranial EEG experiments have enabled the examination of oscillatory activity in humans during navigation, with theta activity in the MTL during navigational mazes associated with movement (Ekstrom *et al.*, 2005), anticipation of movement (Bush *et al.*, 2017) and speed of

movement (Aghajan *et al.*, 2017) in desktop tasks. Critically intracranial EEG of the hippocampus revealed heightened low-frequency theta oscillations during a navigation task with real world movement that were not present in when stationary or in a desktop (i.e. stationary) navigation task. This study highlights the importance of motor, vestibular and proprioceptive input generated through ambulation during navigational tasks (Bohbot *et al.*, 2017).

Whilst the distribution and organisation of IEC cells are thought to have a more tenuous homology to the anterolateral EC (alEC) in humans, mEC cells are highly conserved in the human posteromedial EC (pmEC, Naumann *et al.*, 2016). However both the alEC and pmEC exhibit conserved reciprocal connectivity with other brain areas implicated in spatial behaviours (Naumann *et al.*, 2018). The discrete specialisation of the EC suggests a homology in the neural architecture than underpins the functional mediation of spatial behaviours. A plethora of research consistently demonstrates the specialisation of the IEC/mEC in rodents (Hunsaker *et al.*, 2013; Van Cauter *et al.*, 2013; Wilson *et al.*, 2013b, a; Diehl *et al.*, 2017; Kuruvilla and Ainge, 2017a; Rodo *et al.*, 2017, see Knierim *et al.* (2014) for review) and alEC/pmEC in humans for processing object and spatial information, respectively (Schultz *et al.*, 2012, 2015; Ciavarro *et al.*, 2013; Reagh and Yassa, 2014; Maass *et al.*, 2015, 2018a; Navarro Schröder *et al.*, 2015; Reagh *et al.*, 2017, 2018, 2016; Berron *et al.*, 2017a, 2018a; Yeung *et al.*, 2017, 2018; Berron *et al.*, 2018b; Olsen *et al.*, 2017). The distinct roles of the pmEC and alEC in path integration and object-orientated spatial processing are developed further in chapters 2 and 3, respectively.

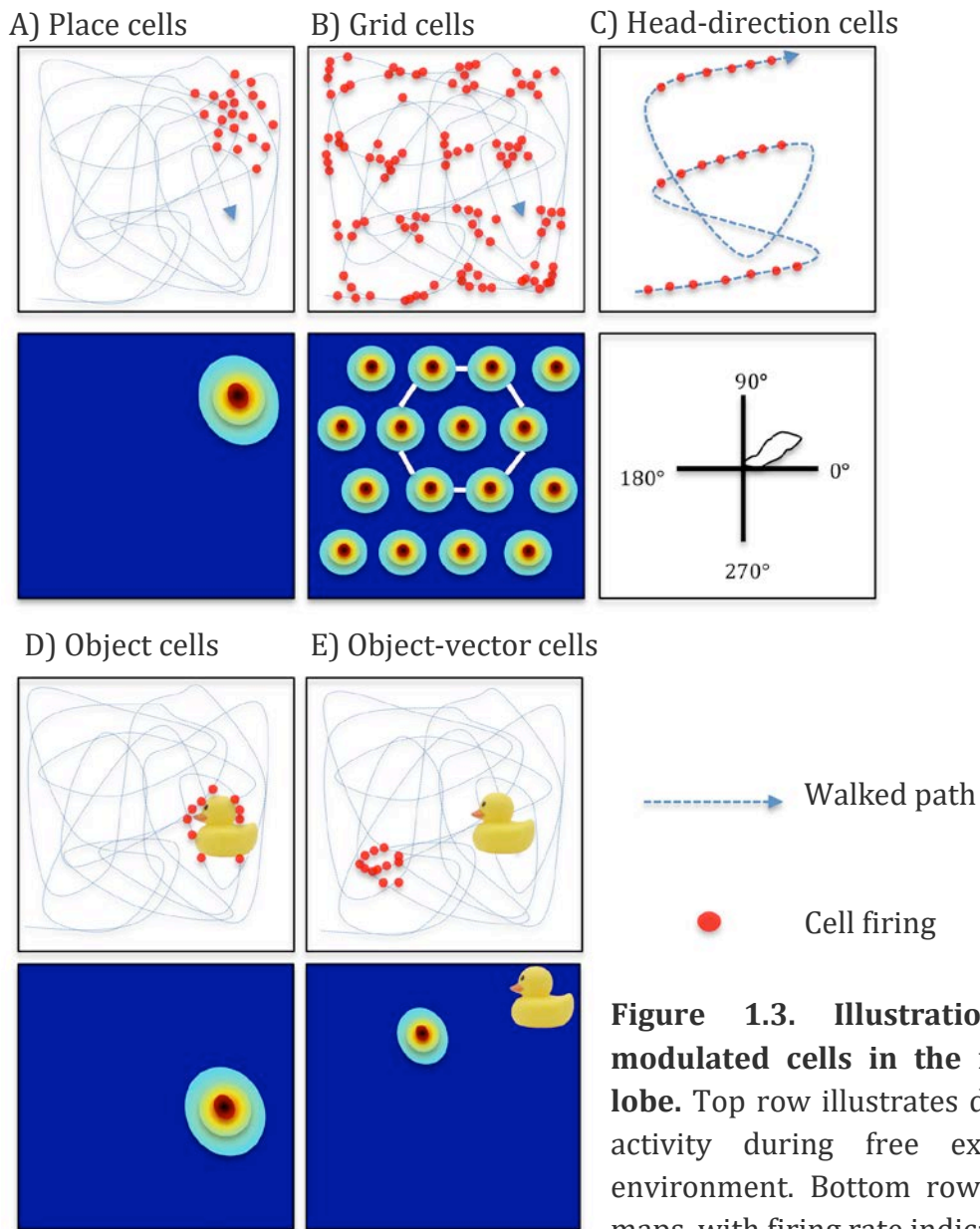


Figure 1.3. Illustration of spatially modulated cells in the medial temporal lobe. Top row illustrates disparate neuronal activity during free exploration of an environment. Bottom row are cartoon rate maps, with firing rate indicated by 'hot' colours

A) Hippocampal place cells fire in response to a specific location within an environment, these cells are qualitatively anchored to the presence of allothetic cues. **B)** Medial entorhinal grid cells' are thought to encode a distance metric of an environment, exhibiting stereotypic activity that is independent of local cues within an environment. **C)** Head-direction cells are predominantly found in the subiculum, thalamic nuclei, retrosplenial and entorhinal cortices. Cell activity is coupled to heading direction in the horizontal (yaw) plane and is independent of environment, this illustration depicts a cell whose activity is selective for north-east. Conjunctive head-direction x grid cells also exists, predominantly in the medial entorhinal cortex and are thought to functionally underpin path integration. **D)** Lateral entorhinal object cell activity (top) occurs around the location of an object in the environment, whereas object-trace cell activity persists when the object is removed (bottom). **E)** Object-vector cells in the medial entorhinal cortex fire at a specific distance and direction from discrete objects, regardless of position.

1.6.2. Spatial cognition in Alzheimer's disease

There is a dearth of literature examining the relationship between AD pathology and spatially-modulated cells, and as such the precise effect of AD pathology on spatial behaviour/cognition remains elusive. However, two key studies have been conducted that raise the possibility of a causal relationship between AD pathology and electrophysiological dysfunction that culminate in impaired spatial behaviours. Cacucci *et al* (2008) examined the relationship between hippocampal place cells and spatial cognition in transgenic AD mice that have elevated levels of $A\beta$ pathology. The degeneration of place cells was observed in the aged (16 months) but not younger (3 month) transgenic mice, and was associated with place cell dysfunction and reduced encoding of spatial information. Critically, the degeneration of place cells and the degree of plaque burden was strongly associated with impaired performance on T-maze tasks of spatial memory. Fu *et al.*, 2017 demonstrated similar results in mEC grid cells of aged transgenic mice (30 months) that expressed a highly aggregable form of human tau. The degree of tau pathology in EC-tau mice (Harris *et al.*, 2012) was associated with reduced firing and periodicity of grid cells that culminated in spatial memory deficits in the Morris water maze and in T-mazes. These deficits were accompanied by a 70% reduction in mEC layer ii glutamatergic neurons and a 50% increase in inhibitory neuron firing. This neuronal disequilibrium strengthened theta oscillations that may partially explain the increase in oscillatory changes observed in MCI and AD dementia (Montez *et al.*, 2009; Moretti *et al.*, 2009).

The synaptic and neuronal dysfunction and degeneration induced by the presence of AD pathology is posited to underpin spatial deficits observed in AD dementia, and to date literature has predominantly focused on egocentric and allocentric spatial tasks. Briefly, egocentric navigation is a strategy that refers to self-centred navigation, often when following familiar routes, whereas allocentric navigation is dependent upon the perception of landmark positions relative to other landmarks, most frequently deployed in novel environments (Coughlan. *et al.*, 2018). Impairments in egocentric and allocentric memory have been observed in individuals with MCI (Hort *et al.*, 2007a; Weniger *et al.*, 2011) and AD dementia

((Tu *et al.*, 2015), see Serino *et al.* (2014) for review). Furthermore, deficits in the translation of allocentric to egocentric representations are observed (Serino and Riva, 2013). Allocentric spatial processing depends on the MTL, and specifically the hippocampus (Morris, 1984; Astur *et al.*, 2002; Feigenbaum and Morris, 2004; Bartsch *et al.*, 2010; Goodrich-Hunsaker *et al.*, 2010; Banta Lavenex *et al.*, 2014). Performance on the Four Mountains task (4MT), a hippocampal-dependent test of allocentric spatial memory (Hartley, 2007; Hartley and Harlow, 2012), is impaired in AD dementia (Pengas *et al.*, 2010) and differentiates AD from frontotemporal dementia (FTD) (Bird *et al.*, 2010). The 4MT performance also differentiates MCI patients with and without underlying AD (Moodley *et al.*, 2015) and is highly predictive of progression from MCI to AD dementia at two year follow up (Wood *et al.*, 2016). Whilst performance on different allocentric spatial memory tasks were impaired in MCI, performance was not predictive of subsequent conversion to AD dementia (Weniger *et al.*, 2011). More recently, allocentric (4MT), but not egocentric, deficits have been observed in healthy older adults at higher risk of AD dementia, with performance errors being associated with dementia risk (Ritchie *et al.*, 2018).

A growing body of evidence suggests that spatial tests may be both sensitive and specific to AD during preclinical stages. Allison *et al.*, (2016) demonstrated that asymptomatic individuals with preclinical AD, with biomarker positivity defined as CSF A β 42 > 500pg/ml (Fagan *et al.*, 2006), were accurately differentiated from their biomarker negative counterparts based upon performance on a way-finding (allocentric) navigation task (area under the curve (AUC) = 0.77). By comparison tests of episodic memory and egocentric route-learning differentiated preclinical AD from biomarker negative participants at approximately chance-level accuracy (AUC=0.56). These findings indicate that performance in allocentric navigation tasks may yield greater sensitivity and specificity to incipient AD ahead of episodic memory or egocentric navigation impairments. Lastly, young adult *APOE-e4* carriers, representing the strongest genetic risk factor of late-onset AD, exhibit reduced EC activation and grid-cell like representations during an fMRI object-location task (Kunz *et al.*, 2015). Reduced grid-cell like representations in at-risk

participants were associated with spatial memory performance, explained as potential evidence of tau pathology in the EC. Reduced grid-cell like representations were also associated with elevated hippocampal activity and interpreted as evidence of a corresponding compensatory mechanism in response to EC dysfunction.

Recent research from multiple groups suggest that impairments in aEC-dependent object discrimination (Schultz *et al.*, 2012; Reagh and Yassa, 2014; Navarro Schröder *et al.*, 2015; Olsen *et al.*, 2017) is impaired in older adults (Reagh *et al.*, 2016, 2017; Berron *et al.*, 2018b) and is associated with the degree of cognitive decline (Fidalgo *et al.*, 2016). Recent evidence indicates that object, but not scene, discrimination was associated with aEC activity, with performance predicted by CSF phosphorylated tau, but not $a\beta$, levels in cognitively healthy older adults (Berron *et al.*, 2019). Additionally, higher tau deposition in anterior-temporal networks was predictive of impaired object discrimination in unimpaired older adults, whereas higher $a\beta$ deposition was predictive of impaired scene discrimination (Maass *et al.*, 2019). Collectively this body of work indicates that the spatiotemporal propagation of tau and $a\beta$ is related to reduced domain specificity of EC subdivision networks and worse performance in object and scene processing, respectively. Impairments in mnemonic discrimination tasks, particularly in the detection of object novelty, may therefore be invaluable to the detection and discrimination of preclinical AD. The role of the aEC and pmEC in mnemonic discrimination is discussed further in chapters 2 and 3

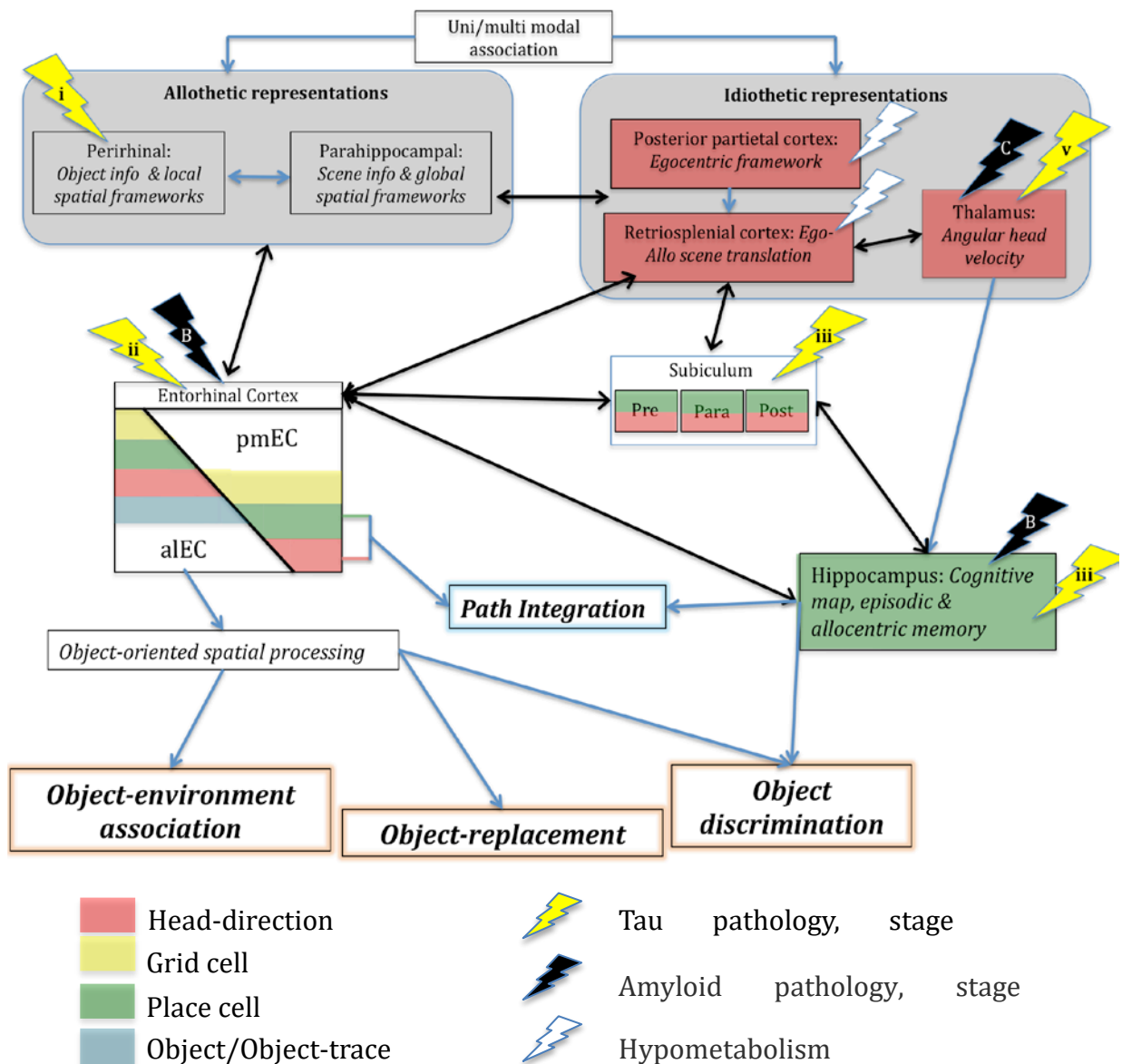


Figure 1.4. Schematic summary of the spatial network, its function and overlap with the spatiotemporal propagation of AD pathology. Brain regions implicated in mediating specific spatial cognitive functions (*italics*). Arrows indicate connectivity between brain structures or the mediation of specific spatial behaviours evaluated in this thesis. Lightning bolts indicate the presence of evidence for these brain areas compromise in AD pathology and the associated staging, where applicable. The highlighted cognitive functions are investigated and discussed at length in chapters 2 (blue) and 3 (orange).

1.7. Summary of study rationale

To date, all interventional trials aimed at slowing the progression of Alzheimer’s disease (AD) have failed. Two of the main contributors to this failure are: i) problems in identifying the initial stages of AD, such that interventional trials are

applied too late in the disease process, and ii) the lack of translatable outcome measures for comparing treatment effect across preclinical testing in animal models of disease and clinical trials in patient populations. Given that the entorhinal cortex (EC) is one of the primary sites of AD neuropathology, detection of AD-related EC dysfunction provides a potential solution to both of these problems.

The EC is a unique brain structure whose cellular physiology and anatomy is tightly coupled to phylogenetically conserved spatial behaviours, the EC is broadly subdivided along its medial-lateral axis, the aIEC (IEC in rodents) is implicated in object-orientated spatial processing whereas the pmEC (mEC in rodents) is required for navigation via path integration and scene processing, both spatial functions are underpinned by specific neuronal physiology. As such, the targeted development of EC-derived spatial cognitive paradigms may be sensitive to the presence of AD pathology in its prodromal and preclinical phases. The degree of impairments in tasks designed around the function of the EC have not been examined in MCI or prodromal AD, doing so would overcome current cognitive task's limited ecological and translational validity.

Therefore, the aim of this thesis is to test the hypothesis that performance in spatial-cognitive tasks based around the disparate function of EC subdivisions are impaired in MCI. It is predicted that MCI patients with CSF positive AD biomarkers (MCI+ i.e. prodromal AD) will be more impaired than MCI patients with negative AD biomarkers (MCI-). It is also predicted that i) performance on both tasks will differentiate MCI from HCs and MCI+ from MCI- more effectively than “gold standard” diagnostic cognitive tasks currently used in clinical and research practice and ii) that performance on tasks probing the functions of the two EC subdivisions correlates with subdivision volume as measured from high resolution MRI.

Chapter 2 - Path integration

We must bear in mind that neither a compass, nor the north star, nor any other such sign, suffices to guide a man to a particular spot through an intricate country, or through hummocky ice, when many deviations from a straight course are inevitable, unless the deviations are allowed for, or a sort of "dead reckoning" is kept... The manner in which the sense of direction is sometimes suddenly disarranged in very old and feeble persons, and the feeling of strong distress which, as I know, has been experienced by persons when they have suddenly found out that they have been proceeding in a wholly unexpected and wrong direction, leads to the suspicion that some part of the brain is specialised for the function of direction. – Charles Darwin (1873), the first report of path integration in homosapiens

2.1. Introduction

Path integration (PI), the ability to keep track of your current position in reference to another location and integrate a direct return path using only idiothetic self-motion cues such as optic-flow, vestibular and proprioceptive information (Etienne and Jeffery, 2004; McNaughton *et al.*, 2006), depends on the entorhinal cortex (EC). Unlike landmark navigation (Doeller *et al.*, 2008), PI is not contingent upon the presence of orientation cues, although performance is improved by their presence (Kalová *et al.*, 2005; Philbeck and O’Leary, 2005). While several other brain regions have been implicated in PI, including the hippocampus, prefrontal and retrosplenial cortices (Chrastil *et al.*, 2015, 2017), there is mounting evidence that the EC is critical for PI and is implicated in route planning (Maguire *et al.*, 1998; Jacobs *et al.*, 2010), the computation of goal direction (Chadwick *et al.*, 2015) and goal distance (Spiers and Maguire, 2007; Howard *et al.*, 2014).

In vivo single cell studies have shown that the firing of EC grid cells and head direction cells is coupled to PI (McNaughton *et al.*, 2006). The medial EC (mEC) is considered to be particularly involved in PI, given that up to 95% of mEC neurons may be grid cells (Diehl *et al.*, 2017). Evidence that the EC underpins navigation in other mammalian species is supported by the demonstration of EC grid cell’s in bats (Yartsev *et al.*, 2011), monkeys (Killian *et al.*, 2012) and humans (Jacobs *et al.*, 2013). The mEC and theoretically the pmEC homolog in humans, mediates PI through grid cells continuous integration of current position and velocity within a distance metric (Hafting *et al.*, 2008), while head-direction cells support the computation of current heading and goal direction (McNaughton *et al.*, 2006; Sargolini *et al.*, 2006).

PI deficits are observed in response to mEC lesions (Van Cauter *et al.*, 2013) and ablation of mEC glutamate receptors that disrupt grid cells but not other spatially modulated cells (Gil *et al.*, 2018). In a VR PI task the inactivation of mEC stellate cells severely disrupted PI-based distance estimates that required multisensory integration (Tennant *et al.*, 2018). Recent research using deep neural networks demonstrated that grid-like representations emerge in artificial agents trained to perform PI in novel, complex and changing environments (Banino *et al.*, 2018).

Importantly PI was impaired in agents unable to develop such representations further indicating a central role of grid cells in adaptive PI, however the utility of deep learning in spatial cognition is yet to be established, although is a rapidly growing field (Cueva and Wei, 2018; Labash *et al.*, 2018). Finally, Stangl *et al* (2018) demonstrated a negative association between grid-cell-like representations during an fMRI object-location task and path integration errors in a separate task requiring real-world movement. The degree of grid cell-like representations predicted impairments in old, but not younger adults. Interestingly, impaired grid cell temporal stability and reduced grid cell-like representations are observed in healthy adults at risk of AD (Kunz *et al.*, 2015).

In the only study of PI in MCI and AD dementia to date, Mokrisova *et al* (2016) demonstrated that patients with MCI and AD dementia exhibit PI deficits compared to healthy older adults, however a step down in PI accuracy between MCI and AD dementia was not observed. Interestingly, performance correlated with EC and parietal thickness as well as hippocampal volume. However, this study is not without limitations; local allothetic landmarks were present at all times during the experiment, enabling participants to navigate and self-localise using either this local landmark or the enclosing boundary thereby impeding the use of *true* PI strategies. The inclusion of such landmarks is particularly problematic for patients with dementia who demonstrate a reliance on such cues, even when these are explicitly manipulated to be inaccurate (Kalová *et al*, 2005). The use of immersive virtual reality (iVR) for the study of path integration overcomes these limitations by enabling environmental cues to be set infinitely far away without compromising on real-world movement. This is vital given that PI is dependent on the function of grid cells which in turn are dependent on the integration of idiothetic self-motion cues that are impaired in the absence of real-world movement (Winter *et al*, 2015). Correspondingly, larger rotational (Klatzky *et al*, 1998) and distance errors (Distler *et al*, 1998; Sinai *et al*, 1999; Adamo *et al*, 2012) have been reported in desktop VR navigation tasks when compared with tasks requiring active movement, possibly reflecting the absence of self-motion cues, leading in turn to reduced grid cell activation (Ólafsdóttir and Barry, 2015).

The requirement for actual movement in iVR also approximates real world navigation and thus has greater ecological validity than desktop VR. There is also evidence of differing neural processes underlying desktop and actual navigation, with desktop VR being associated with lower frequency hippocampal theta oscillations (Bohbot *et al*, 2017).

These previous studies provide the backdrop for the present study, which investigates EC-dependent PI in MCI patients at risk of developing dementia. Given the robust evidence that PI is dependent on EC function and its early compromise in AD, there is a requirement to investigate PI deficits in MCI and prodementia AD using an environment where local landmarks are not present and the environment can be manipulated.

Hypothesis: Performance on an iVR PI task of EC function differentiates MCI patients at increased risk of developing dementia.

Secondary hypotheses:

- i) PI is impaired in older versus but not younger healthy controls.
- ii) Manipulation of environmental cues perturbs PI accuracy.
- iii) PI performance is a better classifier of MCI and prodromal AD than comparator cognitive tests considered to have high diagnostic sensitivity and specificity.

2.2. Methodology

2.2.1. Participants

The studies presented in this thesis predominantly focus on patients with mild cognitive impairment (MCI) and aged-matched healthy controls (HC), described below. This chapter as well as chapter 3 additionally examine the effect of ageing on task performance by comparing younger controls (YCs) to HCs. The

examination of structural atrophy in AD dementia patients is additionally examined in chapter 4. The definition of these groups, method of recruitment, inclusion and exclusion criteria are described here, excluding AD dementia patients that are described in chapter 4.

MCI patients were recruited from the Cambridge University Hospitals NHS Trust Mild Cognitive Impairment and Memory Clinics. MCI was diagnosed by neurologists according to the Petersen criteria (Petersen, 2004), diagnosis of which requires; i) subjective cognitive complaint, ii) objective evidence of cognitive impairment, iii) preserved activities of daily living, iv) functional independence and v) absence of dementia. Objective cognitive decline was evaluated using the Addenbrooke's Cognitive Examination - Revised (ACE-R, Mioshi et al, 2006) and a score of 0.5 on the Clinical Dementia Rating scale (CDR) (Morris, 1997). All patients underwent screening blood tests to exclude reversible causes of cognitive impairment. Exclusion criteria included the presence of a major medical or psychiatric disorder, epilepsy, a Hachinski Ischaemic Score > 4/15 (Moroney et al, 1997), a history of alcohol excess or any visual or mobility impairment of such severity as to compromise ability to undertake the iVR test.

Twenty-six MCI (n=45) patients underwent CSF biomarker and were stratified into biomarker-positive (MCI+, n=12) and biomarker-negative (MCI-, n=14) groups (Table 2.1). The remaining 19 MCI patients did not undergo CSF studies as part of their clinical workup. Aged matched healthy control participants without a history of cognitive impairment (HCs, n=41, Table 2.1), along with thirty-one young control participants (YCs, aged 18-30, mean age = 21.34, 80% female) were also tested.

A proportion of MCI patients underwent CSF biomarker studies (β -amyloid₁₋₄₂, total tau, phosphorylated tau) as part of their clinical diagnostic workup. Biomarker studies were undertaken using ELISA assay kits (Innotest, Innogenetics, Ghent, Belgium) as outlined elsewhere (Shaw et al, 2009). Thresholds for negativity or positivity were set as CSF amyloid <550pg/ml, CSF

tau > 375pg/ml with a CSF tau: amyloid ratio of <0.8 (Mulder et al, 2010). MCI patients were stratified into biomarker-positive (MCI+) and biomarker-negative (MCI-) groups accordingly. Researchers undertaking the VR tests were blinded to the CSF status of patients. The remaining 19 MCI patients did not undergo CSF studies as part of their clinical workup. Healthy control participants without a history of cognitive impairment (HCs) were recruited from Join Dementia Research, an online repository of patients and volunteers interested in participating in dementia research.

The exclusion criteria included:

- Presence of significant cerebrovascular disease
- Major medical co-morbidities e.g. Congestive Cardiac Failure, Diabetes Mellitus with renal impairment
- Major psychiatric disorder
- The use of cognitive enhancing drugs e.g. Cholinesterase inhibitors
- A concurrent diagnosis of Epilepsy
- A history of alcohol excess or illicit drug use
- A history of severe visual impairment, e.g. macular degeneration, diabetic retinopathy, as determined by the clinical team
- A history of repeated head trauma.

The study was undertaken in line with the regulations outlined in the Declaration of Helsinki (WMA, 2013) and was approved by the NHS Cambridge South Research Ethics Committee (REC reference: 16/EE/0215).

2.2.2. Comparator neuropsychological tests

To compare the ability of the iVR test to classify prodromal AD with that of reference neuropsychological tests considered to be highly sensitive to early AD, all participants were administered a battery of tests chosen for their effectiveness in predicting conversion from MCI to AD dementia (A-C), inclusion in the

Preclinical Alzheimer's Cognitive Composite approved by the FDA for use as cognitive outcome measures in trials aimed at preclinical AD (A, D), or prior work indicating high sensitivity and specificity for prodromal AD (E). These tests are as follows (cognitive domains assessed in parentheses):

- A. Free and Cued Selective Reminding Test (FCSRT, episodic memory – verbal, Buschke, 1984)
- B. Rey figure recall (RFR, episodic memory – nonverbal, Osterrieth, 1944)
- C. Trail Making Test B (TMT-B; executive function, attention, processing speed, Bowie and Harvey, 2006)
- D. Digit Symbol test (DST, attention, processing speed, Ryan and Lopez, 2001)
- E. 4 Mountains Test (4MT, allocentric spatial memory, Hartley et al, 2005)

All participants also underwent global cognitive testing with the Addenbrookes Cognitive Examination-Revised (ACE-R, Mioshi et al, 2006) and the National Adult Reading Test (NART, Nelson, 1982), as a measure of premorbid IQ.

2.2.3. Immersive virtual reality

Immersive virtual reality tasks were administered using the HTC Vive iVR kit, which uses external base stations to map out a 3.5x3.5m space within which participants walked during the VR task. If participants went beyond the tracked boundary by 30cm, an 'out of border' warning appeared in their sightline to encourage them to not walk any further. Researchers were also in the immediate proximity to ensure that participants did not venture beyond the test space. Both the PIT and OLT was programmed by Andrea Castegnaro (UCL) in the Unity game engine and ran on Steam VR software, running on an MSI VR One backpack laptop.

Participation in the VR tasks and cognitive testing were conducted at either the MRC Cognitive Brain Sciences Unit or Cambridge Institute of Public Health, University of Cambridge.

2.2.4. The path integration task

The PI task was undertaken within virtual open arena environments with boundary cues projected to infinity (Figure 2.1C). Three environments were used, each with unique surface details, boundary cues and lighting. The absence of local landmarks ensured EC-grid cell dependent strategies rather than striatal-mediated landmark-based navigation (Doeller *et al*, 2008).

Pre-trial practice sessions consist of 20 seconds of habituation to the iVR environment, during which participants were encouraged to explore the environment. Following habituation, participants performed five practice trials, where cone one was re-presented at the end of each trial in order to provide direct visual feedback to participants on the distance error between the remembered and actual locations of cone one. The task consisted of nine trials conducted within each of the three environments, totalling 27 trials per participant. To examine the effects of environmental cues on PI, the environment was altered during the return path when participants were attempting to return to the remembered location of cone one. Three return conditions were used: A) No environmental change (Figure 2.1E), (B) removal of boundary cues (Figure 2.1D), (C) removal of surface detail (Figure 2.1F).

Each return condition was presented three times per environment, with return conditions presented pseudo-randomly in each environment in order to ensure participants were relying more on proprioceptive and self-motion cues rather than allothetic strategies.

Condition B was designed to increase dependence on self-motion cues and homing vector calculation by removing boundary cue information (Burgess *et al*, 2004), thereby placing a greater cognitive load on the PI network (Zhao and Warren, 2015). Condition C was designed to prevent feedback from surface motion during locomotion, thereby disrupting optic flow (Kearns *et al*, 2002) and increasing dependence on allocentric representations of space (Nardini *et al*, 2008). As such, return conditions B and C were considered analogous to “stress tests” for EC-network dependent navigation, with the prediction that a greater impairment in task performance would be observed during these conditions, compared with condition A.

Performance in the iVR PI task was assessed using three outcome measures. Absolute distance error, the primary outcome measure, was defined as the Euclidean distance between estimated and actual location of cone one.

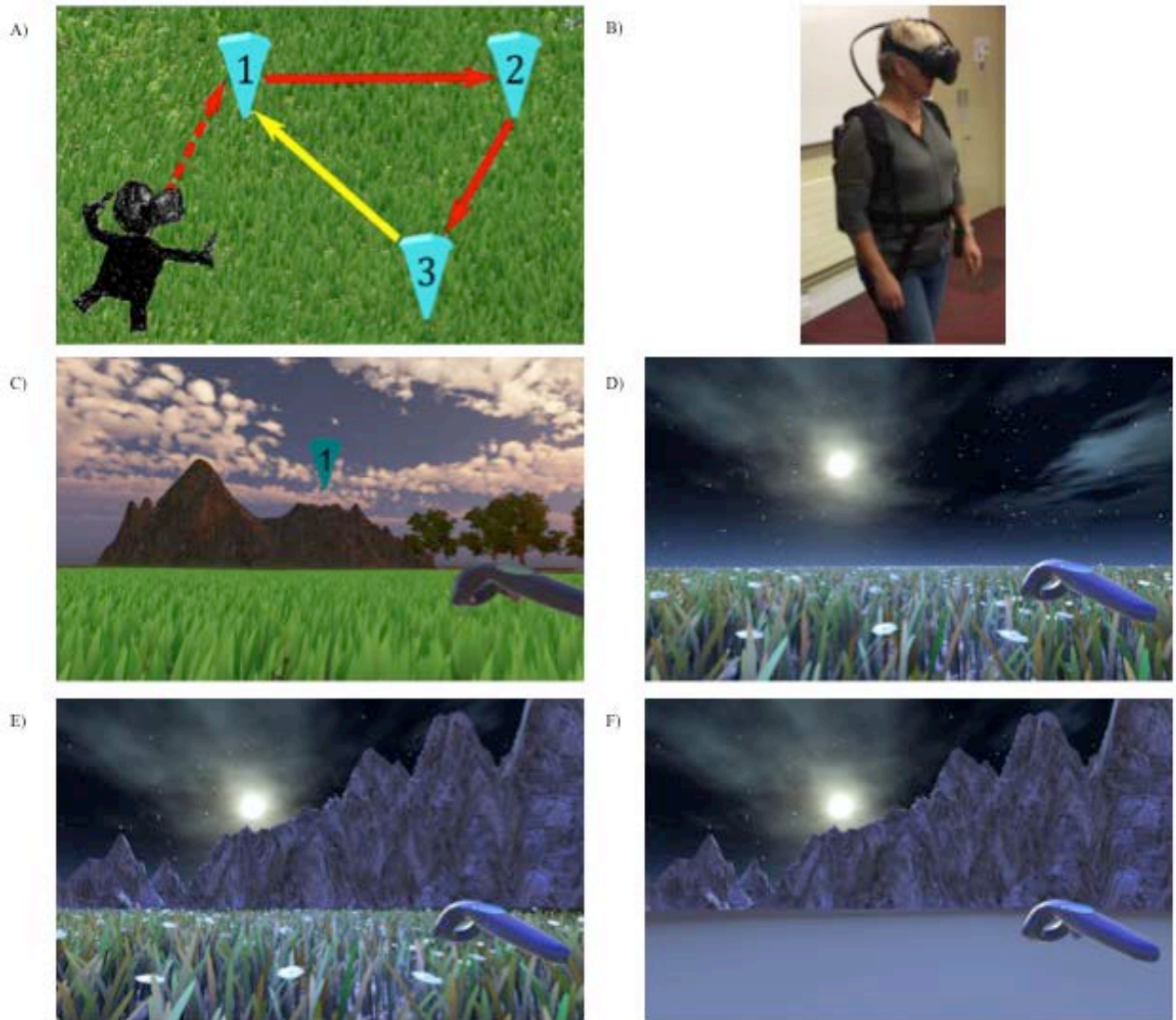


Figure 2.1. Path Integration Task. **A)** Illustration of the path integration task. Each numbered inverted blue cone is a location marker. Only one cone was visible at a time; upon reaching a blue cone it disappeared and the next one in the sequence appeared. Red arrows indicate the guided sequence along two sides of the triangle. The yellow arrow, the last side of the triangle, signifies the assessed return path, performed in the absence of any cones. **B)** Demonstration of VR equipment on a participant during the task, used with permission. **C)** Example environment from the head mounted display with textural and boundary cues present, with cone one and the controller shown. Texture and boundary cues are present in all trials when navigating between cones. **D-F)** Return conditions applied when attempting to return to the location of cone one only (yellow arrow (**A**)) and included removal of environment boundaries (**D**), no change (**E**) and removal of surface detail (**F**).

2.2.5. Calculation of outcome measures

Absolute distance error reflects the Euclidean distance between the estimated position of cone 1 (coordinates) and the actual location of cone 1, as recorded by

the trigger pull in line with previous research (Figure 2.2, Chrastil *et al*, 2015; Mokrisova *et al*, 2016). Calculated as Pythagorean formula:

$$AbsDisErr = \sqrt{(x_1 - y_1)^2 + (x_2 - y_2)^2}$$

where x_1 and y_1 are the coordinates of the participant's estimated location of cone 1, x_2 and y_2 are the coordinates of the actual location of cone 1.

Two secondary outcome measures were included to deconstruct absolute distance errors into its proportional angular and linear components. These measures additionally controlled for between-trial variance in triangle geometry owing to the pseudo-random generation of cone locations that could affect task difficulty, although variance is minimal in paths less than 10 metres long (Harris and Wolbers, 2012). Proportional angular errors reflect the accuracy of performed rotation at cone three toward the participant's estimated location of cone one compared to the optimal rotation required to align with cone one. Proportional linear errors reflected the accuracy of distance estimation, with the Euclidean distance travelled between cone three and the participant's estimated location of cone one compared to the distance between cone three and actual location of cone one.

Proportional angular errors (Figure 2.2B) are calculated as the ratio of rotation performed at cone 3 toward estimated location of cone 1 over the amount of rotation required at cone 3 for an optimal return to cone 1. Calculated by dividing the angles α by β . α and β were calculated using the following formula:

$$\theta = atan2(\vec{v}_1 \times \vec{v}_2, \vec{v}_1 \cdot \vec{v}_2)$$

where the arctangent of the cross and dot product of two vectors (v_1 and v_2) gives the angle between them (θ). After translating data to the same space, α is the angle between the vector of cone 2 and cone 3, and the vector of cone 3 and triggered

position (estimated position of cone 1). β is the angle between the vector of cone 2 and cone 3 and the location of cone 1.

Proportional linear errors (Figure 2.2C) were calculated using the same formula as absolute distance error, this is calculated twice using the x and y coordinates to estimate the Euclidean distance between cone 3 and triggered position (v_1) and cone 3 and cone 1 (v_2). Proportional linear error is the result of $v_1 \div v_2$.

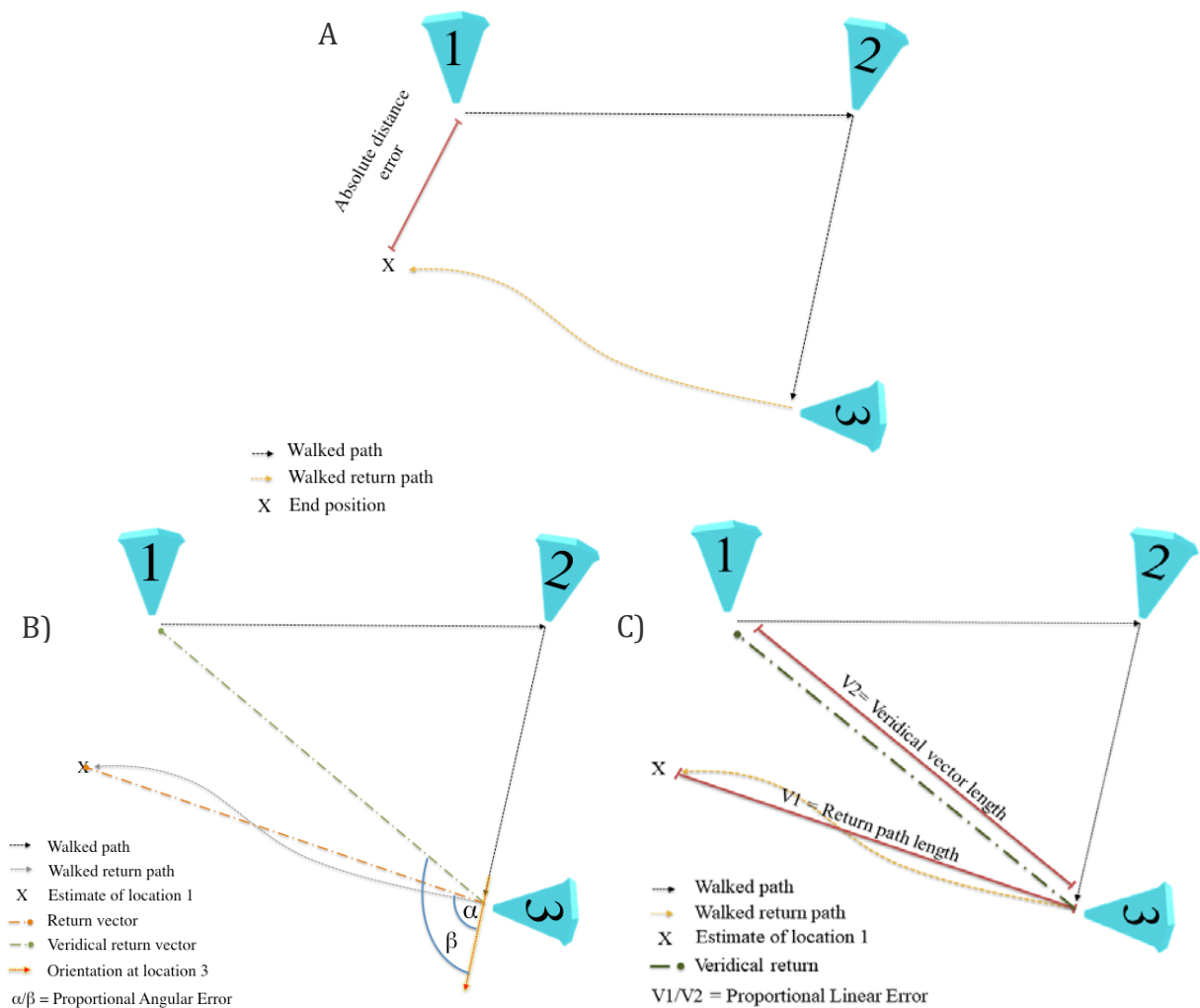


Figure 2.2. Illustrations of outcome measures for the path integration task. A) Absolute distance error is the primary outcome measure that reflects the distance between the estimated locations of cone 1 (goal) and the actual location of cone 1. **B)** Proportional angular error is a measure of rotation accuracy, represents the ratio of performed rotation toward the estimated location of cone 1 at cone 3 (α) divided by the degree of rotation required toward cone 1's actual location (β). **C)** Proportional linear error represents the length of the performed return vector.

2.2.6. Statistical Analysis

Demographic differences between MCI+, MCI- and HCs were assessed using one-way ANOVA or Kruskal Wallis test where parametric assumptions were violated, whereas differences between HCs and total (combined) MCI were assessed using t-tests or non-parametric Mann-Whitney U test. Categorical variables (e.g. sex) were assessed using Fisher's exact Test.

Between-group performance in the PI task compared all MCIs against HCs, as well as MCI+ against MCI-. Linear mixed effect modelling (LME) was used to assess the effect of MCI status on absolute distance error, proportional angular error and proportional linear error. LMEs are the most suitable method for analysing clustered datasets (27 trials with one of three return conditions per trial per participant), with missing data (excluded due to travelling 'out of border', see Results), and unbalanced designs (Moen *et al*, 2016). Alternative approaches such as either i) pooling all trials together would neglect between-participant variance, whereas ii) averaging observations for each participant would neglect within-participant variance (i.e. trial-associated variance, e.g. the distance between cones). Both alternative approaches may lead to misleading inferences and statements about statistical precision (Moen *et al*, 2016).

Final model fixed effects included an interaction term between diagnosis and return condition, along with covariates of age, sex, years in education, ACE-R, NART and VR environment. Unique participant identifiers were used as the random intercept and VR environment as a random coefficient. Reported denominator degrees of freedom were computed using the conservative Satterthwaite approximation. Final LME models were informed by a mixture of *a priori* hypotheses and covariates, where appropriate they were refined using likelihood ratio testing for goodness of fit, whereas intraclass correlation coefficient was used to estimate the amount of variance explained by random effects. Separate models were used to assess PI performance in MCI+ vs MCI- and

HCs vs pooled MCI for absolute linear error, proportional angular error and proportional linear error. The final LME used was:

$$\begin{aligned}
 DV_{ij} = & \beta_0 + \beta_1 MCI_j + \beta_2 Cond_{ij} + \beta_3 MCI_j * Cond_{ij} + \beta_4 Age_j \\
 & + \beta_5 Sex_j + \beta_6 Edu_j + \beta_7 ACER_j + \beta_8 NART_j + \beta_9 Env_{ij} + U_{0j} \\
 & + U_{1j} Env_{ij} + e_{ij}
 \end{aligned}$$

where DV_{ij} is the dependent variable (e.g. absolute distance error, separate models for each outcome measure) in trial i (1...27) of participant j (1..86). β_0 is the population mean, $\beta_1 MCI_j$ is the diagnostic status of participant j (HC vs MCI or MCI+ vs MCI- vs HC), $\beta_2 Cond_{ij}$ is the return condition (no change, no boundary cues, no textural cues) of trial i for participant j . An interaction term between MCI status and return condition (β_3) is also included. There were additional fixed effects of participant's age (β_4), sex (β_5), years in education (β_6), ACE-R (β_7) and NART (β_8) scores. U_{0j} is the random intercept for each participant, while the three different VR environments were modelled as a fixed effect (β_9), as well as random slopes that depended on participant (U_{1j}). The term e_{ij} is the trial-level error for each trial i of participant j . Visual inspection of residual plots did not reveal any significant deviations from homoscedasticity or normality.

Finally, a separate LME was used to assess the effect of ageing on PI, this was required owing to the YCs not having as much demographic or neuropsychological data available, the final model was as follows:

$$\begin{aligned}
 DV_{ij} = & \beta_0 + \beta_1 AgeCat_j * Cond_{ij} + \beta_2 AgeCat_j + \beta_3 Cond_{ij} + \beta_4 Sex_j + \beta_5 Env_{ij} \\
 & + U_{0j} + U_{1j} Env_{ij} + e_{ij}
 \end{aligned}$$

where variable nomenclature are consistent with the above formula except $\beta_2 AgeCat_j$ which refers to the category 'young' or 'aged'.

Between-group differences in cognitive performance across the neuropsychological test battery were investigated using one-way ANCOVA - rank

ordered where parametric assumptions were violated (Conover and Iman, 1982) - covarying for age, sex and years in education. Analyses were conducted across all participants and between MCI+ vs MCI-. Between group differences in CSF tau and $a\beta$ were z-scored (non-normal) and entered as predictors of all PI outcome measures using the GLM. Bonferroni correction was used to control for planned multiple comparisons. Residuals were visually inspected for violating linear assumptions, leverage and outliers.

2.3. Results

2.3.1. Demographics and neuropsychological testing

No significant difference in the distribution of sex was observed across younger and old adults ($X^2(1,72)= 0.51, p>0.05$) and no differences in age, gender, or years in education were observed between all MCI and HCs, or between MCI+ and MCI- (Table 2.1). Following Bonferroni correction with an adjusted α of 0.002, the MCI group as a whole exhibited significantly more errors in all neuropsychological tests compared to HCs ($p<0.002$), whereas no difference between MCI+ and MCI- survived multiple comparisons ($p>0.002$).

2.3.2. Immersive VR path integration task

522 of the 2223 trials were excluded (23.48%) due to the 'out of border' boundary being reached during the return path across aged and young healthy controls. A significant difference in collisions with the 'out of border' boundary was apparent between younger and older adults ($X^2(1, 2223)= 106.40, p<0.001$), older adults reached the boundary 18.65% more than younger adults. The remaining 1701 trials were used for analysing performance differences between young and aged adults.

Across all MCI, MCI-, MCI+ and HCs, 775 of the 2295 trials were excluded (33.77%) due to the 'out of border' boundary being reached during the return path, leaving 1520 viable trial remaining for analysis, no between group difference in 'out of border' warnings were observed ($p>0.05$). All participants successfully completed the PI task with no reported nausea or tolerability issues.

Critically, no differences in out of bounds collisions were observed between return conditions within each volunteer group, indicating that any effect of return condition on performance is not attributable to out of bounds exclusions.

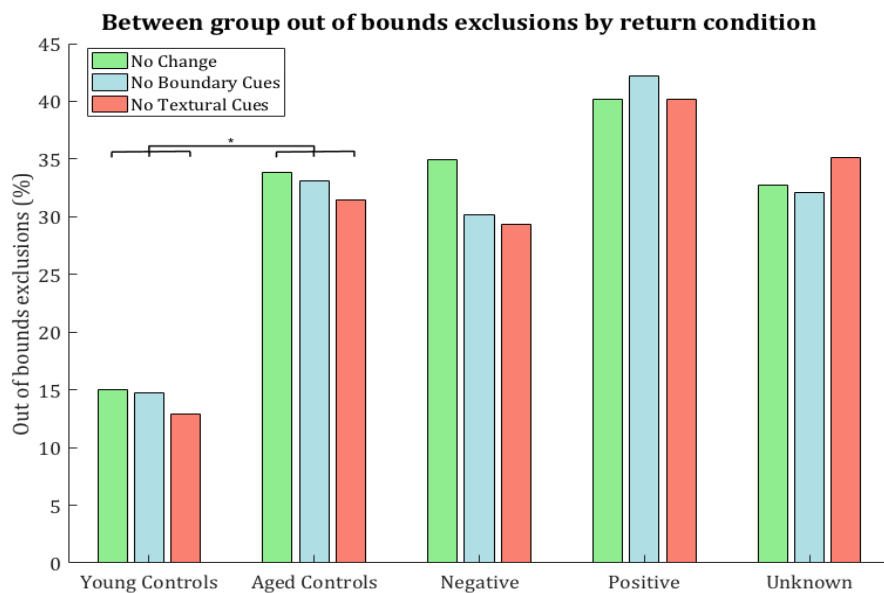


Figure 2.3. Proportion of data excluded due to reaching the 'out of bounds' subdivided by participant group and return condition. Each bar represents the percentage of exclusion for that given return condition only. No within group difference in exclusions were observed across return conditions. *= $p<0.05$.

		Healthy Controls (n=41)	Mild Cognitive Impairment (MCI, n=45)		
			MCI (n=45)	Biomarker Negative (n=14)	Biomarker Positive (n=12)
Age		69.3 ± 7.5	71.7 ± 8.3 ^{n.s}	71.1 ± 9.0	75.4 ± 7.0 ^{n.s}
Males (%)		15 (36%)	12 (63%) ^{n.s}	10 (71%)	9 (75%) ^{n.s}
Years in Education		14.8 ± 3.61	14.2 ± 3.37 ^{n.s}	14.5 ± 4.4	14.5 ± 3.8 ^{n.s}
ACE-R		97.2 ± 3.2	89.3 ± 5.4*	86.6 ± 7.6	80.1 ± 12.1 ^{n.s}
MMSE		29.7 ± 0.6	27.90 ± 1.7*	27.6 ± 2.6	25.0 ± 1.7 ^{n.s}
NART Errors		6.28 ± 3.40	17 ± 10.95*	13.1 ± 8.9	9.1 ± 6.8 ^{n.s}
Rey Figure Recall	Copy	36 ± 0	34.2 ± 2.7*	34.4 ± 1.7	33.1 ± 4.4 ^{n.s}
	Immediate	22.2 ± 7.6	17.5 ± 9.8*	13.8 ± 8.3	9.6 ± 9.1 ^{n.s}
	Delayed	21.3 ± 7.9	15.8 ± 11.0*	12.8 ± 9.8	8.3 ± 9.6 ^{n.s}
FCSRT immediate	Free	34.3 ± 5.1	24.9 ± 11.5*	22.1 ± 9.2	15.4 ± 11.4*
	Total	47.6 ± 0.6	44.7 ± 5.7*	43.1 ± 8.3	36.1 ± 11.5 ^{n.s}
FCSRT delayed	Free	13.4 ± 1.5	9.3 ± 5.3*	7.9 ± 5.1	4.8 ± 4.8 ^{n.s}
	Total	16 ± 0	14.8 ± 2.3*	13.9 ± 4.1	12.3 ± 4.0 ^{n.s}
Trails B seconds		77.2 ± 26.5	145.6 ± 72.8*	130.1 ± 42.2	152.6 ± 88.6 ^{n.s}
Digit Symbol		64.2 ± 14.5	49.9 ± 14.1*	47.0 ± 7.5	43.7 ± 13.7 ^{n.s}
Four Mountains		10.8 ± 1.8	9.3 ± 3.0*	7.3 ± 3.4	6.8 ± 2.2 ^{n.s}

Table 2.1 Between group differences in neuropsychological test performance were assessed between HCs vs MCI as a whole, and MCI+ vs MCI-, scores indicate number of correct responses unless otherwise indicated. * = $p < 0.05$, n.s = $p > 0.05$). Abbreviations: 4MT – Four Mountains Test, ACE-R - Addenbrookes Cognitive Examination-Revised; MMSE - Mini-Mental State Examination; NART = National Adult Reading Test; FCSRT = Free & Cued Selective Reminding Test; Trails B = Trail Making Test B; Digit Symbol = Digit Symbol Substitution test.

2.3.3. Absolute distance error

Aged controls, compared to the young group, exhibited larger absolute distance errors ($t(1,121)=2.57$, $p=0.01$, Figure 2.4A), with an estimated increase of $0.24\pm 0.09\text{cm}$ compared to younger adults. No effect of sex or return condition was observed on absolute distance error. Figures 2.4b and 2.4c are discussed in section 2.3.4. and 2.3.5., respectively.

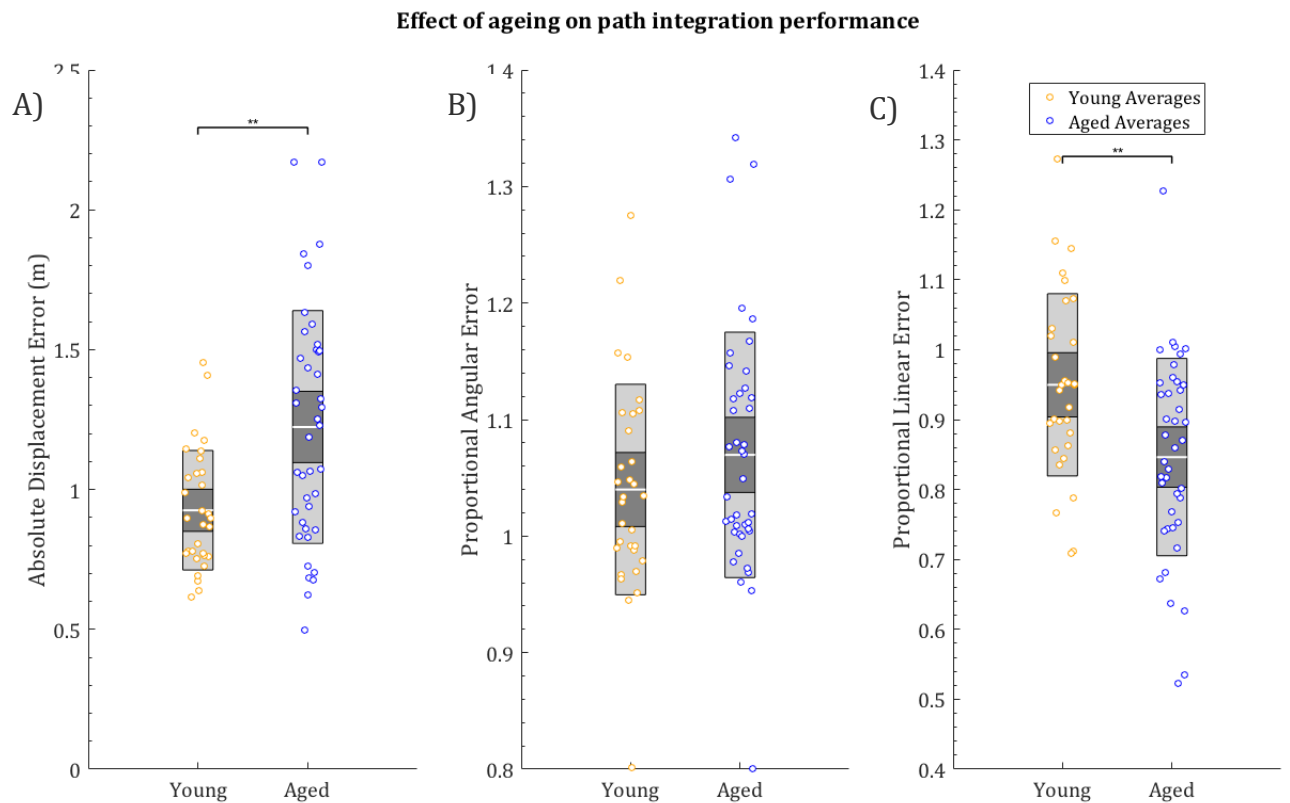


Figure 2.4. Effects of ageing on path integration performance (A-C). Group comparison of young and aged control participants across absolute distance errors (A), proportional angular errors (B) and proportional linear errors (C). Each marker represents the mean performance across trials of each individual: blue circles = aged controls, orange circle = young controls. ** = $p<0.01$.

The MCI group as a whole exhibited significantly larger absolute distance errors than the HC group ($t(1,107) = 3.24$, $p<0.01$, Figure 2.5A), with an estimated $57.33\pm 17.87\text{cm}$ increase in absolute distance error compared to HCs. MCI+ patients exhibited significantly larger absolute distance errors compared MCI- patients ($t(1,163)= 4.69$, $p<0.001$, Figure 2.5B), with an estimated increase of $97.56\pm 20.34\text{cm}$ compared to MCI-. ACE-R score correlated with absolute distance

errors across HCs and total MCI patients ($t(1,85)= 2.89, p<0.01$) and across MCI+ and MCI- groups ($t(1,26)= 4.01, p<0.01$), with lower ACE-R scores being associated with greater distance errors.

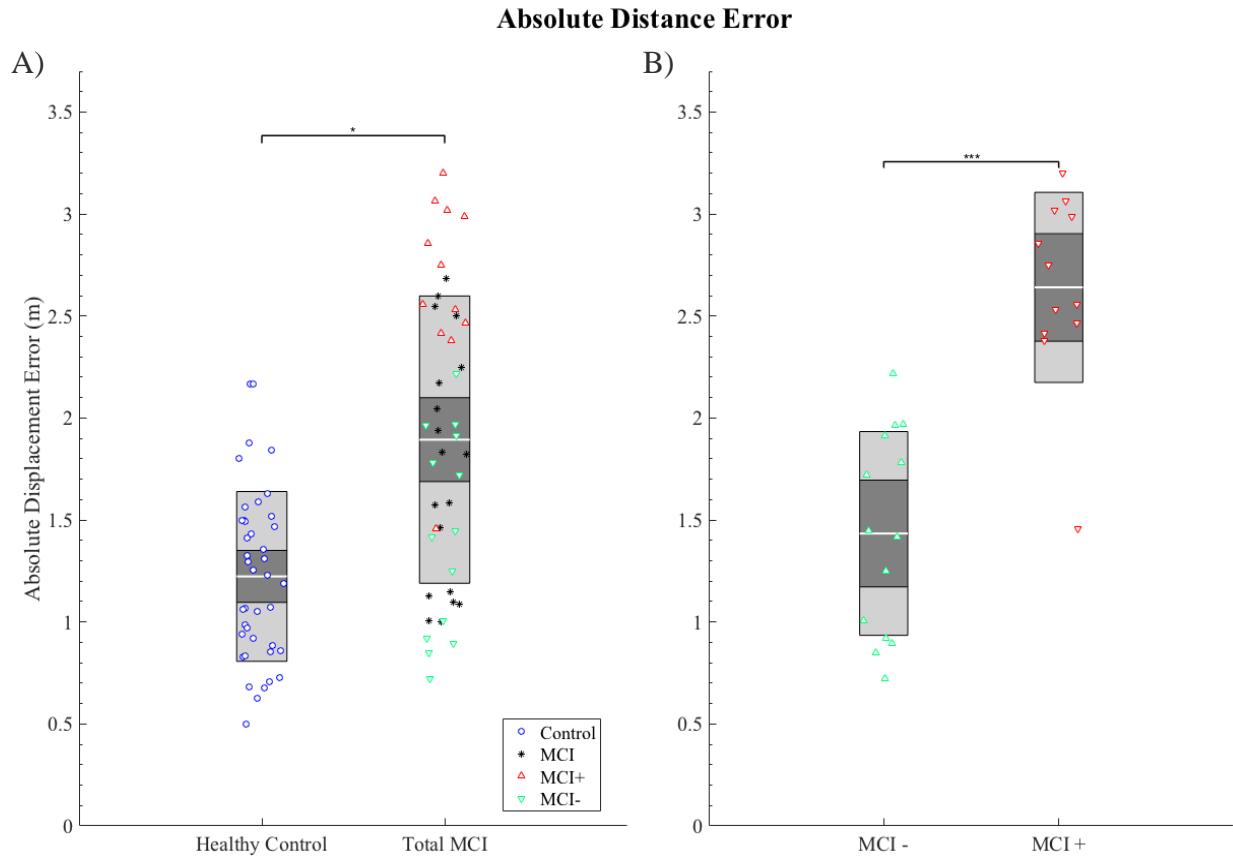


Figure 2.5. Graph summarising the between group differences in path integration performance. Absolute distance error (Euclidean distance) error in metres **(A-B)**. **A)** Group comparison between healthy controls and total MCI and **B)** between MCI- and MCI+. Each marker represents the mean performance across trials of each individual: blue circles = HCs; black asterisks = MCI without biomarkers; red triangles = MCI+; green inverted triangles = MCI-; Central gray line = mean; dark grey inner box= 95% confidence intervals; light grey outer box= 1 standard deviation. * $p<0.05$, *** $p<0.001$.

The contribution of CSF amyloid and tau to absolute distance errors was assessed in a separate model, controlling for age, sex and years in education. CSF total tau predicted absolute distance errors ($t(1,19)= 2.18, p<0,001$) whereas CSF $a\beta$ was

negatively associated with absolute distance errors ($t(1,19) = -4.39$, $p < 0.001$, figure 2.6).

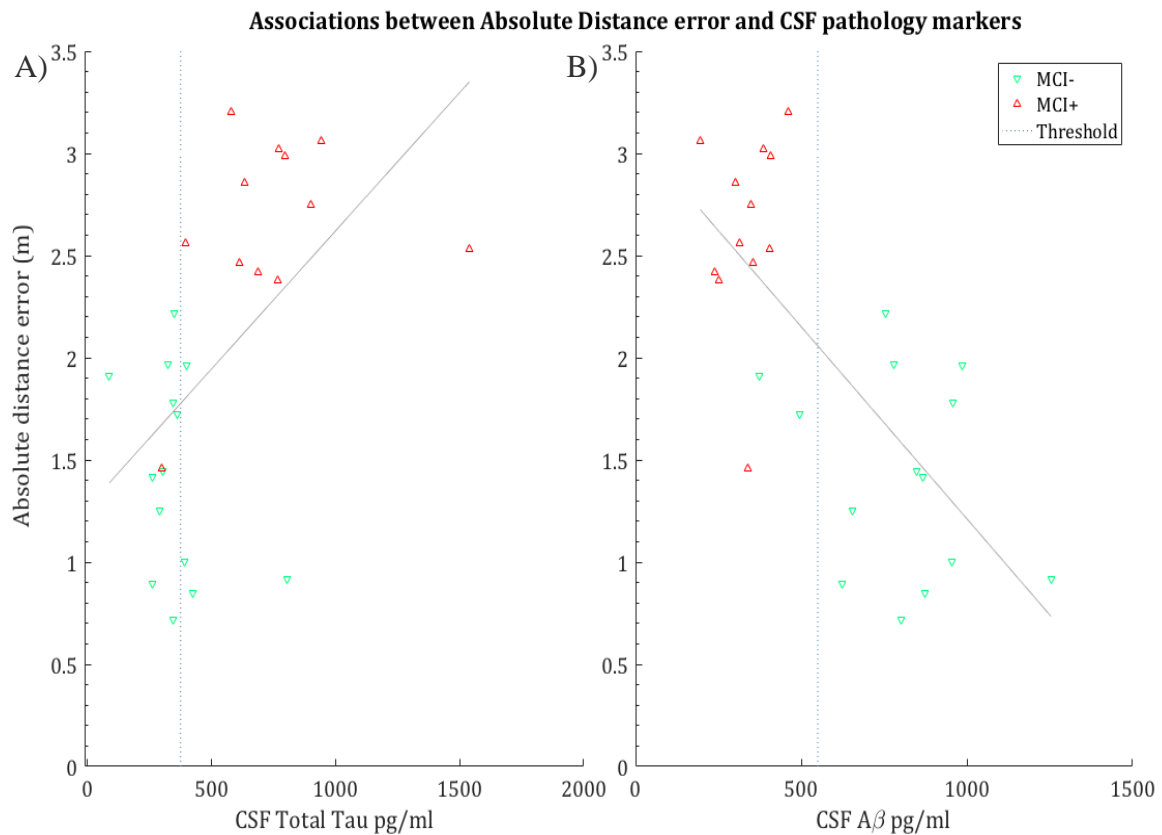


Figure 2.6. Association between absolute distance error and CSF measures of A) tau and B) $a\beta$ across MCI+ (red triangle) and MCI- (green triangle) subgroups. Grey dotted line indicates thresholds for AD positivity or negativity (see Mulder *et al*, 2010).

2.3.4. Proportional Angular Error

No significant difference in proportional angular errors were observed between young and aged controls ($t(1,158) = 0.27$, $p > 0.05$, Figure 2.4B), nor between total MCI and HCs ($t(1,128) = 1.79$, $p > 0.05$, Figure 2.7A) or between MCI+ and MCI- ($t(1,136) = 1.06$, $p > 0.05$, Figure 2.7B). Although between total MCI and HCs, the fixed effect of MCI exhibited a non-significant trend toward a positive association with proportional angular error ($p = 0.07$). Across MCI+ and MCI- an association was observed between proportional angular errors and CSF tau ($t(1,19) = 2.29$, $p < 0.05$) but not $a\beta$ did not ($t(1,19) = -1.08$, $p > 0.05$).

2.3.5. Proportional Linear Error

A significant difference in proportional angular errors were observed between young and aged controls ($t(1,102)= 2.69$, $p<0.01$, Figure 2.4C) where older controls exhibited an estimated decrease in proportional linear error of $0.09\pm 0.03\text{cm}$. A significant difference between MCI and HCs ($t(1,95)= 2.27$, $p<0.05$, Figure 2.7C), as well as between MCI+ and MCI- ($t(1,87)=3.09$, $p<0.01$, Figure 2.7D) was also observed for proportional linear error. Interestingly, an association between proportional linear error and CSF $a\beta$ ($t(1,19)=3.11$, $p<0.05$) was observed but not CSF tau ($t(1,19)= -1.46$, $p>0.05$). Compared to HCs, total MCI participants exhibited a decreased proportional linear error of 0.12 ± 0.01 , whereas MCI+ patients exhibited a decrease of 0.23 ± 0.07 compared to MCI-. These between group differences were replicated using a purer measure of error $(v_1 - v_2)^2$ that is less influenced by the area of the triangle and test space, such an approach should be considered in future research with larger spaces.

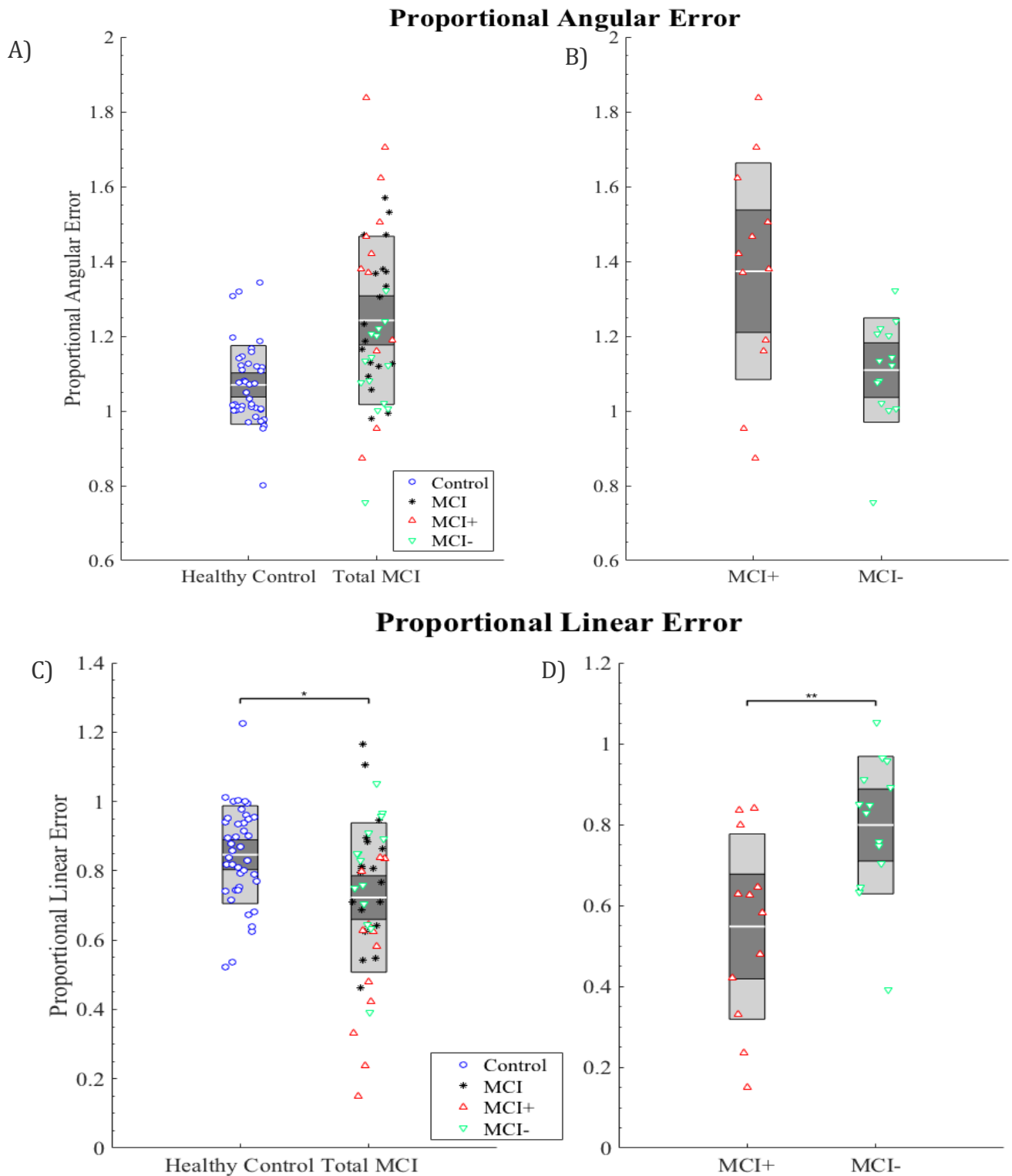


Figure 2.7. Graph summarising between group differences in proportional errors. Performance was evaluated between **A-C)** total MCI and healthy controls and **B-D)** healthy controls, MCI+ and MCI-. Each marker represents the mean performance across proportional angular errors (**A-B**) and proportional linear errors (**C-D**). Blue circles = HCs; black asterisks = MCI without biomarkers; red triangles = MCI+; green inverted triangles = MCI-; Central gray line = mean; dark grey inner box= 95% confidence intervals; light grey outer box= 1 standard deviation.

2.3.6. Effect of return condition

No main effect of return condition ($F(2,1597)= 1.43, p>0.05$) or interaction between return condition and age category ($F(2,1585)= 1.43, p>0.05$) was observed on absolute distance error across young and aged control participants. Similarly, no main effects of return condition were observed on absolute distance error between HC and total MCI groups ($F(2,1318)= 0.86, >0.05$, Figure 2.8A) or between MCI+ and MCI- groups ($F(2,384) = 0.56, p>0.05$). Interaction terms between return condition and participant grouping were also included in the analyses to examine the differential influence of return conditions on PI performance for MCI+ (compared to MCI-) and MCI as a whole (compared to HCs). No significant main effect of return condition on proportional angular error was observed between HCs and total MCIs ($F(2,1317)= 1.37 p>0.05$) as well as across MCI+ and MCI- ($F(2,395)= 0.13, p>0.05$, Figure 2.8B). However, a trend toward an interaction between biomarker status and return condition was observed on proportional angular errors ($F(2,398) = 2.93, p<0.05$), however this did not survive multiple comparison correction. No interaction between MCI status and return condition was observed across MCI and HCs on proportional angular errors ($F(2,1317) = 1.37, p>0.05$).

No significant main effect of return condition on proportional linear error was observed across HCs and all MCI patients ($F(2,1310) = 0.96, p>0.05$) or MCI+ and MCI- ($F(2,381) = 0.37, p>0.05$, Figure 2.8C). No significant interaction was observed between MCI status and return condition on proportional linear error ($F(2,1317) = 0.38, p>0.05$), nor between biomarker status (MCI+ and MCI-) and return condition ($F(2,382) = 0.35, p>0.05$).

A summary of all HC/MCI data is displayed in Figure 2.9, along with 40% of YC data. Absolute distance errors are summarized in 2.9A (distance from centre, angle is arbitrary and included for visual purposes only). Proportional linear errors and proportional angular errors are concurrently displayed in figure 2.9B.

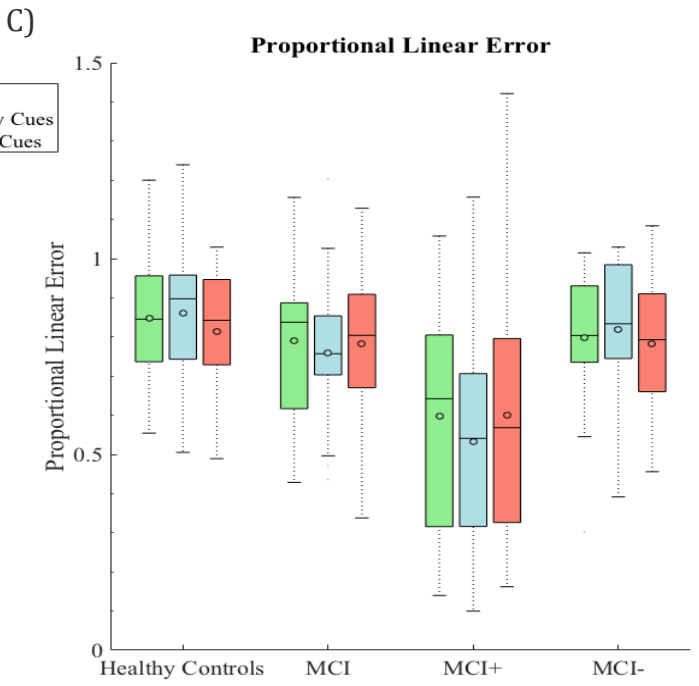
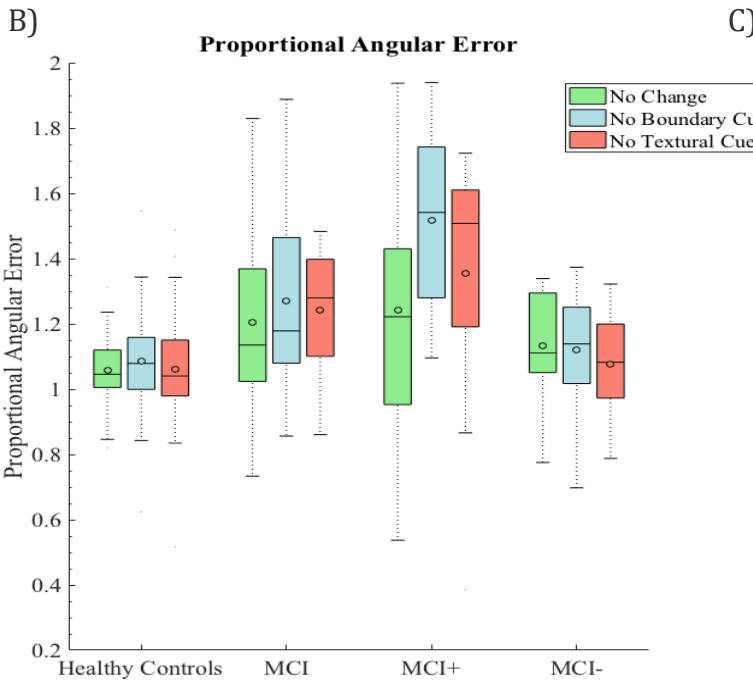
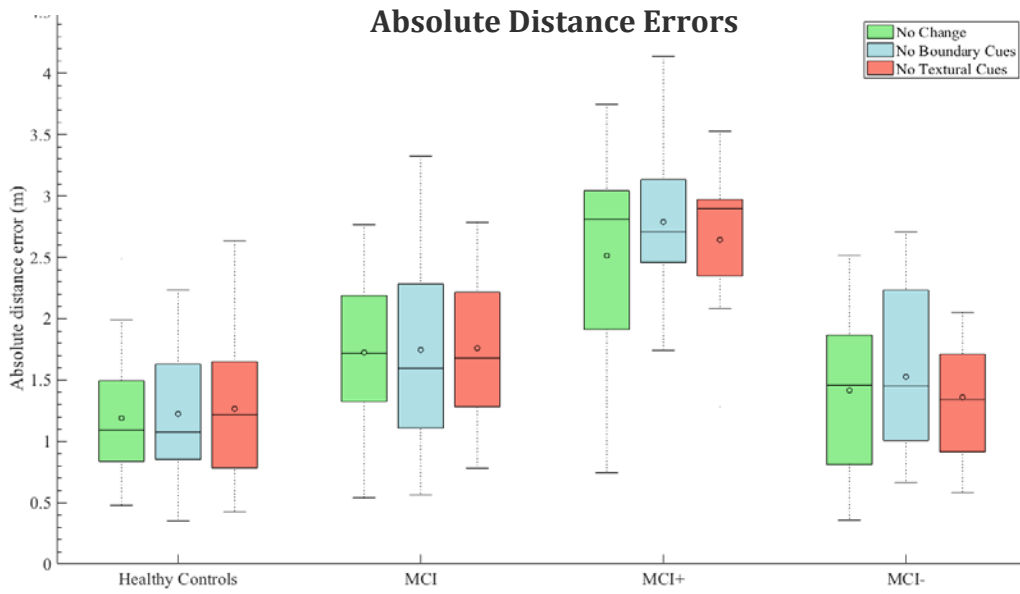


Figure 2.8. Within group effects on return condition for A) Absolute distance error, B) proportional angular error C) proportional linear errors.

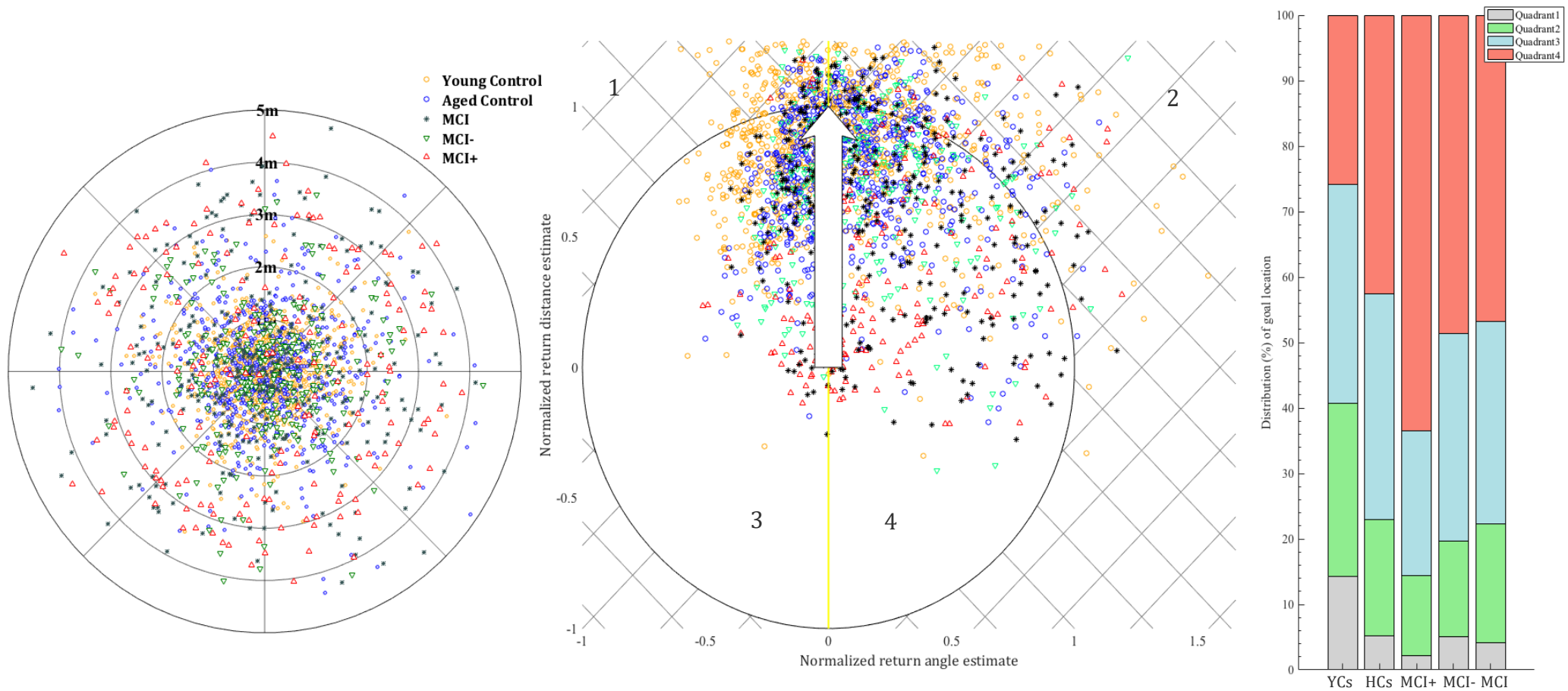


Figure 2.9. Distribution of goal location (cone 1) errors by group. **A)** Illustration of absolute distance error from goal (cone 1, centre), each concentric circle represent 1 metre of absolute distance error. **B)** Distribution of normalized estimated location of cone 1 translated and normalized to Cartesian space. Tip of the white arrow (0,1) represents the optimal linear return path to location of goal (cone 1). The border of the circle indicates optimal distance estimate, outside = overestimate (quadrants 1 and 2), inside = underestimate (quadrants 3 and 4). Yellow line indicates optimal rotation toward goal performed at cone 3, left of yellow line = under-rotation (quadrants 1 and 3), right = over-rotation (quadrants 2 and 4). **C)** Distribution of estimated location of cone 1 by quadrant, expressed as a percentage of the group's total responses. Each marker represents the outcome of a trial which did not reach 'out of bounds': yellow circles = young controls, blue circles = aged controls; black asterisks = MCI without biomarkers; red triangles = MCI+; green inverted triangles = MCI-.

2.3.7. ROC curves and classification accuracy.

Area under the curve (AUC), sensitivity and specificity were estimated using k-fold cross-validation (k=10), adjusted for age, sex and years in education. For the classification of total MCI patients from HCs, absolute distance error was associated with an AUC of 0.82 (Figure 2.10A, 95% confidence intervals (CI) = 0.71-0.89), with an error ≥ 157 cm yielding a sensitivity of 0.84 and specificity of 0.68. By comparison, the ACE-R was associated with an AUC= 0.86 (CI= 0.79-0.94), TMTB (AUC= 0.79 (CI= 0.68-0.87)), 4MT (AUC= 0.73, (CI= 0.6-0.83)), delayed RFR (AUC= 0.72 (CI= 0.60-0.83)) and the immediate (AUC= 0.82 (CI= 0.71-0.89)), delayed (AUC= 0.73 (CI= 0.61-0.85)) and total recall of the FCSRT (AUC= 0.69 (CI= 0.55-0.79)). Lastly, all of the above predictors were taken together as a combined classifier of MCI patients (AUC= 0.83, (CI= 0.73-0.9), this differentiated MCI patients from healthy control comparably to the PI task but was over specified with the ACE-R being a more accurate classifier of MCI.

Classification accuracy of MCI+ from MCI- using absolute distance error was very high, with an AUC of 0.90 (Figure 2.10B, CI= 0.59-1), and errors ≥ 196 cm yielding a sensitivity and specificity both of 0.92. This AUC was considerably higher than that of the comparator reference cognitive tests: ACE-R (AUC= 0.53 (CI= 0.24-0.73)), TMTB (AUC= 0.57 (CI= 0.22-0.69)), 4MT (AUC= 0.56, (CI= 0.22-0.72)), delayed RFR (AUC= 0.55 (CI= 0.22-0.68)) and the immediate (AUC= 0.56 (CI= 0.24-0.70)), delayed (AUC= 0.57 (CI= 0.22-0.68)) and total recall of the FCSRT (AUC= 0.60 (CI= 0.17-0.64)). The aforementioned neuropsychological tests were combined as a single classifier which differentiated MCI+ from MCI- with an AUC of 0.71 (CI= 0.6-0.85) indicating a marked improvement in classification accuracy of combined neuropsychological tests over any one individual test. Despite this improvement, the PI test demonstrated superior differentiation of MCI+ from MCI-.

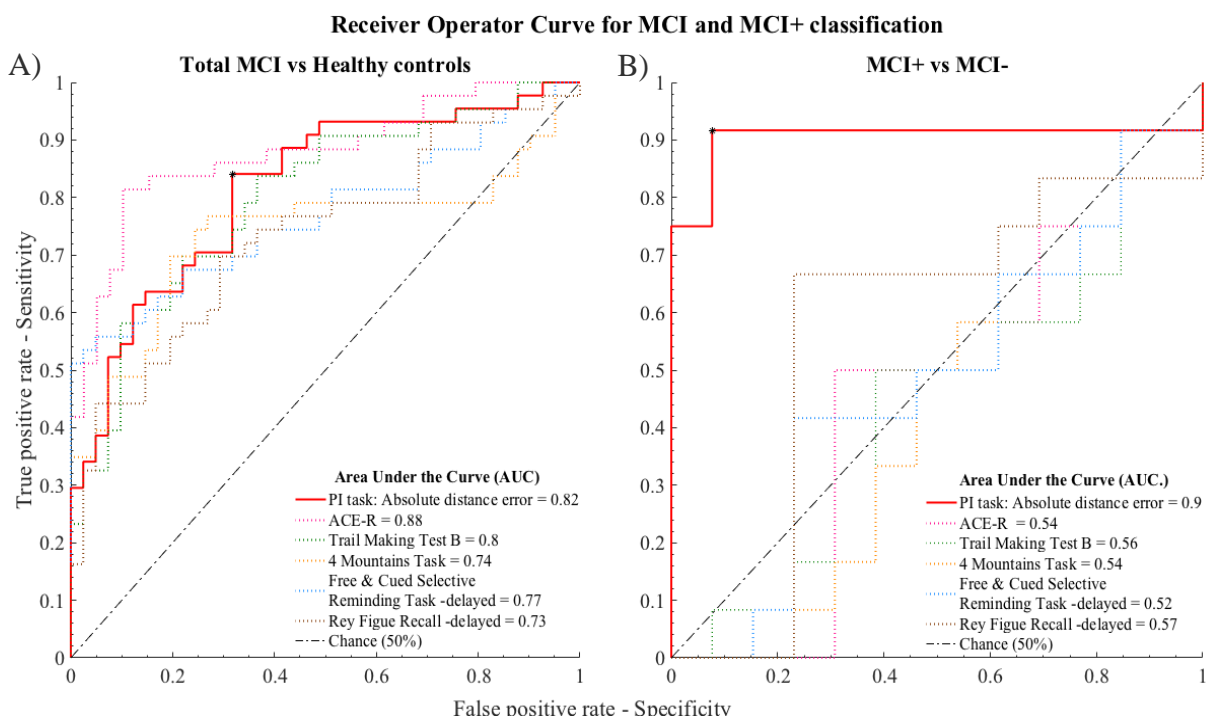


Figure 2.10. Receiver Operating Characteristic plot. Accuracy of path integration task performance for classifying **A)** total MCI from HCs and **B)** MCI+ from MCI- patients. PI performance is represented by absolute distance error (solid red line). Classification of reference cognitive tests is represented by dashed lines for comparison. Addenbrookes Cognitive Examination-Revised (grey), Trail Making Test B (green), 4 Mountains Test (yellow), Free and Cued Selective Reminding Test – delayed free recall (blue) and Rey Figure Recall – delayed recall (purple). Abbreviations: ACE-R - Addenbrookes Cognitive Examination-Revised. Asterisk indicates optimal operating point for absolute distance error.

2.4. Discussion

This study demonstrated that performance on a novel immersive virtual reality path integration paradigm, based on the central role of the entorhinal cortex (EC) in navigation, declines with age and was impaired in MCI patients compared to healthy controls. In keeping with the study hypothesis that an EC-based navigation task can differentiate MCI patients at increased risk of developing dementia, we found that AD biomarker-positive patients drove the difference in navigation accuracy between MCI patients and controls. Finally, and of high relevance for potential diagnostic usage, PI performance differentiated MCI biomarker-positive patients, i.e. those with prodromal AD, from biomarker-negative patients with markedly higher sensitivity and specificity than a battery of “gold standard” cognitive tests used in clinical and research practice.

In keeping with previous research, older adults demonstrated impaired path integration compared to younger adults (Allen *et al.*, 2004; Mahmood *et al.*, 2009; Adamo *et al.*, 2012; Harris and Wolbers, 2012), consistent with the decline of hippocampal and EC function with age (Lister and Barnes, 2009), although the neural correlates of younger controls could not be evaluated in the present study. Age-related reductions in grid-cell like activity in the EC of humans has been linked to PI deficits, particularly their magnitude and temporal stability (Stangl *et al.*, 2018a) mirroring the temporal instability observed in the place cells of older rats (Barnes *et al.*, 1997) as well as the reduced peak firing rate of grid cells in aged rodents (Fu *et al.*, 2017). However, these deficits may also be explained by age-related deficits in the vestibular system (Agrawal, 2017), that have shown to affect PI (Glasauer *et al.*, 2002; Xie *et al.*, 2017). More recently, Stangl *et al.* (2018b) computationally deconstructed the source of age-related PI errors, finding that PI errors may result from noise in the neural integrator, likely the EC, arising from imperfect velocity estimation that accumulates proportional to distance and not time. Such approaches may explain the present study’s findings that relative to younger controls, aged participants underestimate linear distance which contributes to larger absolute distance errors.

The navigational impairments observed in MCI patients are in line with previous navigation research (Hort *et al*, 2007; Laczó *et al*, 2014; Peter *et al*, 2018) and with the sparse literature on real-space PI in patients with MCI and AD dementia (Mokrisova *et al*, 2016). In the present study, significantly larger absolute distance errors were observed in MCI+ than in MCI-, with near-total separation of these two groups on this primary outcome measure, with the latter group exhibiting comparable performance to HCs. Additional analyses revealed that both CSF total tau and CSF amyloid- β were highly predictive of absolute distance error, independent of age, sex and years in education, supporting the notion that path integration deficits are related to Alzheimer's disease molecular pathology. These data suggest that navigational deficits are relatively specific to AD and unrelated to deficits in other cognitive domains, such as attention or episodic memory that might underlie the symptomatology of MCI- patients.

Secondary outcome measures suggested that MCI+ patients are specifically impaired in distance estimation, as evidenced by reduced proportional linear errors, in line with previous research (Hort *et al*, 2007), and may relate to disruption of grid cell activity (Fu *et al*, 2017; Tennant *et al*, 2018), given the role of grid cells in computing a distance metric of an environment (Bush *et al*, 2015) as part of path integration (McNaughton *et al*, 2006). However, decreased proportional linear errors (i.e. linear undershoot) were predicted by lower CSF $a\beta$ (indicative of prodromal AD) but not by tau deposition. This finding indicates that amyloid pathology may affect the path integration network, for example by colocalising with tau in the MTL or by effecting upstream perceptual or multisensory convergence sites. Lastly, we observed that increased CSF tau predicted larger proportional angular errors (i.e. over-rotation) that may relate to neurodegeneration in brain areas dense in HDCs or conjunctive grid x HDCs such as the EC, thalamus and subiculum. However, fluid biomarkers lack spatial specificity and such hypotheses should be explored in future research.

No group differences in performance errors were observed in response to the removal of boundary or surface detail cues. In the MCI+ group, a trend toward

increased proportional angular errors in response to the removal of boundary ($p=0.02$) and textural ($p=0.08$) cues was observed, but this did not survive multiple comparison correction. Given that this effect did not reach corrected statistical significance, any inferences need to be made with caution. Nonetheless it is worth noting that this trend is consistent with previous research that reported heightened increased reliance on landmark cues (Kalová *et al*, 2005) and heightened rotational deficits in response to the disruption of optic flow (Kavcic *et al*, 2006; Mapstone *et al*, 2008). Importantly compared to the no change return condition, the manipulation of environmental cues during triangle completion had no effect on any of the outcome measures or the frequency of out-of-bounds collisions. This absence of effect indicates that's neither distal boundary cues nor textural cues were used as local landmarks that could be used for self-localisation or return vector calculation. Whilst this finding provides evidence that the PIT is a *true* PI task that cannot be informed by rich environmental cues, future research should seek to exclude out of bounds collisions by increasing the size of the test area (discussed further below) as between group and between condition differences may have been masked by the small test area. Another explanation is that some distal landmarks were present in all conditions (e.g. sun/moon) which could potentially be used for broad orientation, however these could not be used reliably to precisely inform distance or angle to goal. When participants recounted their strategy for triangle completion none reported using these cues, nevertheless future research should exclude permanent landmarks during return conditions.

PI performance differentiated the total MCI patient group from HCs with moderate classification accuracy (AUC 0.82), reflecting the large variance in performance within the former group. The classification accuracy of MCI patients from the PI task was comparable to both the ACE-R (AUC 0.86) and the combined battery of neuropsychological tests (AUC 0.83). By comparison, PI performance was highly sensitive and specific for prodromal AD, classifying this group with an accuracy (AUC 0.90) that was markedly higher than that of reference cognitive tests. Greater classification accuracy was observed over the combined battery of tests

(AUC 0.71) encompassing episodic memory, attention and processing speed widely used to diagnose prodromal AD and as outcome measures in clinical trials. The present study found the optimal thresholds for delineating MCI from HCs and MCI+ from MCI- was an absolute distance error of 157cm and 197cm, respectively. However, unlike other neuropsychological metrics it is difficult to produce a reference 'chance' level for the PIT which may constrain the differentiation of incipient AD in future research.

This work therefore contributes to the growing body of evidence that spatial behavioural tests may have added value, above and beyond traditional cognitive tests, in detecting pre-dementia AD (Moodley et al. 2015, Allison *et al* (2016), Ritchie *et al*, 2018, Coughlan. *et al*, 2018). The use in this study of an EC-based navigation task potentially allows detection of AD in its very earliest stages, prior to hippocampal involvement, and builds on previous work showing reduced grid cell-like activation in the EC during an fMRI navigation task in young adults at risk of AD due to *APOE-e4* genotype (Kunz *et al*, 2015).

This study has limitations. The sample size of both MCI+ and MCI- groups was relatively small, and these results therefore need to be considered initial findings that require replication in larger scale studies. Whilst MCI+ patients are at high risk of converting to AD dementia, the aetiologies and prognosis of the MCI- cohort is less certain and more heterogeneous encompassing a range of neurodegenerative and psychiatric conditions. The repetitive nature of the task serves both as an advantage and disadvantage. It is advantageous as the instructions of the task do not change, just the shape of the triangle and the return conditions, as such the task has minimal cognitive load and our results are unlikely due to patients not remembering the task instructions (these were reiterated if patients ever looked confused or requested a reminder). On the other hand task performance may be influenced by fatigue effects, although we attempted to reduce this by changing the test environments. Although it is not anticipated that practice effects would influence PIT performance as the position of flags are generated randomly, we cannot test this formally due to the variability in out of

bounds exclusions between participants. The study would have benefitted from more complete data, for example neuropsychological measures in younger controls as well as measures of gaming/VR experience, real-world navigation ability or activities of daily living all of which likely explain variance in participant performance. Another limitation concerns the test space available with the commercial iVR hardware. The use of a larger space, which will be possible with next generation iVR, would likely result in the i) exclusion of fewer trials, ii) evaluation of proportional linear errors that is not skewed toward an undershoot, and iii) the compounding of vector computation errors (angular and linear estimates) that would likely culminate in larger between group performance differences.

In conclusion, this study demonstrates that performance on an EC-based iVR path integration task is sensitive and specific for prodromal Alzheimer's disease, with greater classification accuracy than that of a battery of current "gold standard" cognitive tests. Given that this test is based on understanding of EC grid cell activity, these findings have implications not just for early diagnosis but also for translational AD research aimed at understanding mechanistic links between impaired cell activity and behaviour in AD. The task used in this study, combined with analogous navigation tasks in animal models of AD, would help address the need for outcome measures capable of comparing treatment effects across preclinical and clinical phases of future treatment trials aimed at delaying or preventing the onset of dementia.

Chapter 3 - Object-Location Task

3.1. Introduction

Object-location memory is an everyday cognitive function that is contingent upon the complex binding of object and contextual representations, a key component of episodic memory (Postma *et al.*, 2008). Episodic memories are partially comprised of information pertaining to objects and environments, the processing of which is localized to the parahippocampal gyrus via the ventral ‘what’ and dorsal ‘where’ visual streams that converge on the lateral and medial EC, respectively (Postma *et al.*, 2008; Knierim *et al.*, 2014; Gillis *et al.*, 2016). The EC appears to partially bind object and environment representations (Hunsaker and Kesner, 2013; Tsao *et al.*, 2013; Wilson *et al.*, 2013b; Yoo and Lee, 2017; Hoydal *et al.*, 2018), that are subsequently projected to the hippocampus where they are cohesively bound with salient temporal, identity and emotional information (Ranganath, 2010; Yonelinas *et al.*, 2019). Therefore the detection of deficits in object and object-environment association processing may aid in the detection of Alzheimer’s disease (AD)-induced EC deficits prior to hippocampal-dependent episodic memory decline.

The perirhinal cortex (PC) is a phylogenetically conserved structure whose function in the encoding and recognition of object detail and location is implicated in the mediation of object processing by both human neuroimaging (Buffalo *et al.*, 2006; Awipi and Davachi, 2008; Staresina and Davachi, 2008, 2010; Staresina *et al.*, 2011; Clarke and Tyler, 2014, see Brown *et al.*, 2012 for review) and animal research (Winters and Bussey, 2005; Barker *et al.*, 2007; Albasser *et al.*, 2009; Savić and Jukić, 2014). Specifically, the PC supports feature encoding that culminates in a holistic conceptual representation of a given object (Winters and Bussey, 2005; Buckley and Gaffan, 2006; Bellgowan *et al.*, 2009b; Knierim *et al.*, 2014; Connor and Knierim, 2017) that is required for disentangling the ambiguity of perceptually or semantically complex objects (Bussey *et al.*, 2003, 2005; Tyler *et al.*, 2004; Barense *et al.*, 2010; Cowell *et al.*, 2010; Taylor *et al.*, 2011; Kivisaari

et al., 2012). The strong evidence for the PC's role in object processing is underpinned by neurons that exhibit little spatial modulation in the proximity of objects (Buckley and Gaffan, 2006). Recently, performance of healthy older adults in an object-recognition paradigm, targeting the function of the PC and IEC, was predictive of future cognitive decline (Fidalgo *et al.*, 2016).

The IEC is a central relay for PC afferents to the hippocampus and is critical for the 'object processing stream' model of spatial cognition (Knierim *et al.*, 2014) whose function heavily overlaps with the PC, given the high interconnectivity and proximity of these regions (Witter *et al.*, 1989; Burwell and Amaral, 1998; Lavenex *et al.*, 2004; Ribeiro *et al.*, 2007). In rodents, IEC lesions induce deficits in object recognition (Murray and Richmond, 2001; Vago and Kesner, 2008; Kuruvilla and Ainge, 2017a) thought to support the hippocampus' role in novelty detection via the lateral perforant path (Murray *et al.*, 2007). Van Cauter *et al.*, 2013 demonstrated that IEC lesions produce significant deficits in object processing but not in spatial tasks, mirroring the non-spatial impairments induced by selective inactivation of the lateral perforant path (Hunsaker *et al.*, 2007). Recently two complementary experiments have demonstrated that the human anterolateral EC (alEC) volume was associated with both object-configuration processing and object-location memory (Yeung *et al.*, 2017, 2018). These findings coincide with IEC activity observed during object discrimination fMRI tasks; where correct identification of object foils was associated with IEC activity (Reagh and Yassa, 2014; Reagh *et al.*, 2018). This also mirrors the alEC's role in processing object-information, distinct from the posteromedial EC's (pmEC) role in scene processing (Schultz *et al.*, 2012; Maass *et al.*, 2015; Berron *et al.*, 2018b) and path integration.

Unlike the PC, the IEC appears to additionally integrate spatial information (Buckley and Gaffan, 2006; Hunsaker and Kesner, 2013; Wilson *et al.*, 2013a, b; Yoo and Lee, 2017) as evidenced by object-selective cells whose activity is thought to reflect a memory trace of an object removed from a given environment (Deshmukh and Knierim, 2011; Tsao *et al.*, 2013). Homologous trace cells have recently also been reported in humans (Qasim *et al.*, 2018) Importantly, the

activity of these cells exhibit stronger response to 3D objects (Hargreaves *et al.*, 2005; Deshmukh and Knierim, 2011; Yoganarasimha *et al.*, 2011). Evidence suggests that the IEC encodes objects in an egocentric reference frame (Wang *et al.*, 2018) likely supported by spatial information from the mEC which contains object-vector cells thought to selectively encode direction and distance from a proximal object (Hoydal *et al.*, 2018). The inactivation of these cells induce deficits in identifying an object's translocation (Wilson *et al.*, 2013a; Tennant *et al.*, 2018) whereas entire EC lesions disrupt object-context associations (Charles *et al.*, 2004) and appears critical for object-context binding, the foundation of episodic memory and the hallmark cognitive deficit of AD. These findings coincide with the IEC's role in associative memory between objects and contexts (Hunsaker and Kesner, 2013; Wilson *et al.*, 2013b; Chao *et al.*, 2016; Kuruvilla and Ainge, 2017a). Critically, both components of the anterior pathway, namely the IEC and PC, exhibit dysfunction in preclinical AD in both humans and transgenic mice ahead of either mEC or hippocampal impairment (Khan *et al.*, 2014). Interestingly aIEC atrophy has been reported in individuals at risk of AD and were predictive of impaired performance on global tests of cognition in older adults (Olsen *et al.*, 2017). Indeed performance on an object-context association task has demonstrated high sensitivity and specificity for the differentiation of early AD from MCI and MCI from healthy controls (Wang *et al.*, 2013).

The hippocampus is posited to underpin the cognitive map and episodic memory via its role in the consolidation and long-term storage of object-detail (Reger *et al.*, 2009; Clarke *et al.*, 2010; Oliveira *et al.*, 2010), recognition of familiar objects in novel contexts (O'Brien *et al.*, 2006; Piterkin *et al.*, 2008) and processing object-location information (O'Keefe and Nadel, 1978; Wiebe and Stäubli, 1999; Mumby *et al.*, 2002; Crane and Milner, 2005; Buffalo *et al.*, 2006; Komorowski *et al.*, 2009; Manns and Eichenbaum, 2009; reviewed by Bird and Burgess (2008) and Strien *et al.* (2009)). Hippocampal recruitment has been shown to increase when object-representations are dependent upon an allocentric framework (Parslow *et al.*, 2004a, 2005; Hartley, 2007; Fidalgo and Martin, 2016) or in reference to a landmark or boundary (Doeller *et al.*, 2008). Furthermore, the encoding and

consolidation of object-location information is dependent on the hippocampus (Yamada *et al.*, 2017), although the degree of hippocampal recruitment is influenced by the duration between encoding and retrieval (Thorne, 2015), as well as the configuration, repetition and congruency of stimuli (Goh *et al.*, 2004; Spanswick and Sutherland, 2010). Transgenic AD mice exhibit greater deficits in object-location than object recognition (Creighton *et al.*, 2019, see Bengoetxea *et al.*, 2015 for review), correspondingly object-location deficits have been observed in MCI patients (Troyer *et al.*, 2008; Kessels *et al.*, 2010b; Külzow *et al.*, 2014; Hampstead *et al.*, 2018) and are highly pronounced in patients with AD dementia (Bucks and Willison, 1997; Brandt *et al.*, 2005; Vacante *et al.*, 2013; Wang *et al.*, 2013).

Knerim *et al.* (2014) posited that object-spatial binding occurs in the hippocampus (Lee *et al.*, 2005; Langston and Wood, 2010; Barker and Warburton, 2011a), however recent evidence suggests that object-location within binding occurs upstream of the hippocampus in the IEC. This notion is supported by the presence of object-trace cells in both the rodent IEC (Tsao *et al.*, 2013) and human EC (Qasim *et al.*, 2018). Furthermore, lesions to the IEC also impair object-location memory (Wilson *et al.*, 2013a; Kuruvilla and Ainge, 2017b). This notion is also complimented by recent human evidence indicating that aIEC, but not hippocampal, volumes predicted object-in-scene memory (Yeung *et al.*, 2019). Similar results were also observed in a continuous measure object-location paradigm that found that the EC, but not the hippocampus was predictive of object-replacement accuracy in MCI patients (Hampstead *et al.*, 2018). In these clinical cohorts, object-location performance was coupled to bilateral parahippocampal and entorhinal cortex volumetry (Hampstead *et al.*, 2018) and activity in the left hippocampus (Hampstead *et al.*, 2011). These functional correlates are vital to the early diagnosis of AD given that EC atrophy is associated to the spread of tau pathology and episodic memory decline (Maass *et al.*, 2018b). However, the aforementioned human studies have relied on non-immersive environments and/or 2d representations of objects, compromising both the direct translation from animal research and the ecological validity of the task. The

current study aims to address this by using a multicomponent iVR object-location task (OLT) comprised of three subtasks: i) object-replacement, as a function of the aIEC/hippocampus; ii) object recognition, as a function of both the aIEC and PC; and iii) object-context association, as a function of the aIEC.

The primary objective of this study was to test the hypotheses that compared to aged-matched controls (HCs), MCI patients are impaired on the iVR object location task designed around the function of the aIEC and medial PC (Brodmann's area 35 (BA35)) and hippocampus. It is predicted that these deficits will be more pronounced in those with CSF evidence of underlying AD (MCI+) than those without (MCI-).

Secondary hypothesis include:

1. Impairments in the OLT will differentiate MCI from HCs and MCI+ from MCI- with greater sensitivity and specificity than a battery of neuropsychological tests.
2. Greater impairment in all components of the OLT will be observed in HCs compared to younger controls (YCs).

3.2. Methodology

3.2.1. Participants

Analyses examined the effect of aging (YCs (n=53) vs HCs (n=24)), MCI (HCs vs MCI (n=23)) and prodromal AD (MCI+ (n=9) vs MCI- (n=7)). Details of the diagnostic, inclusion and exclusion criteria are detailed chapter 2.2.1, group abbreviations are consistent with chapter 2.

iVR Object-Location Task (OLT)

The object-location task is subdivided into 3 subtasks with distinct aims to evaluate: 1) object-replacement, 2) object recognition, and 3) object-context association memory.

3.2.2. Object-replacement subtask

The subtask consisted of 3 distinct environments, each with unique distal cues and 4 discrete objects per environment, totalling 12 object-replacement trials per participant.

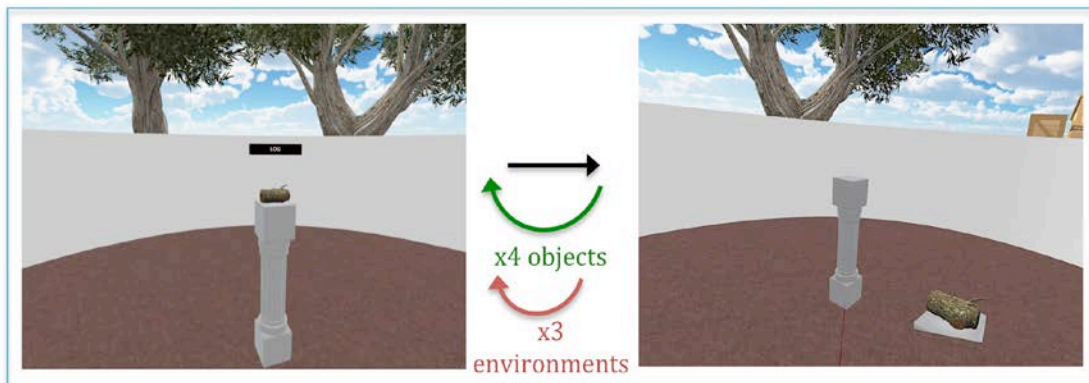
Upon entering an environment, participants had 30 seconds to habituate and explore the environment, and to describe environmental details aloud. For each environment, the subtask was divided into 2 phases: object-position encoding and object-replacement. Object-position encoding comprised:

1. An object appeared within the test space on a pedestal, and participants were instructed to study the details and location of the object.
2. Once satisfied with their study of (1), participants were told to walk into the object, at which point it would disappear and a displacement marker would appear.
3. Participants walked to the displacement marker and a new object would subsequently appear.

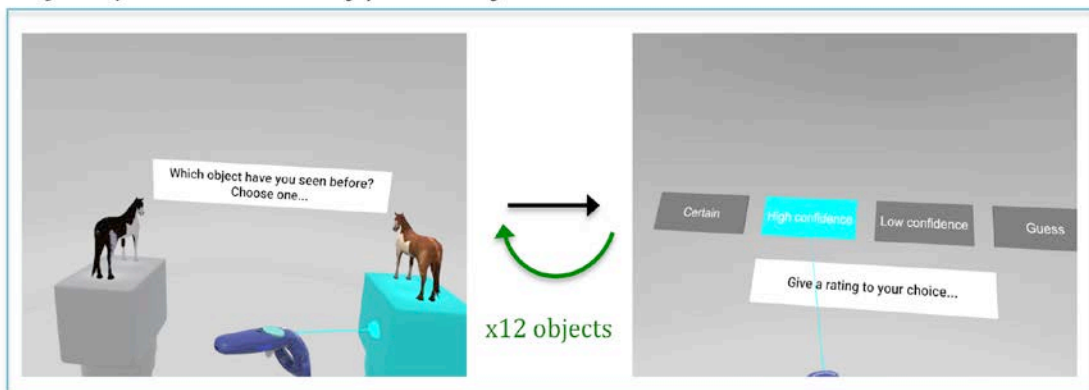
Points 1-3 were repeated for every object in all environments. Objects were presented sequentially on a 1m high pedestal (Figure 3.1A) and could be examined in three-dimensions by walking around the object. No time limit was set for object-position encoding. Displacement markers were designed to force reliance on an allocentric representation of space and distal landmarks by inhibiting positional encoding relative to another object's position (important for the implicit formation of object-context associations). The generation of a new object was pseudorandom from a pool of 25 objects, as such objects varied between participants. Object positioning was also pseudorandom within the environment, although could not be generated within 60cm of either another object or the participant. After all 4 objects had been encoded in a given environment, points 1-3 were repeated for the same object-positions but presented in a new order, giving participants two attempts at encoding all object and positions before replacement.

In total, 3 encoding-retrieval phases took place, one per environment. Encoding-retrieval phases occurred sequentially, each environment comprised two encoding trials and one retrieval trial.

1) Object-Replacement task



2) Object-familiarity/novelty task



3) Object-environment association task

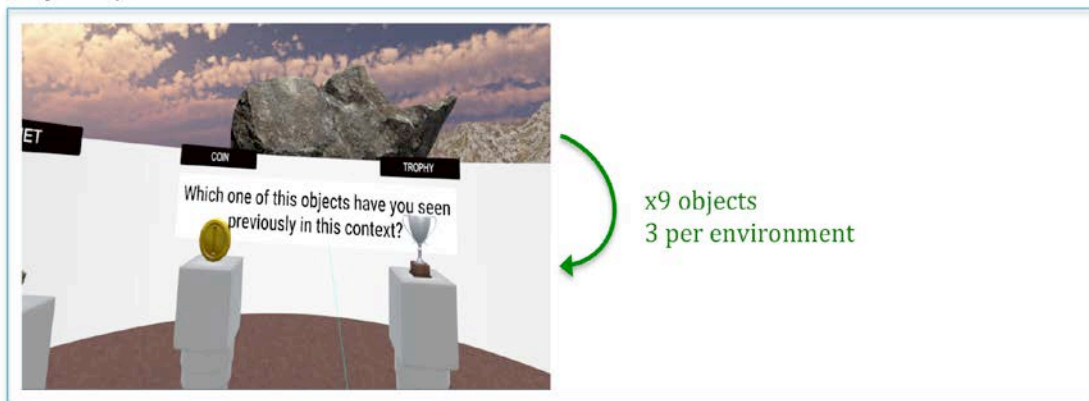


Figure 3.1. Illustration of Object-Location task. 1) Object-replacement task. *Left:* Encoding- 4 objects are presented one at a time in pseudo random order and locations. Participants have two attempts to encode all 4 objects and their locations. *Right:* Retrieval- participants attempt to return objects to their correct location. Encoding and Retrieval are repeated across distinct objects and environments, totalling 12 objects across 3 environments. **2) Object familiarity/novelty task.** Following completion of object-replacement task, participants are tasked with identifying a previously seen object (familiar) from a similar foil (novel, *left*), rating their confidence in their decision (*right*). **3) Finally,** participants attempt to identify which object was present in a given environment during the object-replacement task from a selection of 4 objects.

Immediately following a given environment's second encoding phase, a retrieval phase started in which participants were tasked with returning a given object to its location, in other words, where they found it. Participants were re-immersed in a given environment and asked to estimate a given object's location using a handheld controller; the controller projected a constant laser at the end of which was a transparent pedestal. Object location was indicated by pointing the controller to the estimated location and pulling the trigger. A reminder of the target object was present in the bottom right of the participant's visual field throughout retrieval. Participants were free to walk around the environment, had no time limit to perform any component of the subtask, and no feedback on performance was given. A circular boundary wall enclosed the test space at a height approximately 20cm below the participant's height. This served as a local cue for object-replacements.

Ahead of participant testing, the maximal encoding space was determined by the size of the testing room. However in order to maximise the opportunity for

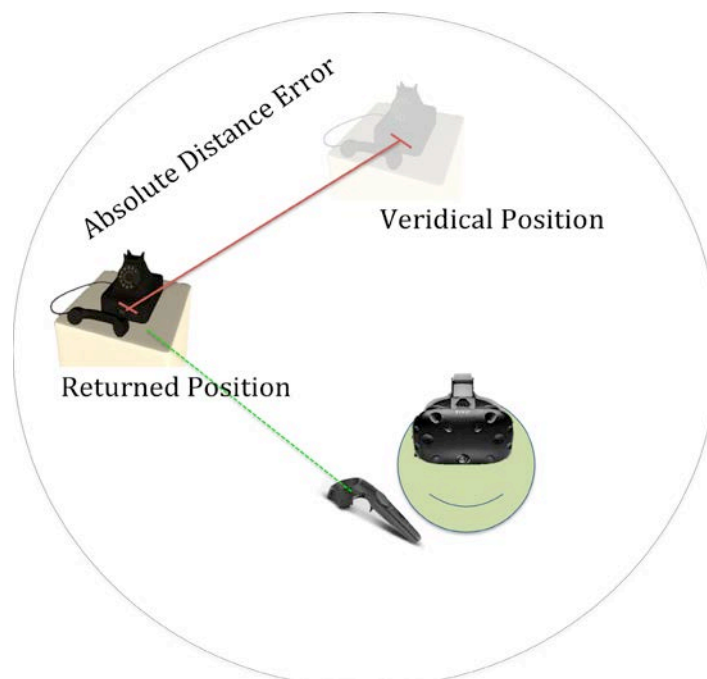


Figure 3.2. Illustration of Absolute distance error 1) Absolute distance error (primary outcome measure) is the distance between the returned object location and veridical object location (red line). The green line shows the laser used by the participant to indicate object location.

retrieval errors, the boundary wall was set at twice the radius of the encoding environment. All HCs and MCI participants were tested using a 3.5m² encoding space, whereas YCs were tested on a variable size arena ranging from 4x3.2m to 4x3.7m, correspondingly YC data was translated to be consistent with a 3.5m² as discussed in section 3.2.3.

Given the complexity and cognitive load of this multicomponent task participants had underwent 5 practice trials using distinct abstract objects/environments from test objects/environments. Participants were reminded of the goal of the task before each stage of the OLT.

The primary outcome measure was the absolute distance error between an object's estimated location and its actual location (Figure 3.2). However, additional outcome measures were defined and evaluated *a posteriori* following researcher observations during testing. Namely, MCI patients seemed more likely than HCs to exhibit specific types of error during object replacement, and these types of errors seemed most pronounced in MCI+ patients. Error types were therefore characterised as follows (summarised in Figure 3.3):

- i) Retrieval failures (i.e. guesses, Figure 3.3B – bottom right quadrant).
- ii) Swap errors (i.e. putting an object in a *different* objects veridical location):
 - A. Misattribution swap error – Object A is returned to the veridical location of object B, indicative of correct location recall but incorrect association between object and location.
 - B. Content swap error – Object A is returned to the veridical location of object B *and* object B is returned to the veridical location of object A.

Retrieval failures, misattribution and swap errors were categorised using a manual protocol that examined the graphical data of all object within each environment. An object was evaluated only if the closest object was not the target location and the following criteria controlled for general inaccuracies. Retrieval failures were defined as object-replacements that appear random deviating from the veridical location of all objects in both angle and proximity. For all scenarios the following were considered: i) the participant's position within the environment relative to both the veridical and estimated location of the object, ii) the distance between the veridical and estimated location of the target object and iii) linear or angular proximity to the veridical location of other objects. Whilst some 2D visual-working memory tasks have achieved success using algorithmic approaches (Pertzov *et al.*, 2012, 2013; Liang *et al.*, 2016), the degrees of freedom in the iVR task were too high and produced too many false positives upon

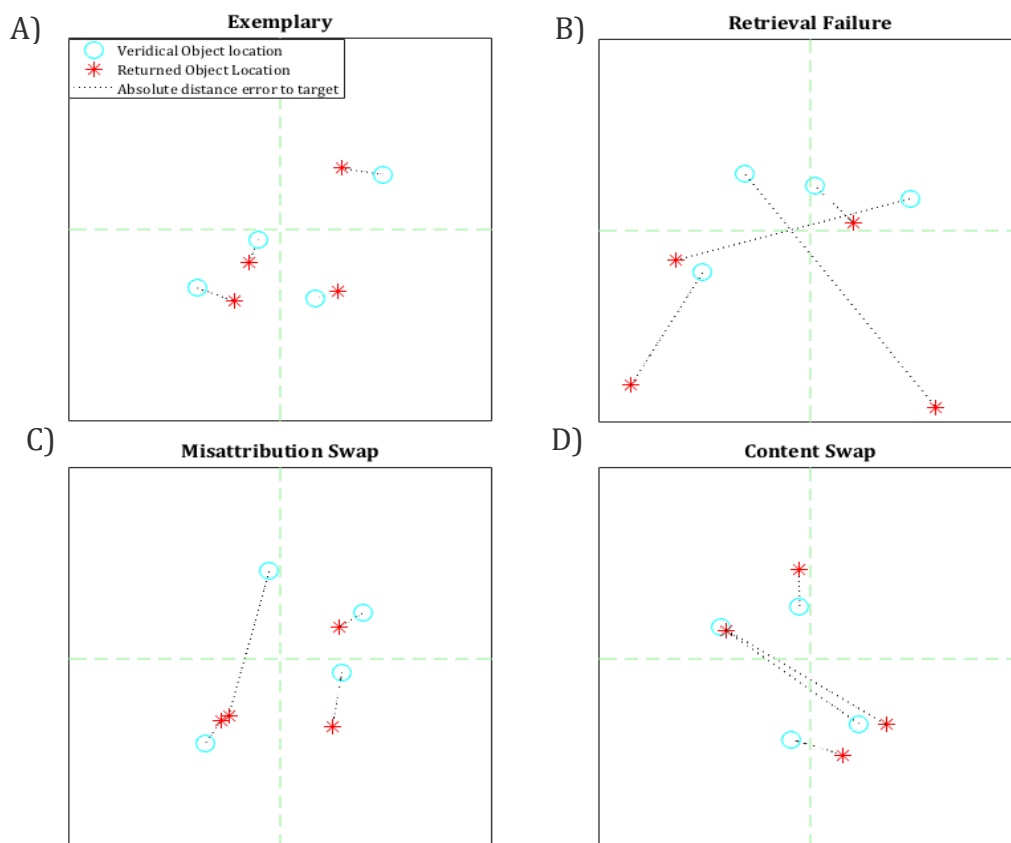


Figure 3.3. Participant data illustrating swap scenarios. A) Exemplary, B) Retrieval Failure, C) Misattribution Error, D) Content-location derived swap error. Cyan circles = true object location; * = estimated return location; dotted lines indicate the absolute distance error between an object and its veridical location.

inspection for such methods to be employed here. Coco Newton and I manually inspected all data and categorised errors according to the aforementioned criteria.

3.2.3. Object-recognition subtask

Following completion of the object-replacement subtask, a two-alternative forced choice object recognition subtask was used to examine participant discrimination accuracy for familiar (i.e. 'old') from novel (i.e. 'new') objects (Figure 3.1B). Novel objects were designed to be very similar to familiar objects with one distinguishing feature, for example a change in colour or property. The presentation order of objects was pseudo-random.

3.2.4. Object-environment association subtask

Following completion of 12 object-recognition trials, participants were re-immersed at random into one of the three environments. Participants were tasked to select the object that was seen in this environment from a choice of 4 (3 foils, Figure 3.1C). No time limit was set. Performance was assessed by the percentage of objects correctly identified. 9/12 object-environment associations were used with unique object combinations per trial. For each object-environment trial, foil objects prioritised objects that were not present in previous trials or had been previously selected (correctly or incorrectly). Given the small amount of objects used (12 total), combined with the 4-object force choice, repetition of foils was unavoidable. This novel approach to studying object-context associations offers two distinct advantages: i) object-context associations are encoded implicitly during object position encoding and ii) participants can re-explore all objects and environments before making a response, mitigating the context shift decrement (Hayes *et al.*, 2007).

3.2.5. Data processing and Statistics

Calculation of absolute distance errors are detailed in 2.2.5. Differences in test arena size between YCs (tested in a variable size test arena ranging from 3.2x4m

to 3.7x4m) and HCs (3.5m²) could mask any effect of aging on object-replacement performance, given that the size of the test arena dictates the distance between objects and larger environments beget larger errors. Therefore all Cartesian coordinates for the YC data were scaled to a 3.5m² room, to match the HC and MCI data.

Demographic data were assessed using two-sample t-tests, or Kruskal-Wallis test if parametric assumptions were violated. Object-replacement outcome measures were not normally distributed as confirmed by both visual inspection of graphs and the Shapiro-Wilks test. Categorical distributions were analysed using Fisher's exact test. Between group differences in CSF tau and a β were z-scored (non-normal) and entered as predictors of all PI outcome measures using the GLM.

Object-replacement data were analysed using a log-linked generalized LME (GLME). GLMEs permit the analysis of non-normal clustered data in the presence of random effects (Bolker *et al.*, 2008), and to compare different linking functions that relate the dependent variable to predictor variables. The log-link Gaussian model was the best fitting distribution. Such an approach also avoids transforming response variables, which can obscure and bias interpretation of the results (Lo and Andrews, 2015).

The final GLME model was refined using likelihood ratio testing for goodness of fit. Separate models were used for YCs vs HCs, for HCs vs pooled MCI and for MCI+ vs MCI-. The final LME used absolute distance error as the response variable, with MCI, environment, age, sex, years of education and ACE-R as predictor variables. Object number and environment number were specified as random coefficients with by-participant random intercepts (similar to the formula outlined in 2.2.6). The effect of ageing was assessed between YCs and HCs in a similar model using age category (young or aged) as the predictor variable but without ACE-R or years in education covariates.

Finally, a logistic GLME was used to assess object recognition and object-context association subtask performance. Correct responses were used as the outcome measure with the same aforementioned fixed effects with, participant specified as a random intercept. Object recognition was additionally assessed using multiple regression with measures of signal sensitivity (d') and response bias (C , McNicol, 2005) as response variables, rank ordered where parametric assumptions were violated.

Table 3.1. Demographics and neuropsychological test scores

		Healthy Controls (n=24)	Mild Cognitive Impairment (MCI, n=23)		
			<i>MCI (n=23)</i>	<i>Biomarker Negative (n=9)</i>	<i>Biomarker Positive (n=7)</i>
Age		68.9 ±5.8	72.2 ±7.3 ^{n.s}	68.3 ±6.2	74.1 ±7.2 ^{n.s}
Males (%)		8 (33%)	15 (65%) ^{n.s}	5 (71%)	7 (77%) ^{n.s}
Years in Education		15.5 ±3.9	14.8 ±3.6 ^{n.s}	13.4 ±3.5	15.1 ±4.2 ^{n.s}
ACE-R		97.8 ±2.5	85.3 ±10.8*	89.9 ±7.2	79.2 ±13.5 ^{n.s}
MMSE		29.9 ±0.3	26.7 ±4.5*	28.7 ±2.2	24 ±6.0 ^{n.s}
NART Errors		6.2 ±3	12.0 ±8.7*	16.86 ±10.9	9.4 ±7.0 ^{n.s}
Rey Figure Recall	Copy	36 ±0	33.6 ±3.7*	35 ±1.2	32.7 ±5.0 ^{n.s}
	Immediate	22.9 ±6.9	13.3 ±9.8 ^{n.s}	15.9 ±6.9	9.2 ± 10.7 ^{n.s}
	Delayed	22.2 ±7.1	12.9 ±10.8 ^{n.s}	15.4 ±8.6	8.4 ± 11.1 ^{n.s}
FCSRT immediate	Free	34.3 ±5.1	19.8 ±12.0*	24 ±8.9	13.6 ±11.8 ^{n.s}
	Total	47.8 ±0.5	40.7 ±10.4*	44.6 ±7.8	33.9 ±12.4 ^{n.s}
FCSRT delayed	Free	13.4 ±1.4	7.6 ±5.7*	9.4 ±5.0	4.9 ±5.6 ^{n.s}
	Total	16 ±0	13.74 ±3.6*	15 ±2.7	11.6 ±4.4 ^{n.s}
Trails B seconds		67.8 ±21.1	147.3 ±80*	123.0 ±40.4	167.6 ±97.6 ^{n.s}
Digit Symbol		67.8 ±13.1	45.4 ±12.0*	50.3 ±6.1	42 ±15.5 ^{n.s}
Four Mountains		11.0 ±1.9	8.3 ±3.1*	8.4 ±3.7	7.3 ±2.4 ^{n.s}

Table 3.1. Between group differences in demographics and neuropsychological test performance were assessed between HCs vs MCI as a whole, and MCI+ vs MCI-, scores indicate number of correct responses unless otherwise indicated. * = p<0.05, n.s = p>0.05). Abbreviations: 4MT – Four Mountains Test, ACE-R - Addenbrookes Cognitive Examination-Revised; MMSE - Mini-Mental State Examination; NART = National Adult Reading Test; FCSRT = Free & Cued Selective Reminding Test; Trails B = Trail Making Test B; Digit Symbol = Digit Symbol Substitution test.

3.3. Results

3.3.1. Demographics and neuropsychological testing

No significant differences in age, sex or years in education were observed between either HCs and MCI or MCI+ and MCI- ($p > 0.05$). Following Bonferroni correction with an adjusted α of 0.002, significant differences were observed between HCs and MCI across the neuropsychological test battery, summarised in table 1. No significant differences were observed between MCI+ and MCI- across the neuropsychological test battery ($p > 0.05$).

3.3.2. Object-replacement subtask

Across YCs and HCs, environment ($t(1,907) = -2.82$, $p < 0.01$) was a significant predictor of absolute distance error that survived the Bonferroni correction ($\alpha = 0.01$). No difference between YC and HC groups (i.e. effect of ageing) was observed ($t(1,918) = -1.45$, $p < 0.05$). A significant difference in absolute distance errors were observed between HCs and MCI (Figure 3.4B, $t(1,543) = 4.23$, $p < 0.001$), where MCI was associated with an estimated increase of 50 ± 12 cm compared to HCs. An effect of sex ($t(1,543) = -2.42$, $p < 0.05$) was observed but did not survive the Bonferroni-adjusted alpha of 0.007. No difference in absolute distance error was observed between MCI+ and MCI- (Figure 3.4C, $t(1,183) = 1.30$, $p > 0.05$) and was not predicted by either CSF tau ($t(1,10) = 0.53$, $p > 0.05$) or $a\beta$ ($t(1,10) = 1.47$, $p > 0.05$).

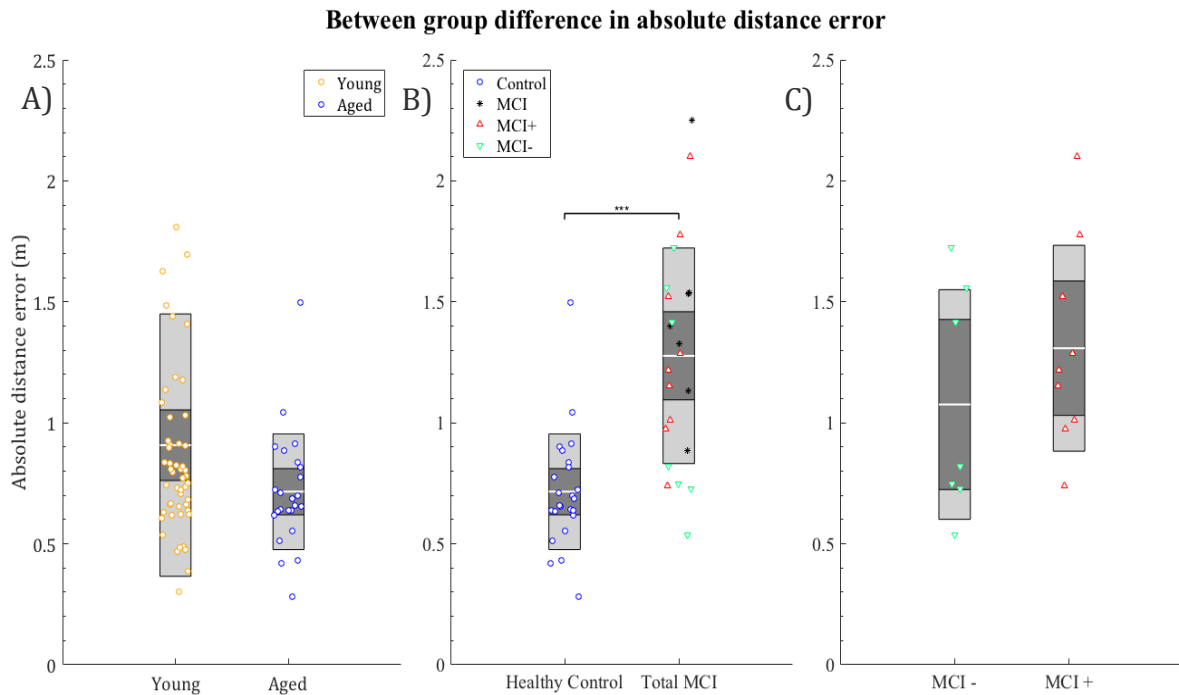


Figure 3.4. Between group differences in performance across A) young and aged controls, B) aged-matched controls and MCI and C) MCI+ and MCI-. Yellow circles = YCs, Blue circles = HCs; black asterisks = MCI without biomarkers; red triangles = MCI+; green inverted triangles = MCI-; Central gray line = mean; dark grey inner box= 95% confidence intervals; light grey outer box= 1 standard deviation.

3.3.3. Object-recognition subtask

The ability to distinguish novel from familiar objects was evaluated using three measures (table 2, Figure 3.5): 1) frequency of correct responses, 2) sensitivity, as measured with d' and 3) response bias, as measured with C (McNicol (2005), note that the latter two measures are obtained by averaging over trials). No difference in the frequency of correct responses were observed between YCs and HCs (Figure 3.5A, $t(1,920)= 0.85, p>0.05$), HCs and MCI ($t(1,557)= 0.26, p>0.05$) or MCI+ and MCI- ($t(1,187)= 0.14, p>0.05$). No association was observed between object-recognition performance and either CSF $a\beta$ ($t(1,10)=1.22, p>0.05$), or tau deposition ($t(1,10)=0.96, p>0.05$). No group differences in d -prime were observed (Figure 3.5B) between YCs and HCs ($t(1,74)=-0.40, p>0.05$), HCs and MCI ($t(1,41)= 0.31, p>0.05$) or MCI+ and MCI- ($t(1,11)=-1.96, p>0.05$). No differences were found in response bias between YCs and HCS ($t(1,74)=-1.03, p>0.05$) or MCI+ and MCI- ($t(1,11)= -0.71, p>0.05$), though MCI patients exhibited a more conservative

response bias than HCs (Figure 3.5C, $t(1,42)= 2.38, p<0.05$).

Summary of between group differences in object recognition

Group	Trials (n)	Hits	False Alarms	Correct Rejections	Misses	Sensitivity (<i>d</i> -prime)	Response Bias (<i>C</i>)
YCs	536	214 (39.9)	122 (22.7)	280 (52.2)	20 (3.7)	1.48	-0.39
HCs	288	133 (46.2)	57 (19.7)	91 (31.6)	7(2.4)	1.50	-0.50
MCI	182	103 (56.6)	43 (23.6)	103 (56.6)	12 (6.6)	1.61	-0.29
MCI+	108	48 (44.4)	19 (17.6)	39 (36.11)	2 (1.9)	1.71	-0.40
MCI-	84	37 (44.0)	12 (14.3)	28 (33.3)	7 (8.3)	1.35	-0.20

Table 3.2. Raw numbers used for signal detection in object recognition task. Brackets indicate percentage of total trials, sensitivity and response bias are mean of group.

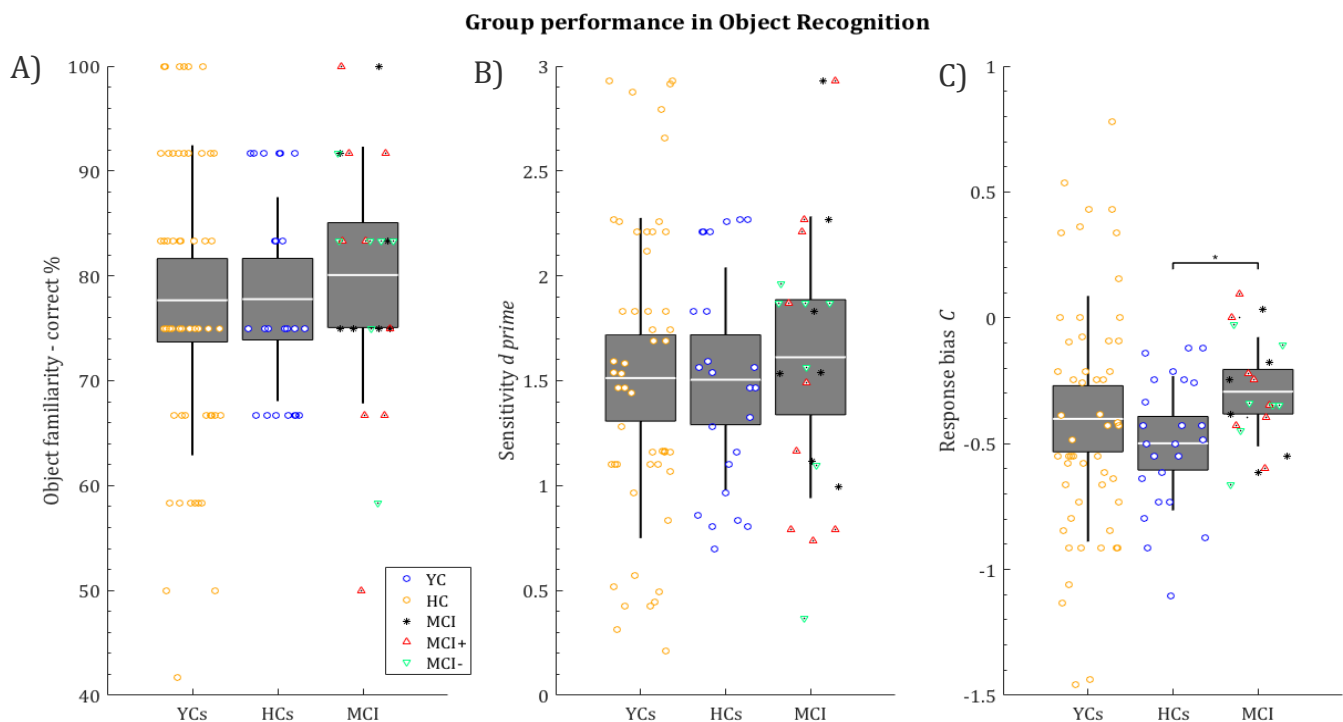


Figure 3.5 Discrimination of object familiarity between groups. **A)** Percentage correctly identified as either novel or familiar, **B)** Discrimination sensitivity as measured by *d'* and **C)** Response bias as measured by *C*. Yellow circles = YCs, blue circles = HCs; black asterisks = MCI without biomarkers; red triangles = MCI+; green inverted triangles = MCI-. Central line = mean; dark grey box= 95% confidence intervals; whisker = 1 standard deviation.

3.3.4. Object-environment association subtask

Across YCs and HCs, a significant effect of environment ($F(2,687)= 9.86, p<0.001$) was observed on hit rate (i.e. the number of correct object-context associations), which survived Bonferroni correction ($\alpha = 0.01$). Hit rate was greater in environment 3 compared to either environment 1 (Figure 3.6D, $\beta=0.89\pm 0.22$) or environment 2 ($\beta=0.93\pm 0.21$). However, no effect of ageing was observed (Figure 3.6A, $p>0.05$). Across HCs and MCI, a significant effect of environment ($t(2,415)=1.84, p<0.05$) was observed, however environment did not survive Bonferroni correction ($\alpha = 0.008$). However, no effect of MCI status was observed (Figure 3.6B, $p>0.05$). Across MCI+ and MCI- an effect of years in education ($t(1,136)= 2.81, p<0.01$) was observed, with more years in education predicting more correct responses ($\beta=0.17\pm 0.06$). Whilst no effect of biomarker status was observed (Figure 3.6C, $p>0.05$), object-context association performance was predicted by CSF $a\beta$ ($t(1,10)=3.18, p<0.05$) but not by CSF tau ($t(1,10)=0.65, p>0.05$).

Table 3.3. Object-environment association performance as indicated by hit rates

<i>Group</i>	<i>Trials (n)</i>	<i>Total Hit Rate</i>	<i>Env 1</i>	<i>Env 2</i>	<i>Env 3</i>
YCs	477	334 (70%)	106 (66.7%)	98 (61.6%)	130 (81.8%)
HCs	216	152 (70.4%)	45 (62.5%)	49 (68.1%)	58 (80.6%)
MCI	207	126 (39.1%)	41 (59.4%)	39 (56.5%)	46 (66.7%)
MCI+	81	45(55.6%)	14 (51.9%)	13 (48.2%)	18 (66.7%)
MCI-	63	44 (69.8%)	16 (76.2%)	15 (71.4%)	13 (61.9%)

Object-Environment Association

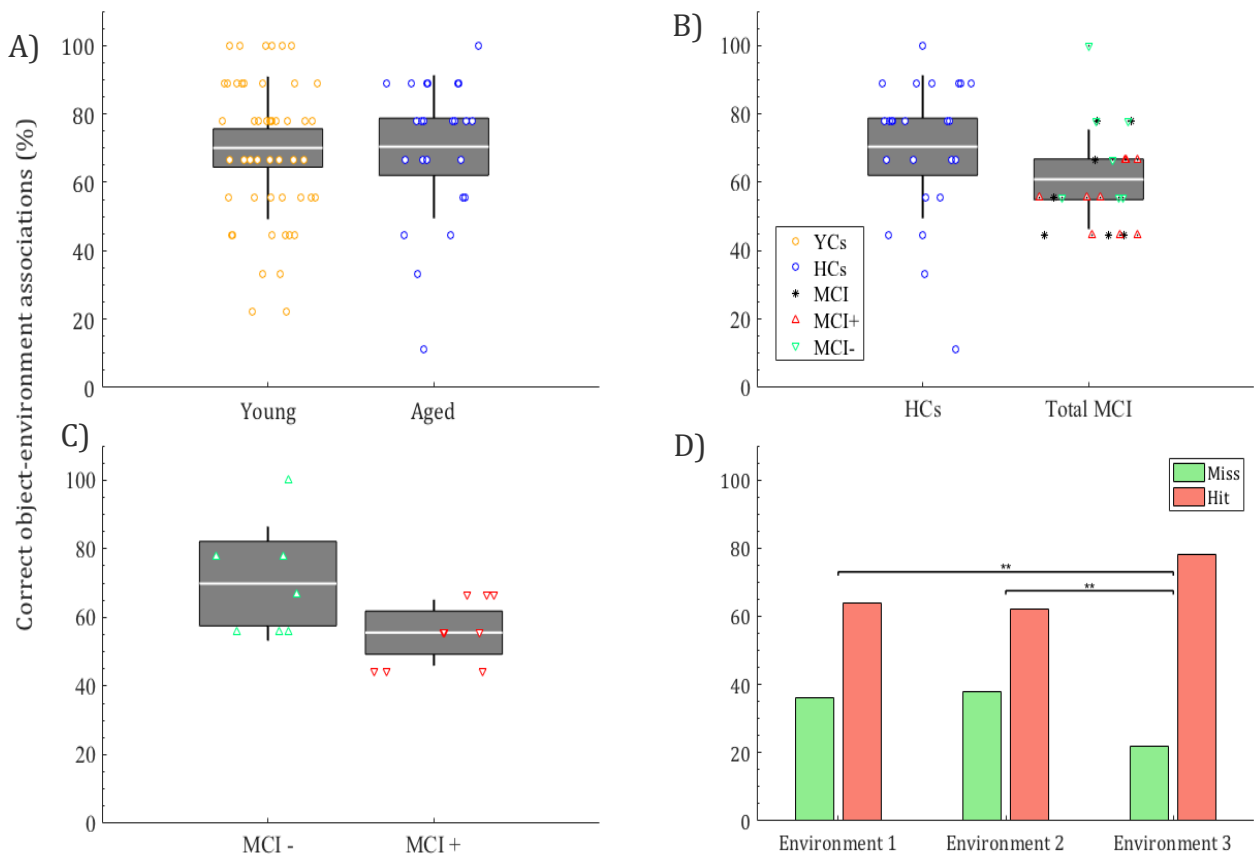


Figure 3.6. Correct discrimination of object-environment association. A-C) Percentage of objects correctly identified as belonging to the environment in question. Yellow circles = YCs, blue circles = HCs; black asterisks = MCI without biomarkers; red triangles = MCI+; green inverted triangles = MCI-. Central line = mean; dark grey box= 95% confidence intervals; whisker = 1 standard deviation. **D)** Effect of environment on association accuracy across all participants (% correct). **= $p < 0.01$.

3.3.5. Classification accuracy of the object-location task

Area under the curve (AUC), sensitivity and specificity were estimated using k-fold cross-validation ($k=10$), adjusted for age, sex and years in education. For the classification of total MCI patients from HCs, absolute distance error was associated with an AUC of 0.89 (Figure 3.7, 95% confidence intervals (CI) = 0.73-0.95), with an error ≥ 82 cm yielding a sensitivity of 0.87 and specificity of 0.92. Whereas performance in both object recognition (AUC= 0.52 (CI= 0.31-0.66)) and object-environment association (AUC= 0.67 (CI= 0.48-0.80)) subtasks were less effective at differentiating MCI from HCs. By comparison, the ACE-R was

associated with an AUC= 0.84 (CI= 0.69-0.94)), TMTB with an AUC= 0.83 (CI= 0.67-0.93), 4MT with an AUC= 0.73 (CI= 0.53-0.93), the delayed conditions of FCSRT with an AUC= 0.73 (CI= 0.55-0.85) and RFR with an AUC= 0.74 (CI= 0.57-0.86). Classification accuracy for neuropsychological predictors when combined exceeded any individual comparator test performing analogously to the object replacement task (AUC= 0.87, (CI= 0.66-0.93). Insufficient sample size in the biomarker positive and negative groups precludes ROC analysis.

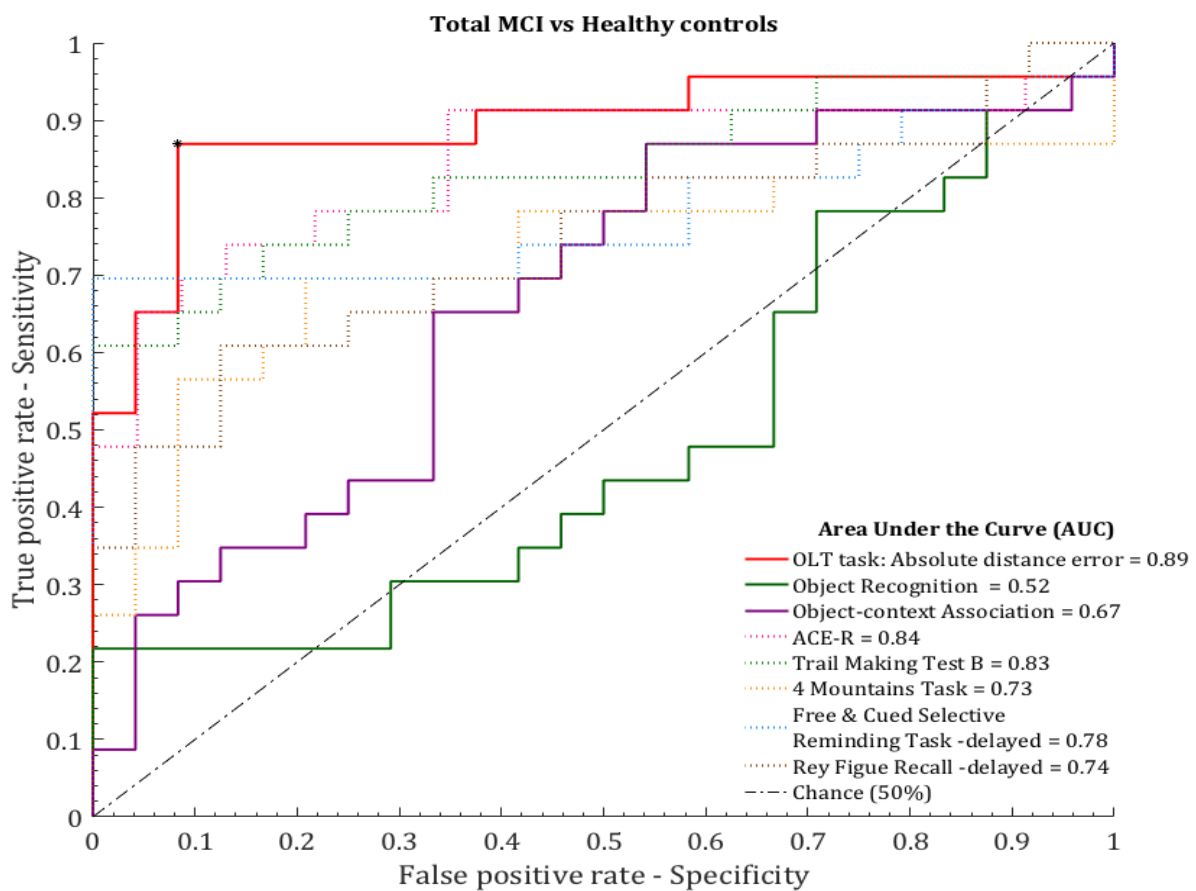


Figure 3.7. Receiver Operating Characteristic plot. Accuracy of object-location task performance for classifying total MCI from HCs. Absolute distance error (solid red line) and the percentage of hits was used for object recognition (solid purple line) and object-context association (solid green line). Classification of reference cognitive tests are represented by dashed lines for comparison: Addenbrookes Cognitive Examination-Revised (grey), Trail Making Test B (green), 4 Mountains Test (yellow), Free and Cued Selective Reminding Test – delayed free recall (blue) and Rey Figure

3.3.6. *A posteriori hypothesis*

A manual approach to categorising retrieval failures and swap errors was undertaken to test the prediction that MCI patients will exhibit such errors more

frequently than HCs. Two raters manually assessed all object replacement trials for the error source as outlined above. High inter-rater reliability was observed across all measurements with an overall agreement of 91.45% and an S score (Bennett *et al.*, 1954) of 0.89 (1= perfect agreement).

Group differences in the number of trials where the returned object was closer to its target location than to a different object’s location (i.e. nearest neighbour) were examined. Between YCs and HCs, a significant difference was observed, with YCs (24.06%) exhibiting fewer ‘non-target’ trials than HCs (30.56%, Figure 3.8A, odds ratio (object-recognition) = 0.71, $p < 0.05$). A significant difference was also observed between HCs and MCI patients, with MCI patients exhibiting more ‘non-target’ errors (45.57%) than HCs (object-recognition= 0.54, $p < 0.001$). However, no significant difference in ‘off-target’ trials was seen between MCI+ (43.52%) and MCI- (36.9%, object-recognition = 0.75, $p > 0.05$). Interestingly the frequency of any swap error (misattribution + content swap errors) significantly differed between

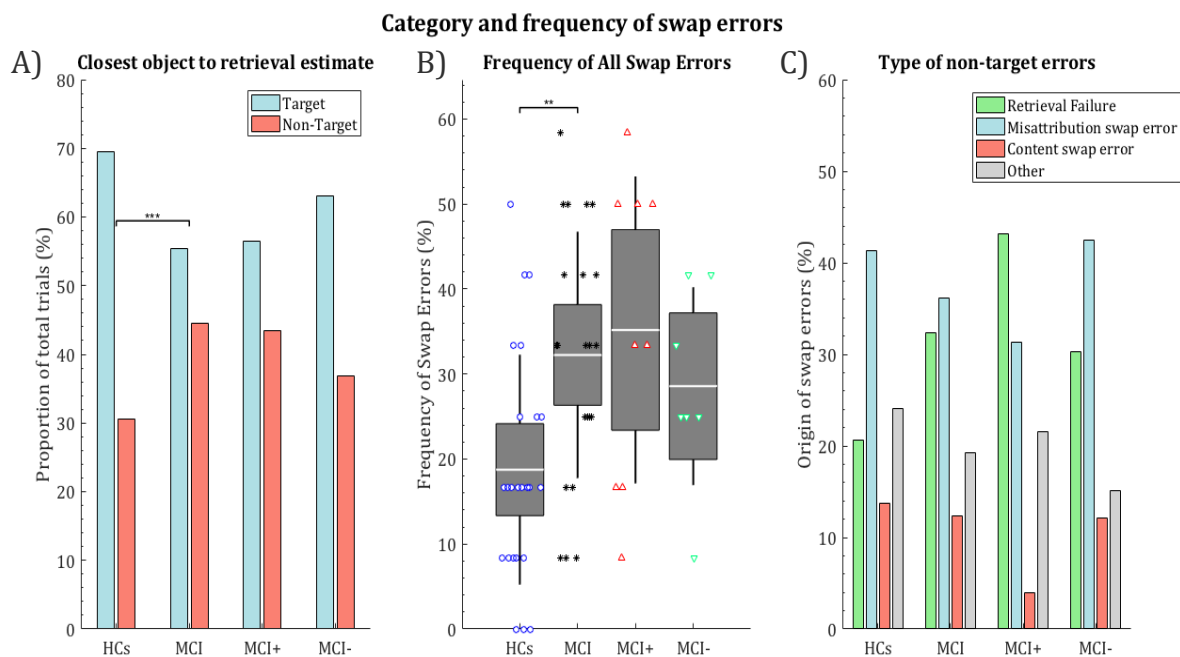


Figure 3.8. Distribution of swap errors. **A)** Proportion of trials when the location of a returned object is closest to its veridical location (target) or another object’s veridical location (non-target). **B)** Frequency of any swap error by group (misattribution or content) **C)** Within group errors, defined in section methodology, “other” constitute trials when a decision about the error cannot be reliably made, usually owing to the similar angle or close distance between two objects.

HCs and MCI (Figure 3.8B, $t(1,559) = 2.95$, $p < 0.01$), but not between MCI+ and MCI- ($t(1,187) = 1.11$, $p > 0.05$). However, no difference in the frequencies of retrieval failures, misattribution errors or content swap errors was observed between HCs and MCI ($p > 0.05$) or MCI+ and MCI- ($p > 0.05$, Figure 3.8C).

Finally, swap errors category was entered as an additional covariate to the GLME models previously described to evaluate whether their inclusion explains variance in performance associated with MCI. It was found that the inclusion of swap increased model fit (LRStat = 320.65, $p = 0$) and were highly significant predictors of absolute distance error ($F(5,539) = 124.2$, $p < 0.001$), with retrieval failures, misattribution swap errors and content-swap errors being associated with an increase in absolute distance errors of 77 ± 10 , 42 ± 9 and 62 ± 11 cm, respectively. Importantly, however MCI still explained a unique proportion of the variance in absolute distance errors ($t(1,539) = 2.88$, $p < 0.01$), although the proportion of variance associated with diagnosis was reduced (difference in $t = 1.35$).

3.4 Discussion

This study demonstrated that performance on a novel immersive virtual reality (iVR) object-location task (OLT), designed to explicitly test the function of the aEC, PC and hippocampus, is impaired in MCI. In line with the study hypothesis, performance on the object-replacement subtask successfully differentiated MCI from HCs with greater accuracy than comparator gold standard global and domain-specific cognitive tests. However, no group differences were observed in either object recognition or object-environment association memory, suggesting that the deficit was selective to object-position memory, rather than whole task. Finally, contrary to the study hypothesis, no effect of ageing or underlying pathology (MCI- vs MCI+) was observed in any of the three iVR subtasks.

The larger absolute distance errors observed in MCI compared to HCs are consistent with matrix-dependent location-learning (Bucks and Willison, 1997; Kessels *et al.*, 2010a, b) and placing tests (Vacante *et al.*, 2013) as well as free recall object-location paradigms (Wang *et al.*, 2013; Külzow *et al.*, 2014; Hampstead *et al.*, 2018). However contrary to the study hypothesis, no performance difference in object replacement was observed between young and healthy controls or between MCI patients with positive and negative AD biomarkers. This finding is unexpected given that categorical object-replacement tasks have shown efficacy in differentiating AD dementia from MCI patients (Bucks and Willison, 1997; Kessels *et al.*, 2004, 2010b; Wang *et al.*, 2013) and it was anticipated that errors would become more pronounced in a task with greater difficulty and degrees of freedom. Subsequent analyses did not reveal an association between object replacement performance and either CSF tau or $\text{A}\beta$ levels, these contrasting findings to chapter 2 may be explained by methodological limitations discussed below. However, in line with the *a posteriori* hypothesis, swap errors were more frequent in MCI compared to HCs, indicative of an object-position binding deficit that may be localised to EC dysfunction, specifically deficits in lEC object and object-trace cells (Tsao *et al.*, 2013) and mEC object-vector cells (Høydal *et al.*, 2019) both of which require conjunctive representations of the object and its allocentric position. This notion that object-

location processing is dependent on EC trace cells is reinforced by the observation of these cells in humans; in an object-location task these cells were shown to remap to the position of a target object's remembered position within the environment (Qasim *et al* (2018), submitted). However, swap errors did not fully explain the larger absolute distance errors observed in MCI indicating a deficit in spatial precision that is independent of the aforementioned binding impairment. Swap errors were highly predictive of object-replacement performance in line with prior research using a coordinate-dependent object replacement paradigm (Liang *et al.*, 2016). However, unlike the present task, Liang *et al* (2016) demonstrated that the frequency of swap errors differentiated asymptomatic familial AD from HCs, and was negatively correlated with hippocampal volume. By comparison, in the present study patients with biomarker evidence of prodromal AD did not exhibit more swaps than MCI patients with negative AD biomarkers.

Contrary to the study's secondary hypothesis, no effect of ageing, MCI or prodromal AD was observed on object-recognition performance. This was surprising given the role of the PC and IEC in object-recognition (Murray and Richmond, 2001; Bellgowan *et al.*, 2009b; Berron *et al.*, 2018b) and its reported deficits in MCI (Barbeau *et al.*, 2004; Dudas *et al.*, 2005; Bennett *et al.*, 2006) as well as mild AD dementia (Hudon *et al.*, 2006; Clark *et al.*, 2012). Previous research demonstrated a strong link between increased CSF tau and impaired mnemonic discrimination of objects (Düzel *et al.*, 2018; Berron *et al.*, 2019), with tau deposition in anterior-temporal networks being heavily implicated in such deficits (Maass *et al.*, 2019). However in the present study, object-recognition was not predicted by either CSF tau or $a\beta$ levels. These results may be due to the limited quantity of stimuli, constrained by the number of items that could be viably tested during both object replacement and object-context association subtasks (approximately 20% of those used in other tasks, e.g. Barbeau *et al.*, 2004; Bennett *et al.*, 2006). However, despite the limited stimulus size and variability in the saliency and distinctiveness of the test and foil objects few participants exhibited floor or ceiling effects, the absence of effect in MCI may be explained by methodological limitations as outlined below. A group difference in response bias

was observed in the object-recognition subtask whereby MCI patients were less likely to select 'old' responses than HCs. This finding contrasts with previous research that more liberal response biases (i.e. more likely to select 'old' responses) are observed in patients with MCI and AD dementia compared to HCs (Gomar *et al.*, 2017; Russo *et al.*, 2017); an effect that appears to be invariant of the quantity or type of stimulus (Beth *et al.*, 2010). Given these findings an explanation for the opposite bias in the present data is not posited, but note that any such differences in response bias should not confound the d' measure of sensitivity (accuracy), which did not differ between groups.

No between group differences were observed in object-environment association accuracy. This finding is contrary to the study hypothesis and previous studies which demonstrated impaired object-environment association memory in MCI, with moderate differentiation of MCI and mild AD dementia (Wang *et al.*, 2013). The present study's results are particularly surprising given the demonstrated role of the IEC in object-environment association recognition (Wilson *et al.*, 2013a) and the deficits in hippocampal-dependent associative encoding in MCI and AD dementia (Sperling *et al.*, 2003; Atienza *et al.*, 2011; Hanseeuw *et al.*, 2011). Previous work has demonstrated that anteriortemporal $a\beta$ and posteromedial tau are associated with scene and object processing, respectively (Maass *et al.*, 2019). It is therefore surprising that a task requiring conjunctive object and scene encoding was associated with CSF amyloid but not CSF tau. This discrepancy may be explained by amyloid deposition in posteromedial networks, encompassing posterior default mode networks which are involved in scene construction (Hassabis *et al.*, 2007; Andrews-Hanna *et al.*, 2010) which is impaired in AD (Irish *et al.*, 2015), potentially through impaired functional connectivity with the MTL (Palmqvist *et al.*, 2017). However, conclusions about the relationship between pathology and OLT performance are limited by methodological issues as discussed below. Object-environment association memory was consistently more accurate in the third environment than either the first or second environment, which were equivalent. This finding is partly explained by a recency effect (better memory for more recent experiences), as observed in other object-environment

association paradigms (Tam *et al.*, 2015), and partly by the heightened saliency of environmental cues in environment 3 anecdotally reported by participants. Future research would benefit from avoiding such distinctive environments and the repetition of object stimuli in alternative forced choice paradigms.

Performance on a brief object-replacement subtask successfully differentiated MCI from HCs and was more sensitive and specific for the detection of MCI than separate or combined global and domain-specific cognitive tests. Importantly, the iVR paradigm differentiated MCI from controls with higher classification accuracy than what was previously reported in study's employing 2D object-replacement paradigms (Wang *et al.*, 2013; Hampstead *et al.*, 2018). While few object replacement paradigms using coordinate-dependent free recall have been assessed in prodromal AD, these results are in line with 2D visual short-term memory experiments in familial AD patients. Compared to controls, symptomatic and asymptomatic carriers were impaired in object replacement accuracy, but no difference was observed between asymptomatic and symptomatic carriers (Liang *et al.*, 2016). However, both the object-recognition and object-environment association subtasks were less accurate at classifying MCI compared to all tests on the neuropsychological test battery. In the present study, insufficient sample size prohibited examining the classification accuracy of MCI with positive CSF AD biomarkers (i.e. prodromal AD) from MCI with negative CSF AD biomarkers. However, there was no significant effect of CSF status on performance across all components of the OLT, classification accuracy is therefore not likely to be much better than chance.

The present study has several limitations. As a whole, the memory load required for retaining the instructions and format of the OLT is large, prohibiting the use of a greater quantity of stimuli in patients with cognitive impairment. However, despite the inherent complexity of the OLT, no floor effects were observed in object recognition/object-environment association subtasks (as were observed during piloting with larger number of objects and environments). The design of the experiment could be improved by counterbalancing environment order: this

would clarify whether the performance advantage of environment 3 is driven by the saliency of environment-specific cues, or was the manifestation of practice effects during object-replacement and recency effects for object-context associations (Tam *et al.*, 2015). Furthermore, the discontinuity of objects between participants presents a similar confound, given that the strength of the association is likely to be influenced by the salience and congruency of the object and environment (for example comments like “the pizza will be frozen” – comment made by a participant when viewing the ‘pizza’ object in the third snowy environment). Indeed, both stimulus and schema congruency have a significant effect on memory, although whether this confers an advantage or disadvantage remains controversial (Buuren *et al.*, 2014; Greve *et al.*, 2017, 2019; Frank *et al.*, 2018), this is particularly problematic given that patients with mild AD dementia attend more to incongruent stimulus pairings (Lenoble & Corveleyn, 2018). Lastly, the limited stimulus size driven by the format of the OLT reduces the power of these findings and interpretation of the data; each component of the OLT represents an interesting investigative question and warrants its own dedicated task. Despite these limitations, the present study demonstrated the viability of implementing a novel multicomponent OLT using 3D iVR. Unlike 2D tasks, iVR enables encoding of both objects and environmental cues in 3D that elicits greater recruitment of IEC object and object-traces cells compared to 2D objects (Hargreaves *et al.*, 2005; Deshmukh and Knierim, 2011; Yoganarasimha *et al.*, 2011). Future research should seek to resolve these design limitations and additionally incorporate a stepwise systematic increase in either objects or environments. Increasing task difficulty until a maximal performance threshold is reached would add a capacitive outcome measure that may improve classification of prodromal AD (Kessels *et al.*, 2010a) and have greater utility in detecting subtle impairments in preclinical AD.

In conclusion, this is the first study to utilise a multicomponent iVR object-location task in MCI patients with and without CSF evidence of Alzheimer’s pathology. It was found that performance on a coordinate-based object replacement task differentiates patients with mild cognitive impairment from aged-matched

healthy controls with high sensitivity and specificity. However, performance on the object-replacement task did not differentiate MCI patients with CSF biomarker evidence of AD pathology from those without. No effect of MCI or prodromal AD was observed in either object recognition or object-environment association accuracy, and no effect of ageing was found in any of the three iVR tasks. The conclusions of the present study are confounded by the small number of stimuli and environments that were not counterbalanced or consistent between participants which should be resolved in any future research using this paradigm.

Chapter 4 - MRI measures of Entorhinal Cortex structure and their relationship to spatial cognition

4.1. Introduction

The EC exhibits significant atrophy in AD dementia (Juottonen et al., 1998), in MCI patients smaller EC volumes are predictive of disease severity and subsequent conversion to AD dementia (Dickerson et al., 2001) with greater specificity than hippocampal atrophy (Killiany et al., 2002; DeToledo-Morrell et al., 2004; Pennanen et al., 2004; Devanand et al., 2007, 2012). EC atrophy is also more predictive of memory decline, and more resistant to age-related degeneration than the hippocampus (Raz et al., 2004). However, the EC's superior diagnostic differentiation is limited by the morphological heterogeneity of the parahippocampal gyrus and its sulci which vary in both quantity (i.e. bifurcation) and depth (Insausti et al., 1998) reducing the reliability of current automated approaches (Leng et al., 2019). Moreover, current automated approaches do not delineate the functionally disparate role of EC subdivisions. Manual segmentation of EC thickness, volumetry and diffeomorphometry overcomes these challenges with demonstrably high reliability, sensitivity and specificity as a biomarker for AD dementia (Tward *et al.*, 2017a; Kulason *et al.*, 2019a). Krumm *et al.* (2016) manually segmented the parahippocampal gyrus in patients with MCI and early AD dementia demonstrating atrophy in the EC and medial bank of the collateral sulcus (Brodmann's area 35 (BA35)). This area encompasses the transentorhinal cortex, an area primarily affected by tau pathology, thought to be involved in the formation of complex associations pertaining to identity, semantics and object-location (Jo and Lee, 2010; Watson *et al.*, 2012; Eradath *et al.*, 2015) and is densely connected with the EC.

Given the EC's role as the cortical gateway to the hippocampus and the impaired connectivity associated with EC atrophy in both MCI and early AD dementia (Li *et al.*, 2002; Wang *et al.*, 2006; Allen *et al.*, 2007) there is increasing interest in mnemonic discrimination fMRI tasks that probe the distinct functions of EC subdivisions (Schultz *et al.*, 2012; Reagh and Yassa, 2014; Navarro Schröder *et al.*,

2015). Recently, reduced activity in object discrimination tasks associated with activity in aLEC-PC networks was observed in older adults (Ryan *et al.*, 2012; Berron *et al.*, 2018b). These findings mirror previous research that found age-related deficits in the detection of changes in object identity (Reagh *et al.*, 2016) and pattern separation associated with aLEC activity (Reagh *et al.*, 2017). Importantly, reduced aLEC volumetry was predictive of cognitive performance both of which were impaired in 'at-risk' older adults, defined by below-average scores on the Montreal Cognitive Assessment (MoCA) without subject cognitive complaint (Olsen *et al.*, 2017). The regional vulnerability of the EC has even been demonstrated in preclinical AD, Khan *et al.* (2014) found hypometabolism and reduced cerebral blood volume in the IEC, PC and transentorhinal cortex of asymptomatic individuals who subsequently converted to AD dementia at 3.5-year follow-up. These results were mirrored in transgenic AD mice that overexpress both human amyloid and tau in the EC which induced hypometabolism in the IEC and posterior parietal cortex, key nodes of the posteromedial network. The aforementioned studies suggest that the detection of aLEC impairments may be sensitive to tau-related neurodegeneration given its dense connectivity with the transentorhinal cortex, these impairments may be detectable using targeted imaging biomarkers.

To date object and scene discrimination tasks, used respectively to represent functions of the aLEC and pmEC, have focused on age-related cognitive decline and have not been fully explored in patients with MCI or early AD dementia. However, preliminary evidence demonstrate an intriguing relationship between the deposition of tau and performance in mnemonic discrimination tasks. Berron *et al.* (2017, poster) found that in a complex object-in-scene task, object discrimination was predicted by CSF tau whereas scene discrimination was more associated with CSF amyloid in patients with subjective cognitive impairment and MCI. These results were echoed in healthy older adults where object-discrimination performance was associated with CSF phosphorylated tau levels, a biomarker of preclinical AD (Berron *et al.*, 2019). Lastly, object discrimination performance, but not scene discrimination, was associated with tau deposition in the medial temporal lobe of older adults, whereas amyloid deposition was not associated

with either task (Maass *et al.*, 2019) . These studies provide initial evidence that impaired mnemonic discrimination of objects and scenes as respective functions of the aEC and pmEC may be sensitive to the presence of tau pathology. Taken together, these studies raise the possibility that the spatiotemporal propagation of AD pathology within the EC occurs with a lateral to medial gradient. Therefore the detection of incipient AD may therefore be aided by object discrimination tasks that are associated with aEC structure (Olsen *et al.*, 2017) and function (Berron *et al.*, 2018b). However, given the extensive evidence for the role of the aEC and pmEC in object-location and path integration it is of considerable interest to delineate the neural correlates of the work outlined in chapters 2 and 3.

The present study seeks to investigate EC structure-function associations in MCI and prodromal AD, via manual segmentation of the EC, including aEC and pmEC subdivisions, and BA35, containing the transentorhinal cortex.

This study's primary objective is to test the hypothesis that impairments in path integration and object-location correlate respectively with reductions in pmEC and aEC volume in MCI and early AD dementia. It is predicted that pmEC volumes will be associated with absolute distance errors in the path integration task (PIT), whereas performance in the object-replacement task (OLT) will correlate with aEC volumes. With regard to the OLT subtests, it is predicted that performance on the object recognition subtask will correlate with both aEC and BA35 volumes whereas object-environment memory will correlate with aEC volume. Additionally, it is predicted that PI and OLT performance will be associated with the parahippocampal gyrus and hippocampus in a whole-brain, voxel-based morphometry (VBM) analysis. It is further anticipated that aEC and BA35 atrophy occur in a stepdown manner from HCs to MCI to AD dementia, and will be more sensitive and specific to the presence of AD pathology than other regions of interest. Lastly, this study will evaluate whether the high classification accuracy of both iVR tasks can be improved by the addition of pmEC and aEC volumes.

4.2. Methods

4.2.1. Participants

Structural and morphometric differences were compared between two participants groupings i) HCs (n=34), MCI (n=54) and AD dementia (n=15) and ii) MCI+ (n=12) and MCI- (n=9). AD dementia was diagnosed accordingly to the McKhann criteria (McKhann *et al.*, 2011); mild dementia was determined by Mini-Mental State Examination scores >22 and a Clinical Dementia Rating of one (Morris, 1997). Details of the diagnostic, inclusion and exclusion criteria for MCI, MCI+ and MCI- are detailed in 2.2.1, abbreviations are consistent with previous chapters.

4.2.2. MRI acquisition parameters:

MRI scanning was conducted on 32 channel Siemens 3T Prisma scanners based either at the MRC Cognition and Brain Sciences Unit, Cambridge, or the Wolfson Brain Imaging Centre, Cambridge, with the same acquisition parameters used at the two scan sites. The volumetric scan protocol included whole brain 1mm isotropic T1-weighted MPRAGE (TA 5:12, TR 2300ms, TE 2.96ms) and high-resolution 0.4x0.4x2 mm T2-weighted scans through the hippocampal formation with scans aligned orthogonally to the long axis of the hippocampus (TA 8.11, TR 8020ms, TE 50ms).

4.2.3. Voxel-based morphometry preprocessing

T1 scans were manually inspected and reoriented to Montreal Neurological Institute (MNI) space if required. Whole brain voxel based morphometry was conducted using Matlab 2016a and computational anatomy toolbox (CAT12, (Gaser and Kurth, 2016)). Images were registered to the MNI template ahead of undergoing modulated segmentation into grey matter, white matter and CSF, thereby conserving the volumes of the original image. Normalised segmented data were visually inspected for segmentation errors and checked for inhomogeneities and outliers. Data were smoothed using an 8mm kernel before model estimation.

4.2.4. Manual Segmentation of the Parahippocampal gyrus

Segmentation of BA35, whole EC, anterolateral EC (alEC), posteromedial EC (pmEC) and subdivisions was undertaken. While segmentation protocols are available at ultrahigh-resolution 7T (Maass *et al*, 2015), the delineation of boundaries using 3T (Olsen *et al*, 2017; Yeung *et al*, 2017, 2018) is incomplete in intermediate slices that do not exclusively contain alEC or pmEC. Therefore, for this study, an in-house protocol was devised, which partially segmented alEC and pmEC using the three anterior-most and three posterior-most slices of the EC that contained exclusively alEC or pmEC (Maass *et al*, 2015). Intermediate slices were not used for alEC and pmEC segmentation owing to the overlap of the two subdivisions within this part of the EC and the absence of consistent landmarks to reliably delineate the progressive boundary between alEC and pmEC. As such, this protocol prioritised specificity of segmentation over completeness. Manual segmentation was performed in ITK-SNAP (Yushkevich *et al*, 2006) (Figure 4.1).

The EC, alEC, pmEC and BA35 were manually segmented on coronal slices of high resolution T2-weighted 3T MRI scans, as summarized in Figure 4.1. The partial segmentation of alEC began two slices anterior to appearance of the hippocampal head and subiculum. pmEC segmentation extended one slice anterior from, to one slice posterior to, the emergence of the incisura temporalis and the separation of the uncus from the medial temporal lobe. The medial extent of the anterior EC was the semiannular sulcus of the ambiens gyrus, whereas more posteriorly borders the medial subiculum. The complete segmentation of the EC and BA35 was adapted from the protocol outlined in Berron *et al* (2017) that aims to accommodate the anatomical variability of the collateral sulcus in this region (Ding and van Hoesen, 2015). The lateral border of the EC extends $\frac{1}{4}$ of the depth of the collateral sulcus (CS), unless it is < 4mm deep in which case it extends to the fundus of the CS. The segmentation of BA35 is dependent upon the type and depth of the CS, the lateral extent of BA35 extends from the lateral extent of the EC to:

- Very deep CS (>10mm): $\frac{3}{4}$ the depth of the medial CS bank
- Deep CS (7-10mm): the fundus of the CS.

- Shallow (4-7mm): $\frac{1}{2}$ the depth of the lateral CS bank.
- Very shallow: the crown of the fusiform gyrus.

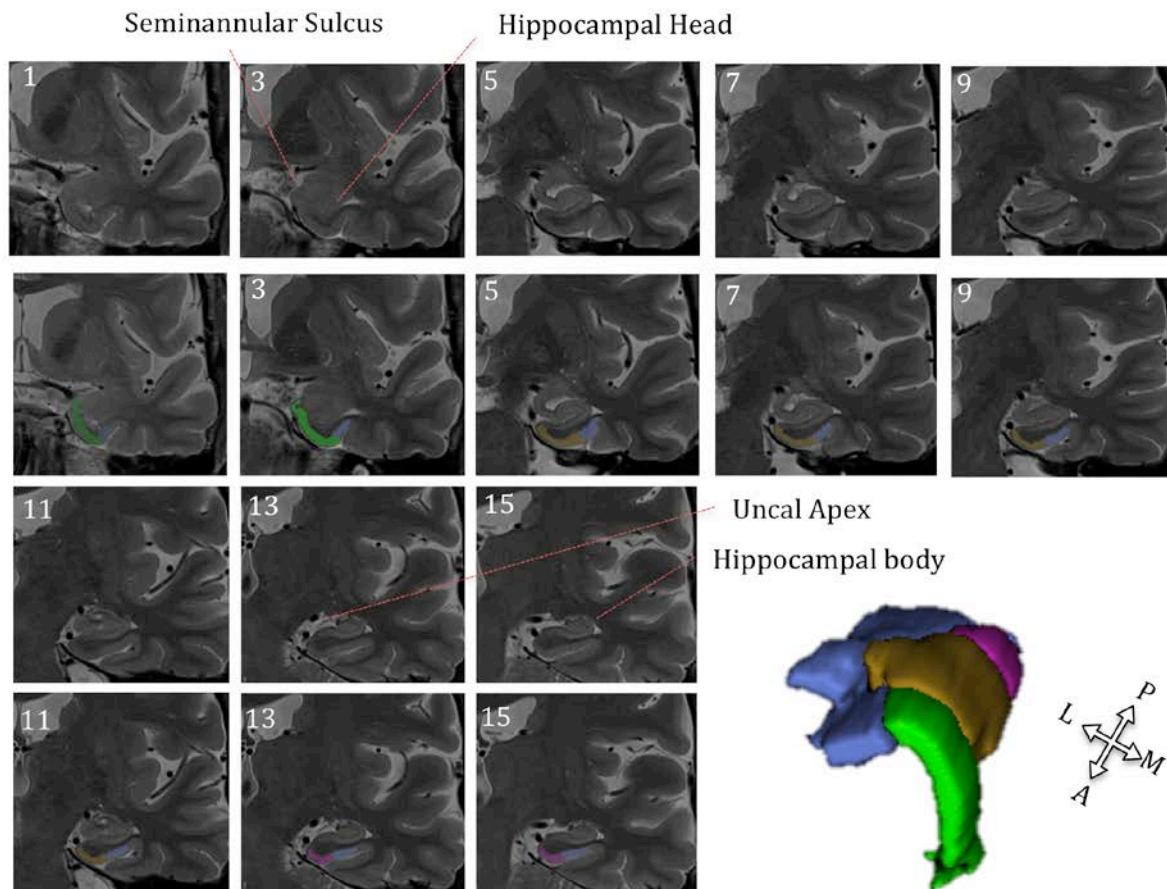


Figure 4.1. Illustration of entorhinal subdivisions and BA35 segmentation.

Anterolateral (aLEC, green) is segmented two slices anterior to the emergence of the hippocampal head (slice 3). Posteromedial (pmEC, pink) is segmented from one slice anterior to, and one slice posterior from, the uncal apex (slice 13). All intermediate slices between aLEC and pmEC are segmented as EC (brown), total EC volume is produced by summing all 3 EC subdivision volumes. BA35 is segmented on all slices as the EC and one additional slice posterior to the end of the pmEC. Arrow schematic indicates anatomical plane for 3D segmentation only.

Given the involvement of brain areas in PI (e.g retrosplenial cortex (RSc) Worsley *et al*, 2001; Chrastil *et al*, 2015) and OLT (e.g. hippocampus, Parslow *et al* (2004a, b, 2005)) that were not included in this manual segmentation protocol, these additional regions of interest (ROIs) were segmented using the Destrieux atlas in Freesurfer 6.0 (Fischl *et al*, 2002; Iglesias *et al*, 2015).

All segmentations were manually inspected to exclude cysts, CSF and meninges. The residual method was used to adjust ROI volumes:

$$adjROI_i = ROI_i - \beta(ICV_i - ICV_{HC_mean})$$

Where $adjROI_i$ is the intracranial volume (ICV)-corrected ROI, ROI_i is the raw volume, coefficient β represents how ROI volume is expected to change with ICV and ICV_{HC_mean} is the mean ICV of HC participants. This approach removes variation in the ROI associated with intracranial volume (ICV), achieved by regressing raw ROI volumes to ICV, the resulting adjusted volumes are therefore not correlated to ICV. The mean ICV from HCs was used to normalize and adjust ICV across all participants, removing variation in an ROI associated with ICV in “neurotypical” individuals likely to be altered in the presence of pathology (Voevodskaya *et al.*, 2014; Jack, 1989). This approach has demonstrated less sensitivity to stochastic and systematic errors (Sanfilippo *et al.*, 2004) and was less influenced by extraneous variables, such as gender disparities (Andreasen *et al.*, 1993; Barnes *et al.*, 2010). Volumetric measurements were summed across hemispheres after ICV correction.

Lastly, intra-rater reliability was assessed over two raters; Johanna Hagman and I, 10 randomly selected scans were re-segmented following a delay of at least one month from initial segmentation. Inter-rater reliability was assessed for both raters by segmenting 5 randomly selected images from the other rater. Intra- and inter-rater reliability was assessed using spatial overlap as measured using Convert3D’s Dice similarity coefficient (Yushkevich *et al.*, 2006). Whereas consistency in volume was assessed using intraclass correlation coefficient (ICC) for intra- (ICC (3,k) - consistency) and inter-rater (ICC(2,k) -agreement) reliability (McGraw and Wong, 1996).

4.2.5. Statistics

Between group differences in demographics were assessed using one-way ANOVAs with between group contrasts (HC vs MCI, HC vs AD and MCI vs AD),

whereas two-sample t-tests were used to assess differences between MCI+ and MCI-. Where parametric assumptions were violated the Kruskal-Wallis or Wilcoxon rank sum test was used in place of ANOVA or t-test. Associations between VBM and performance in either the PIT or OLT were assessed using multiple linear regressions. Separate models examined the effect of absolute distance error (averaged per participant) for both PIT and object replacement across HCs v MCI and MCI+ and MCI-. Additional models examined grey matter (GM) correlates of proportional linear and proportional angular error from the PIT along with percentage correct in the object recognition and object-environment subtasks of the OLT. All variables were mean centered and checked for orthogonality, with voxel values restricted to an absolute threshold of 0.1 prior to contrasts being defined. F-contrasts were used to specify the iVR outcome measure of interest covarying for ICV, age, sex, years in education and diagnostic status. Significant voxel clusters are primarily reported using an FWE correction threshold of $p < 0.05$, in the case that no voxels were significant at this threshold, an exploratory uncorrected threshold of $p < 0.001$. Post statistical thresholding, cluster size (extent threshold) was set to a non-arbitrary value as determined using the `cp_cluster_Pthresh` tool (<https://goo.gl/kjVydz>).

Between-group differences in ROI volume were assessed using multiple regression with the response variable specified as the ROI and group (HC vs MCI vs AD) specified as the predictor variable along with covariates of age, sex and years in education. Contrasts were used to examine specific between group differences (e.g. HC vs MCI, HC vs AD, MCI vs AD). Separate models were used to examine between group structural differences in the ROI of MCI+ and MCI-.

One-way MANCOVA was used to examine the effect of ROIs on iVR performance covarying for group, age, sex and years in education across all participants. For the path integration task, dependent variables were specified as the three response variables (absolute distance error, proportional linear and proportional angular error). The final model included whole EC, pmEC, isthmus cingulate and hippocampal volumes as mean centred predictor variables. For the OLT, response variables were specified as absolute distance errors in the object replacement task

		Healthy Controls (HC)	Mild Cognitive Impairment (MCI)			Alzheimer's Disease
			<i>Total MCI</i>	<i>MCI-</i>	<i>MCI+</i>	
Between Group	n	30	54	9	12	15
	Age	68.3 ±6.5	68.2 ±7.8	70.18 ±7.8	72.1 ±10	74.4 ±9.8
	Males	43.3 %	69.2%	72.7 %	66.7 %	46.6%
	Year in Education	14.1 ±3	13.5 ±3.3	14.5 ±4.4	14.5 ±3.8	11.2 ±1.5
	ACER	97.1 ±2.8	76.5 ±13.1*	85.3 ±8.2	81.3 ±10.8*	72.3 ±11.1*
PIT	n	37	34	9	12	
	Age	68.8 ±6.39	70.2 ±10.2	70.18 ±7.8	72.1 ±10	
	Sex	44.4 %	67.6 %	72.7 %	66.7 %	
	Years in Education	14.8 ±3.6	14.2 ±3.3	14.5 ±4.4	14.5 ±3.8	
	ACER	97.1 ±2.9	80.2 ±11.2*	85.3 ±8.2	81.3 ±10.8*	
OLT	n	24	21	7	9	
	Age	68.9 ±4.4	70 ±9.1	67.4 ±6.3	69.7 ±10.1	
	Sex	52.9 %	65 %	71.4 %	71.4 %	
	Years in Education	15.1 ±2.9	14.4 ±3.6	14.1±4.4	14.5 ±3.4	
	ACER	97.2 ±2.8	82.8 ±9.8*	86.1 ±8.6	79.9 ±11.8	

Table 4.1 Demographic table summary for VBM and manual segmentation analyses. Analyses examined the differences in VBM and manual segmentation of the parahippocampal gyrus between groups and their association with PIT and OLT performance. *Indicates a difference from HCs at $p < 0.01$.

along with percentage correctly identified in both the object recognition and object-context association. Predictor variables included whole EC, aIEC, hippocampal and BA35 volumes which were mean centred. Between group differences in CSF tau and $a\beta$ were z-scored (non-normal) and entered as predictors of all PI outcome measures using the GLM. All models covaried for age, sex and years in education and were inspected for multicollinearity between predictor variables, with residuals visually inspected for normal distribution and homoscedasticity.

4.3. Results

4.3.1. Demographic differences

Across the three cohorts (Between group, PIT and OLT), no significant difference in age or sex ($p > 0.05$) was observed. The Kruskal-Wallis test (non-normal data) revealed that patients with AD dementia had significant fewer years in education than MCI patients ($\chi^2(2,96) = 16.86, p < 0.01$) but not HCs ($p > 0.05$). A significant difference in ACER was observed between HCs and MCI, and between HCs and AD dementia ($\chi^2(2,96) = 55.0, p < 0.01$). No significant differences were observed between MCI+ and MCI- groups.

4.3.2. Reliability of segmentation protocol

High inter- and intra- rater reliability was achieved for the manual segmentation protocol of the EC, alEC and pmEC, consistent with previous research (Berron *et al.*, 2017b; Olsen *et al.*, 2017). Inter-rater reliability on the whole was lower than intra-rater reliability but exhibited moderate to good consistency (Koo and Li, 2016). Intraclass correlation coefficient (ICC) gives an indication of quantitative consistency whereas dice coefficients reveal the proportion of spatial overlap between segmentations (ICC of 1 = complete agreement in volumetric estimates, Dice of 1 = perfect overlap between segmentations).

		EC		alEC		pmEC		BA35	
		LHS	RHS	LHS	RHS	LHS	RHS	LHS	RHS
Intra-rater reliability	*ICC	0.93	0.82	0.88	0.89	0.85	0.77	0.89	0.75
	Dice	0.87	0.87	0.89	0.82	0.88	0.85	0.84	0.81
Inter-rater reliability	ICC	0.98	0.94	0.92	0.98	0.91	0.70	0.79	0.70
	Dice	0.70	0.71	0.75	0.73	0.71	0.69	0.77	0.73

Table 4.2 Dice similarity coefficient was computed for both intra- and inter-rater reliability. ICC(3k) and ICC(2k) was used for intra-rater and inter-rater reliability, respectively. Abbreviations: EC, entorhinal cortex; ICC intraclass coefficient; *ICC – averaged across both raters.

4.3.3. Between group differences in volumetry and morphometry

Between group differences in EC subdivision volumetry were examined across HCs, total MCI and AD patients, as well as MCI+ and MCI-. Across HCs, MCI and AD participants, a main effect of group was observed on EC ($F(2,101)= 20.77$, $p<0.001$), aIEC ($F(2,101)= 14.82$, $p<0.001$), pmEC ($F(2,101)=10.78$, $p<0.01$) and BA35 ($F(2,101)=20.70$, $p<0.001$). Post hoc contrasts examined volumetric differences between HCs and AD, HCs and MCI and MCI and AD (table 4.3).

Between HCs and AD, and between HCs and MCI, differences were observed across all manually segmented volumes, whereas differences between MCI and AD were only observed in total EC volume. Significant differences between MCI+ and MCI- were observed in bilateral aIEC ($t(1,20)= 2.30$, $p<0.05$), pmEC ($t(1,20)=2.36$,

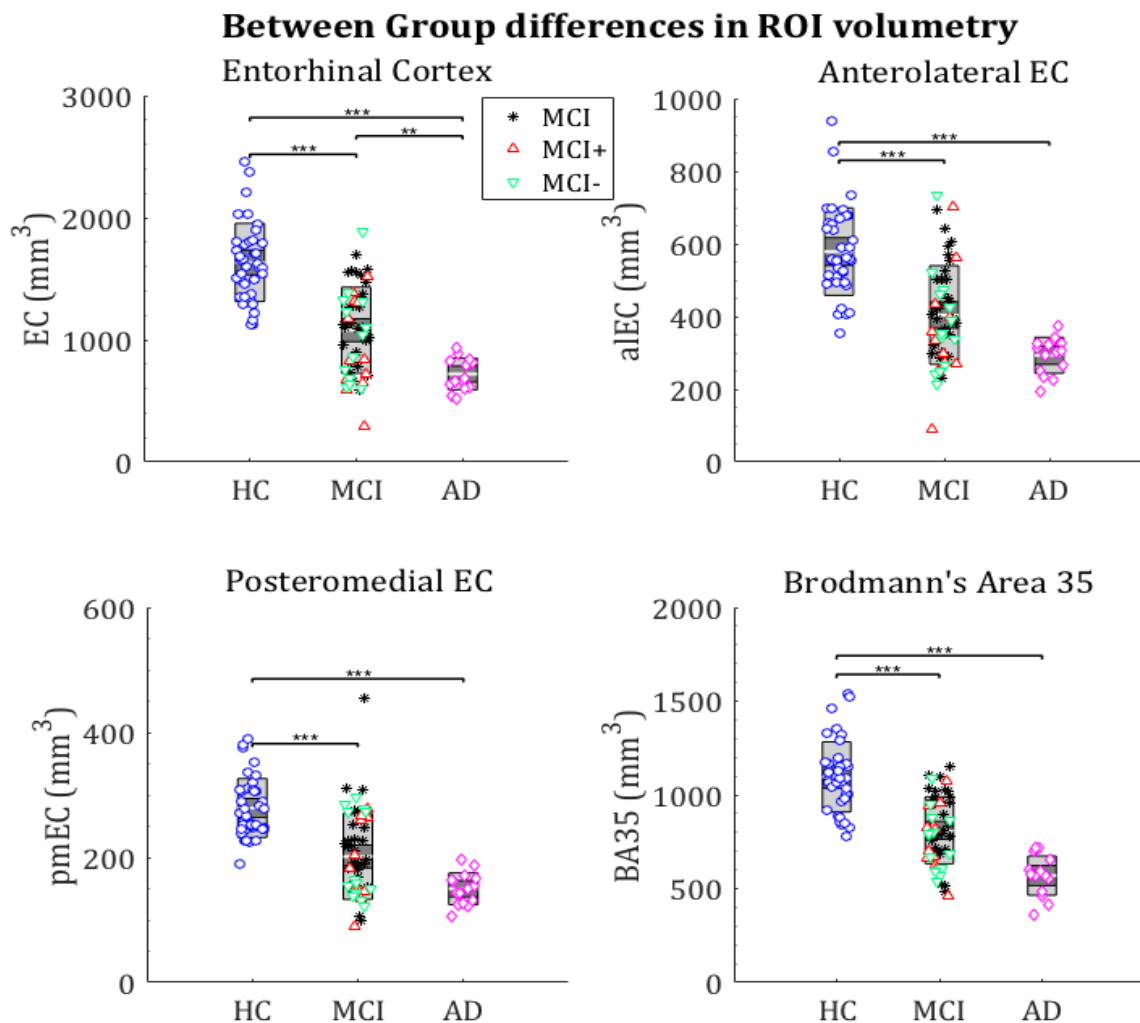


Figure 4.2. Between group differences in ROI volumes ** $p<0.01$, *** $p<0.0001$

$p < 0.05$) and total EC ($t(1,20) = 2.29$, $p < 0.05$), however, none of these contrasts survived control for multiple comparisons. No association was observed between CSF measures and any ROI volume. However trends were observed between $a\beta$ levels and whole EC ($p = 0.09$), aEC ($p = 0.06$) and TE35 ($p = 0.09$) volumes, whereas trends were only observed between tau levels and $pmEC$ volumes ($p = 0.09$).

Contrasts	EC	aEC	pmEC	BA35
HC vs AD	$t = 6.30$, $p < 0.001^*$	$t = 5.23$, $p < 0.001^*$	$t = 4.56$, $p < 0.001^*$	$t = 4.56$, $p < 0.001^*$
HC vs MCI	$t = 5.36$, $p < 0.001^*$	$t = 4.68$, $p < 0.001^*$	$t = 3.79$, $p < 0.01^*$	$t = 3.79$, $p < 0.01^*$
MCI vs AD	$t = 3.31$, $p < 0.01^*$	$t = 2.55$, $p < 0.05$	$t = 2.50$, $p < 0.05$	$t = 2.50$, $p > 0.05$

Table 4.3. Between group differences across EC, aEC, pmEC and BA35 as assessed by post hoc contrasts. * Indicate comparisons that survived multiple comparison correction ($\alpha = 0.01$).

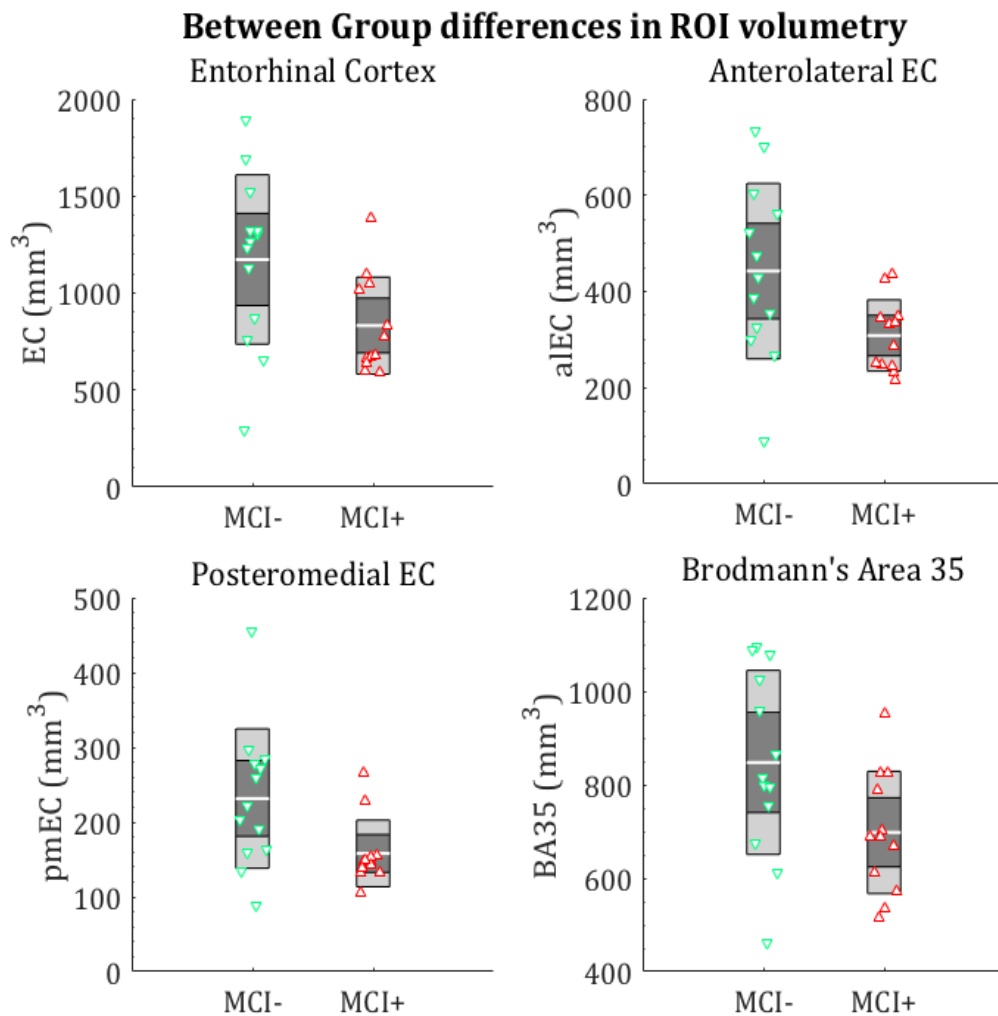


Figure 4.3. Between group differences in ROI volumes across MCI+ and MCI-, all comparisons were significant at $p < 0.05$ but did not survive control for multiple comparisons.

VBM analysis was used to examine the differential patterning of gray matter (GM) voxel values between HCs, MCI and AD. A one-way ANCOVA, adjusted for age, sex, years in education and ICV was performed, and between-group t-tests revealed differences in GM voxel values between AD and HCs in the bilateral hippocampus (BA54), left parahippocampal gyrus (BA 36), left putamen (BA49) and left supramarginal gyrus (BA40, all cluster level FWE $p < 0.05$, table 4.4). Between HCs and MCI differences in GM were only observed in the left middle temporal gyrus (cluster level FWE $p < 0.05$). Whilst no differences between MCI and AD were observed at cluster level FWE $p < 0.05$, an exploratory $p < 0.001$ revealed differences localised to the left putamen.

Comparison	Anatomical location (BA)	MNI coordinates			Cluster size	t/F Stat	Z Values
		X	Y	Z			
Between group differences							
<i>HC vs AD</i>							
	L Hippocampus (BA 54)*	-32	-9	-14	608	6.55	5.92
	L Putamen (BA49)*	-26	18	3	368	6.35	5.77
	L Supramarginal gyrus (BA40)*	40	-48	46	123	5.56	5.15
	L Parahippocampal gyrus (BA36)*	-34	-10	-33	99	5.56	5.15
	R Hippocampus (BA54)*	27	-12	-9	426	5.54	5.14
<i>HC vs MCI</i>							
	L Middle temporal gyrus (BA21)*	-45	-15	-10	235	5.61	5.19
<i>MCI vs AD</i>							
	L Putamen (BA49)	-27	14	-6	1479	4.29	4.09
Path Integration							
<i>Absolute Distance Error</i>							
	L Thalamus	-6	-15	2	1327	17.98	3.8
Object Location							
<i>Object Recognition % correct</i>							
	L Hippocampus (BA 54)	-32	-20	-14	1496	25.64	4.26
	L Parahippocampal gyrus (BA36)	-32	-16	-24			

Table 4.4 VBM differences between groups and associated with PIT and OLT performance. Anatomical locations with * indicate cluster significance at FWE $p < 0.05$, all other anatomical locations were significant at uncorrected cluster threshold of $p < 0.001$, with an extent size determined by $p < 0.01$.

4.3.4. Association between ROI volumetry and path integration performance

Multivariate analysis between PIT performance measures and ROIs (pmEC, EC, isthmus cingulate and hippocampus) covarying for age, sex, years in education and group revealed that, across all participants, pmEC volume was the only significant predictor of PIT performance (Pillai's Trace (PT)= 0.13, $F(3,58)= 2.83$, $p<0.05$). Reduced pmEC volumes were associated with larger absolute distance errors ($t(1,60)= -2.96$, $p<0.01$, $R^2=0.47$), while hippocampal volume showed a trend toward an association with absolute distance errors ($t(1,60)=-2.29$, $p<0.05$, $R^2=0.47$) but did not survive multiple comparison correction. No ROI volume was predictive of either proportional linear or proportional angular errors. The results for PIT distance error are summarised in table 4.4 and Figure 4.4.

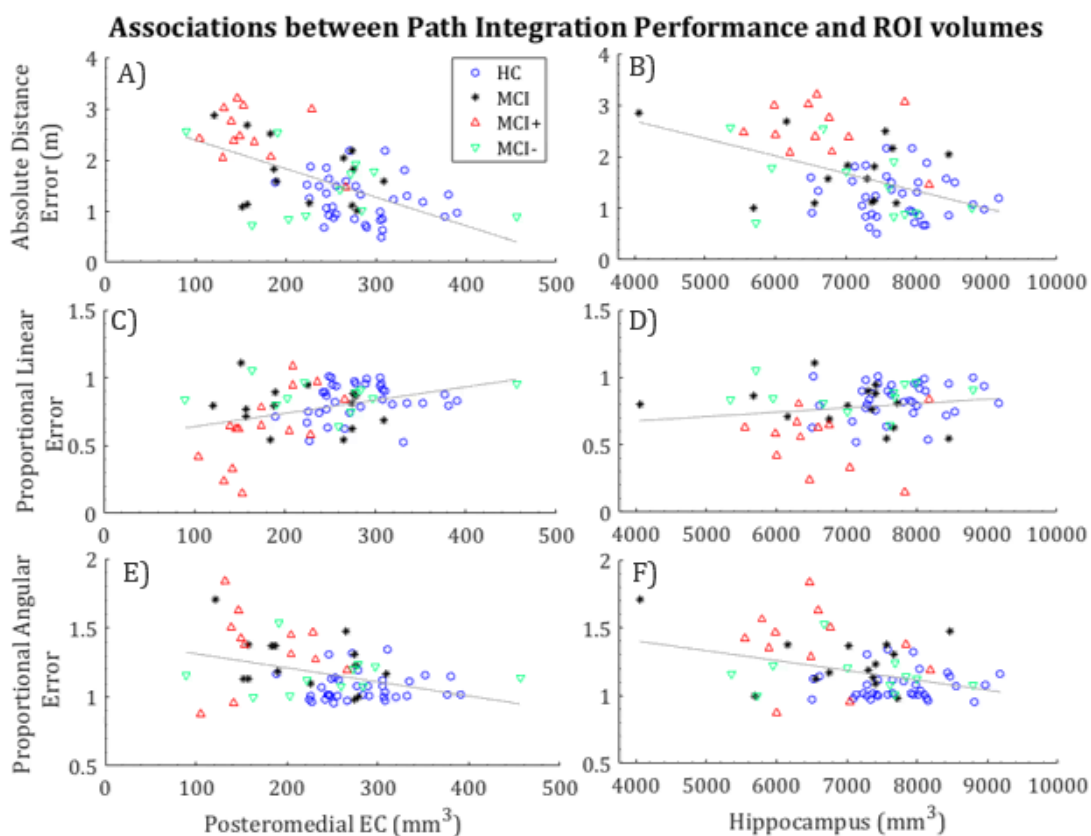


Figure 4.4. Association between path integration outcome measures and regions of interest (ROIs) Bilateral posteromedial entorhinal cortex (A, C, E) and hippocampus (B, D, F) volumes are displayed on the x-axis against absolute distance errors (A, B), proportional linear errors (C, D) and proportional angular errors (E, F) on the y-axis. Least square lines are across all participants.

VBM analysis across all participants revealed no association between GM and PIT performance using a cluster FWE $p < 0.05$. Using an exploratory uncorrected statistical threshold of $p < 0.001$ across HCs and MCI revealed correlations between absolute distance errors and GM values in the left thalamus. Neither proportional linear and proportional angular error were associated with any GM values.

Table 4.5. Univariate statistics summary of ROIs and PIT/OLT performance.

Path integration task performance												
	<i>Absolute Distance error</i>				<i>Proportional Angular Error</i>				<i>Proportional Linear Error</i>			
	β	SE	t	p	β	SE	t	p	β	SE	t	p
Entorhinal Cortex	0.07	0.14	0.55	0.58	0.05	0.04	1.17	0.25	-0.01	0.04	-0.27	0.79
Posteromedial EC	-0.32	0.11	-2.96	0.004	-0.06	0.03	-1.92	0.06	0.07	0.04	2.00	0.06
Isthmus cingulate	0.09	0.08	1.24	0.22	0.04	0.02	1.86	0.07	-0.01	0.02	-0.31	0.76
Hippocampus	-0.24	0.11	-2.29	0.03	-0.06	0.03	-1.96	0.06	0.01	0.03	0.27	0.79
<i>F(8,60) = 3.71, p<0.01, R² = 0.47</i>				<i>F(8,60) = 3.71, p<0.01, R² = 0.33</i>				<i>F(8,60) = 1.86, p>0.05, R²=0.19</i>				
Object Location Task Performance												
	<i>Object Replacement Subtask</i>				<i>Object Recognition Subtask</i>				<i>Object-Context Subtask</i>			
	β	SE	t	p	β	SE	t	p	β	SE	t	p
Entorhinal Cortex	0.20	0.16	1.28	0.21	-0.09	0.05	-1.86	0.07	-0.16	0.07	-2.10	0.04
Anterolateral EC	-0.25	0.13	-1.94	0.06	0.06	0.04	1.53	0.13	0.23	0.06	3.63	<0.001
BA35	0.04	0.08	0.42	0.68	-0.02	0.03	-0.83	0.41	-0.07	0.04	-1.80	0.08
Hippocampus	-0.06	0.07	-0.80	0.46	0.41	0.02	3.94	<0.001	-0.02	0.03	-0.62	0.54
<i>F(8,34) = 5.26, p<0.001, R² = 0.55</i>				<i>F(8,34) = 2.87, p<0.05, R² = 0.40</i>				<i>F(8,34) = 3.53, p<0.01, R² = 0.45</i>				

Table 4.6. Associations between ROIs and iVR performance. Multiple regression models were used to identify which ROI was associated with which outcome measure/subtask following multivariate regression. Emboldened p values were significant predictors of the given outcome measure.

4.3.5. Association between ROI volumetry and object-location task performance

Multivariate analysis examined the relationship between ROIs (aIEC, hippocampus and BA35) and OLT performance (absolute distance error in object replacement and percentage correct in object recognition and object-context association subtasks) across all participants. It was found that OLT performance was predicted by aIEC (PT=0.31, $F(3,33)=4.86$, $p<0.05$) and hippocampal (PT=0.33, $F(3,33)=5.35$, $p<0.01$) volumes. The results for absolute distance error are shown in table 4.4 and Figure 4.6. No volume was associated with absolute distance errors across the object replacement subtask. Larger hippocampal volumes ($t(1,34)=3.94$, $p<0.001$, $R^2=0.4$) were predictive of more correct responses in the object recognition subtask, whereas the proportion of correct responses in the object-environment association subtask was predicted by larger aIEC ($t(1,34)=3.63$, $p<0.01$, $R^2=0.45$).

VBM analysis revealed that, at FWE $p<0.05$ threshold, object recognition performance (% correct) was correlated with GM voxel values in the left hippocampus and left parahippocampal gyrus. However, neither absolute distance errors in the object replacement subtask nor percentage correct in the

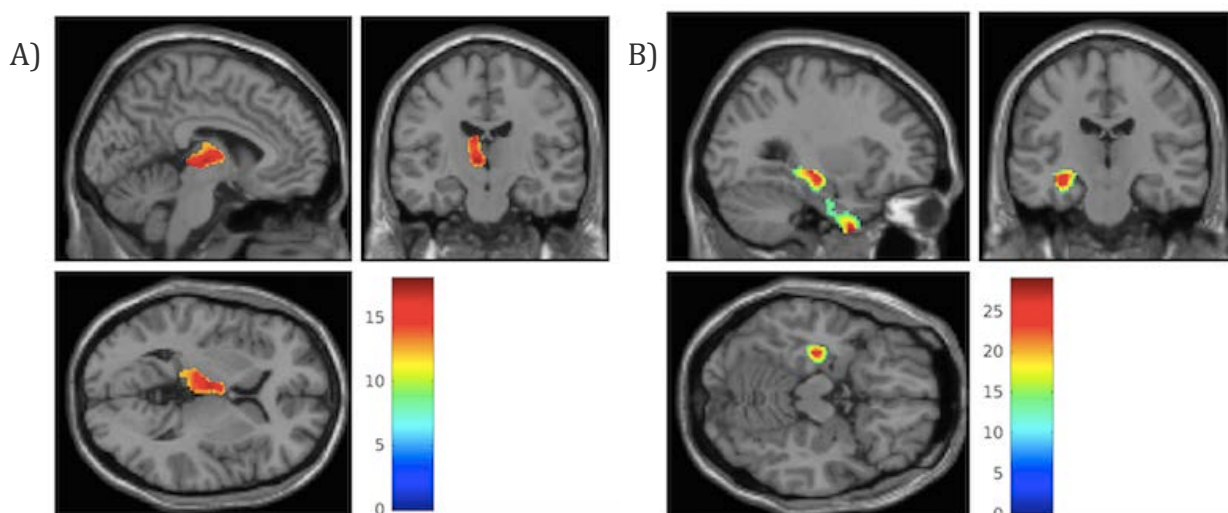


Figure 4.5. Grey matter regions associated with iVR performance. Regions of grey matter associated with absolute distance errors in the path integration task (A) and percentage of correct responses in the object recognition subtask of the OLT (B) using an uncorrected threshold of $p<0.001$.

object-context associations were predictive of any changes in GM at either a corrected FWE threshold of $p < 0.05$ or uncorrected threshold of $p < 0.001$.

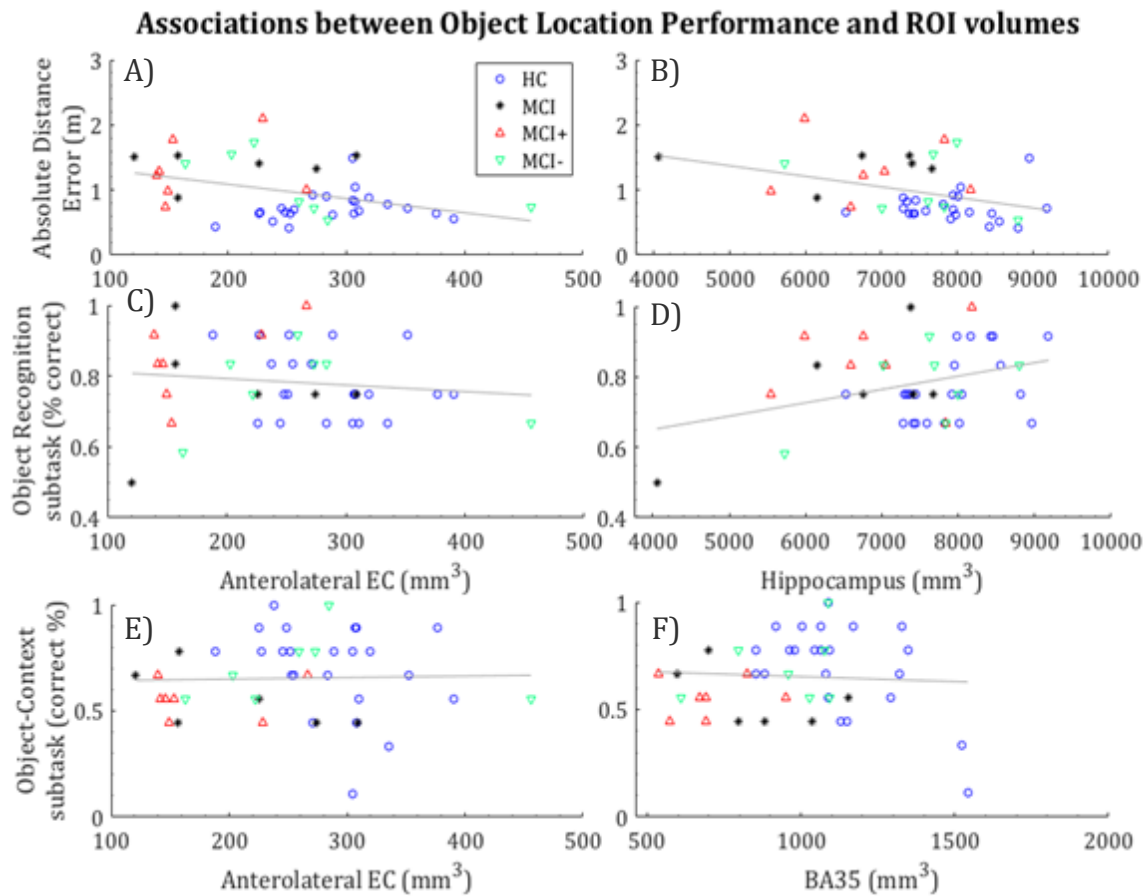


Figure 4.6. Associations between object location performance and regions of interest (ROIs) across all participants (raw data). Absolute distance errors (A, B) were not associated with either aLEC (A) or hippocampal volumes (B), whereas the percentage correct in the object recognition task (C, D) was associated with hippocampal volume (D) but not with aLEC volume (C). Correct object-environment associations were associated with both aLEC (E) and BA35 volumes (F).

4.3.6. Classification Accuracy

The classification accuracy of ROI volumes for differentiating MCI and AD from HCs, AD from MCI and MCI+ from MCI- was assessed using a linear discriminant analysis with 10 fold cross validation and bootstrapped with 1000 replicates, with results summarised in table 4.6. It was found that the most sensitive and specific classifiers of AD pathology were total EC and BA35 volume, exhibiting perfect differentiation of AD from HCs (AUC=1, confidence interval (CI): 1-1). BA35 volume differentiated AD from MCI patients with the highest accuracy (AUC= 0.88

CI: 0.76-0.94), whereas the best classifiers of MCI+ from MCI- groups were pmEC volume (AUC= 0.60, CI=0.34-0.8) and BA35 volume (AUC= 0.60, CI=0.37-0.83) though neither performed much better than chance.

Performance on the iVR tasks was combined with volumetric MRI measures to assess whether this improved the classification of MCI from HCs (Figure 4.7). Not all participants had MRI scans available, so the sample sizes and classifications presented differ from those outlined in chapters 2 and 3. For the path integration task, a marginal improvement in the classification of MCI from HCs on the basis of absolute distance errors (AUC= 0.76 CI: 0.62-0.86) was observed with the addition of pmEC (AUC= 0.79, CI: 0.65, 0.88) and hippocampal volumes (AUC=0.79, CI: 0.65-0.88), and this marginal increase in classification accuracy (0.03) related to proportional linear (AUC increase = 0.05) and proportional angular errors (AUC increase = 0.03). For the OLT, the addition of alEC volumes marginally decreased the classification accuracy of detecting MCI from absolute distance errors in the object-replacement subtask (baseline: AUC= 0.86, full AUC= 0.84 CI: 0.61-0.93). However, compared to baseline, the addition of alEC volumes significantly improved the classification accuracy of both object recognition (baseline: AUC= 0.51, full AUC= 0.79 CI: 0.63-0.9) and object-context association memory (baseline AUC= 0.61, full AUC= 0.80, CI: 0.63-0.93). The effect of combining volumetric measurements with iVR performance to the classification of MCI+ from MCI- could not be evaluated owing to the small sample size; models were unstable and cross-validation could not be performed.

Classifier	MCI vs HCs			MCI+ vs MCI-			AD vs HC			AD vs MCI		
	AUC	Sens	Spec	AUC	Sens	Spec	AUC	Sens	Spec	AUC	Sens	Spec
EC	0.88	0.83	0.74	0.59	0.83	0.62	1	1	1	0.81	0.20	1
pmEC	0.81	0.61	1	0.60	0.75	0.62	0.99	0.93	0.97	0.79	0.47	0.94
alEC	0.84	0.87	0.66	0.55	0.67	0.69	0.99	0.87	0.97	0.81	0.40	0.98
Hippocampus	0.77	0.67	0.84	0.56	0.62	0.68	0.95	0.80	0.95	0.75	0.40	0.96
BA35	0.86	0.94	0.66	0.60	0.50	0.85	1	1	1	0.88	0.40	0.96

Table 4.7. Classification accuracy of regions of interest across group. Abbreviations = AUC = Area under the receiver operating characteristic curve, Sens = Sensitivity, Spec = specificity.

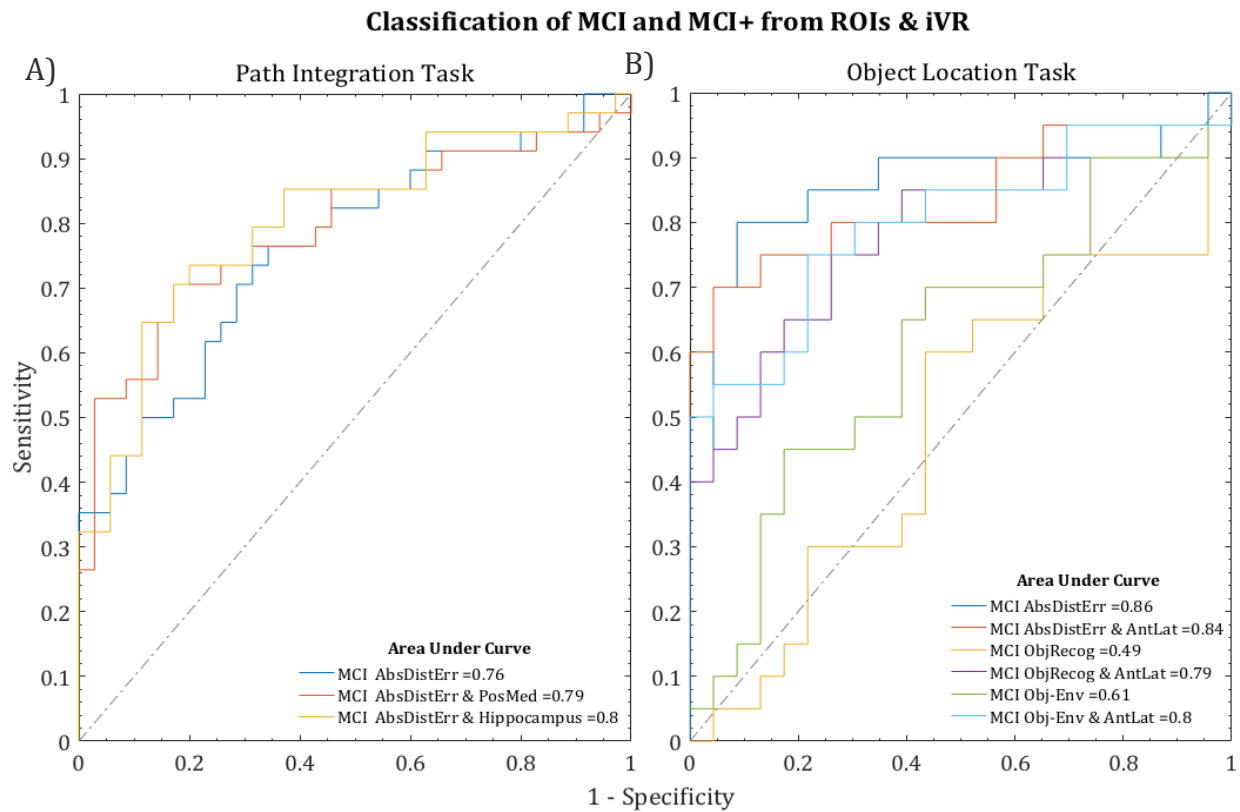


Figure 4.7. Receiver operating characteristic (ROC) curve for iVR tasks combined with ROI volumetry. A) Classification accuracy of absolute distance errors in the path integration task with and without ROIs (pmEC and hippocampus) of MCI versus HCs (positive class = MCI). **B)** Classification accuracy of absolute distance errors with and without ROIs (pmEC and hippocampus) for absolute distance errors in the object replacement subtask and correct percentage in object-recognition and object-environment association subtasks.

4.4. Discussion

This study provides support for the functional specialisation of entorhinal cortex subdivisions and its impairment in MCI and early AD dementia. In line with the existing literature, MCI and AD dementia patients had reduced volumes in all manually segmented regions of interest (ROI) including both EC subdivisions (alEC and pmEC), total EC and BA35. EC volumes exhibited high classification accuracy for differentiating MCI (AUC=0.88) and AD dementia (AUC=1) from HCs, whereas BA35 volumes were highly accurate in differentiating AD dementia from MCI patients (AUC= 0.88). Reduced volumes across all ROIs were observed in MCI patients with AD positive biomarkers (MCI+), compared to MCI patients with AD negative biomarkers (MCI-), however these did not survive planned comparisons and did not differentiate prodromal AD with a high degree of accuracy (best classifier was BA35 (AUC= 0.6)). In line with the primary study hypothesis, path integration performance was strongly predicted by pmEC volumes across all participants, although VBM analyses indicated that left thalamic GM was most predictive of path integration errors across the whole brain. Performance in the OLT was predicted by alEC volumes, although no association was observed between alEC volumes and object-replacement accuracy. However larger hippocampal and alEC volumes were associated with object-context association and object recognition memory, respectively. Taken together these study findings provide further support for the notion of functional deficits occurring before structural atrophy in the pathophysiology of AD.

The present study found atrophy of the EC and BA35 in patients with MCI and AD dementia, in line with previous research (Juottonen *et al.*, 1998; Killiany *et al.*, 2002; Pennanen *et al.*, 2004; Devanand *et al.*, 2007, 2012). In line with the study hypothesis both alEC and pmEC volumes were progressively smaller from HCs to MCI to AD dementia. These findings may have relevance in developing imaging biomarker measures sensitive to the cortical spread of tau pathology ahead of significant cognitive decline (Olsen *et al.*, 2017). In contrast to the pattern of degeneration anticipated by Braak staging (Braak and Braak, 1991, 1995), BA35 (encompassing the transentorhinal cortex) was not significantly more atrophied than other ROIs in MCI+ patients, consistent with other research (Krumm *et al.*,

2016), although other studies demonstrated a pronounced difference (Tward *et al.*, 2017b; Kulason *et al.*, 2019b). It is possible that these discrepant findings reflect differences in measurement protocols relating to the anatomical heterogeneity of this brain region and the lack of any harmonised segmentation protocol for BA35 (e.g. (Krimer, 1997; Insausti *et al.*, 1998; Augustinack *et al.*, 2013; Berron *et al.*, 2017b). However, the possibility that BA35 volume may be a marker of early AD is reinforced by recent research employing the Krimer *et al.* (1997) segmentation protocol at 11T which found greater changes in the thickness of the transentorhinal cortex than in the mEC in prodromal AD patients compared with HCs (Kulason *et al.*, 2019a). In the present study the partial segmentation protocol revealed approximately equal volume loss across the aLEC and pmEC. However given the variance associated with the volumetric measurements and the heterogeneity of MCI this evidence is not sufficient to reject the hypothesised anterolateral-posteromedial atrophic patterning postulated in prodementia AD. Nevertheless this finding is surprising given that metabolic deficits in the IEC are highly predictive of conversion to AD dementia in asymptomatic individuals (Khan *et al.*, 2013), however the rate and patterning of atrophy may be more apparent in the pre-MCI stages of AD as symptomatic patients are likely to have significant atrophy at clinical presentation (Braak and Del Tredici, 2015). Lastly, VBM analysis revealed substantial grey matter atrophy in the left parahippocampal gyrus, supramarginal gyrus, putamen and bilateral hippocampus of AD patients compared to controls in line with previous research (Grignon *et al.*, 1998; Hirata *et al.*, 2005; De Jong *et al.*, 2008; Yang *et al.*, 2012).

Consistent with the study hypothesis, pmEC volumes were negatively associated with absolute distance errors in the path integration task, contrasting with the lack of association with the hippocampus, total EC and isthmus cingulate, as a proxy of the retrosplenial cortex (RSc), all of which didn't survive multiple comparisons. To the author's knowledge, this is the first demonstration that reduced pmEC volumes are associated with impaired path integration in humans, and is consistent with previous research demonstrating a negative association between EC thickness and path integration errors in MCI and AD dementia patients (Mokrisova *et al.*, 2016). Importantly, these findings reinforce previous

work that the EC is critically involved in PI analogous to the rodent mEC (McNaughton *et al.*, 2006; Knierim *et al.*, 2014), and that PI in prodromal AD is primarily related to pmEC dysfunction. The trend toward a negative correlation between hippocampal volume and absolute distance errors is consistent with the higher level spatial processes of the hippocampus (Wolbers *et al.*, 2007) and the deficits observed in temporal lobectomy patients (Worsley *et al.*, 2001). Interestingly, VBM analyses revealed an association with absolute distance errors and grey matter voxel values in the right anterior thalamus. Along with the EC and subiculum, the thalamus contains a high density of head-direction cells (Taube, 1995) that encode horizontal head movements in humans (Kim and Maguire, 2019) that are integral to accurate path integration (Frohardt *et al.*, 2006; Valerio and Taube, 2012). This novel finding may reflect the cognitive impairments associated with thalamic degeneration in MCI (Pedro *et al.*, 2012; Yi *et al.*, 2016) or the spatial disorientation specific to AD dementia (Aggleton *et al.*, 2016). However, a more targeted approach to examining these findings is required given the disparate functions of thalamic nuclei and their later degeneration in the pathogenesis of AD (Braak staging (iv - v)).

Performance across all subtasks of the OLT were predicted by bilateral aIEC and hippocampal volumes. To the author's knowledge, this is the first report that aIEC volumes were associated with an iVR object-location task in humans, and is line with the study's hypothesis and the role of the IEC as a convergent point of anterotemporal networks (Ranganath and Ritchey, 2012). The IEC is postulated to bind object-specific spatial and non-spatial information (Deshmukh and Knierim, 2011; Tsao *et al.*, 2013) as demonstrated by lesion studies (Keene *et al.*, 2016), that indicate that aIEC function extends beyond object discrimination. Given the hippocampus' postulated role as a binding site of object, spatial and temporal information the observation that hippocampal volumes were predictive of OLT performance has face validity. However contrary to the study hypothesis, performance in the object replacement subtask was not associated with aIEC volumes or any other ROIs, although a non-significant trend in aIEC volume was observed. This is surprising given that previous research demonstrated that EC

volumes are associated with object-replacement accuracy in a continuous-measure object replacement task across HCs and MCI (Hampstead *et al.*, 2018).

The finding that object-environment memory was predicted by aIEC volumes supports the notion that the IEC is critical for the integration of event ‘content’ (Knierim *et al.*, 2014) and corroborates impairments in the formation of complex object-environment associations and object-orientated spatial processing induced by IEC lesions (Hunsaker and Kesner, 2013; Wilson *et al.*, 2013b; Kuruvilla and Ainge, 2017b). The present study found no association between object-environment association memory (Charles *et al.*, 2004; Jo and Lee, 2010; Watson *et al.*, 2012; Wilson *et al.*, 2013b) and BA35 volumes, however the role of BA35 may be more important in short-term and working memory tasks (Buffalo *et al.*, 2006; Bellgowan *et al.*, 2009a; Watson *et al.*, 2012) and less relevant to tasks with longer delays. The positive association between object recognition memory and hippocampal volumes coincides with the deficits induced by hippocampal lesions (Broadbent *et al.*, 2004; Fortin *et al.*, 2004) especially in tasks requiring a longer delay (Cohen and Stackman, 2015). However the role of the hippocampus in recognition memory is increasingly understood to depend on the qualia and binding demands of the stimuli (see Bird (2017) for review) with a number of studies demonstrating no effect of hippocampal lesions on object recognition (Bussey *et al.*, 2000a; Winters *et al.*, 2004; Good *et al.*, 2007; Langston and Wood, 2010) suggesting such representations are processed upstream of the hippocampus in BA35/perirhinal cortex (Xiang and Brown, 1998; Bussey *et al.*, 2000b; Norman and Eacott, 2004; Winters *et al.*, 2004; Bussey and Saksida, 2005). It may be that object recognition becomes dependent on the hippocampus when temporal order or spatial context is important (Agster *et al.*, 2002; Fortin *et al.*, 2002; Barker and Warburton, 2011b). Given that the OLT required conjunctive object x position x environment encoding, these findings support the central role of the hippocampus in complex object recognition memory (Mayes *et al.*, 2002; Yonelinas *et al.*, 2019) and particularly the right hemisphere (Kessels *et al.*, 2002; Postma *et al.*, 2008). Although contrary to the study hypothesis and the findings of other object-discrimination tasks (Schultz *et al.*, 2012; Reagh and Yassa, 2014; Reagh *et al.*, 2017, 2018; Berron *et al.*, 2018b), aIEC volumes were not predictive

of object recognition memory performance. Collectively, these findings support the role of the aEC in object-oriented spatial binding that is not explained by BA35 or hippocampal volume and is impaired in response to aEC atrophy. Whilst the present study was restricted by its sample size, future research should examine the role of the effect of aEC atrophy and impaired functional connectivity on object-spatial binding that has demonstrable sensitivity to AD pathology in older adults (Berron *et al.*, 2017a; Olsen *et al.*, 2017; Hampstead *et al.*, 2018; Maass *et al.*, 2019)

The classification accuracy of the EC, its subdivisions and BA35 volumes were assessed in their ability to differentiate both MCI and AD dementia patients from HCs, as well as MCI from AD dementia patients. It was found that all manually segmented ROIs demonstrated near perfect classification of AD dementia patients from HCs, outperforming automated segmentation of the hippocampus. The volume of all ROIs were less accurate in classifying AD dementia from MCI patients, although BA35 atrophy encompassing the transentorhinal cortex (Braak stage I), was highly sensitive and specific for AD (AUC= 0.88) in line with previous research (Krumm *et al.*, 2016). As such BA35 volumes may aid in the detection of prodementia AD and may even extend to pre-mci (Figure 4.3D). The manual segmentation of BA35 conferred a marginal benefit in classifying heterogeneous MCI from HCs in line with previous research (Kulason *et al.*, 2019b). Whilst the small sample sizes of the MCI+ and MCI- groups prevented reliable assessment of the ROI's classification accuracy, a trend toward group separation was observed (Figure 4.3A-C), MCI+ patients exhibited more atrophy across all ROIs than MCI- but was most pronounced in the EC, taken as a whole. The differentiation of prodromal AD based on EC/BA35 atrophy is likely to be more specific to underlying AD than whole brain (Hojjati *et al.*, 2018) or hippocampal-based approaches (Miller *et al.*, 2015; Long *et al.*, 2017), both of which are affected by other neurodegenerative dementias. Conflicting with the study hypothesis, the addition of volumetric measurements to iVR task performance did not improve classification accuracy of either the PIT or OLT. One explanation for this is that both pmEC and aEC explain similar variance as PIT and OLT performance thereby restricting improvements in classification accuracy, though this needs to be

examined in larger samples. In contrast, the classification accuracy of both object recognition and object-environment memory was significantly improved with the addition of aIEC volumes, attributable to the poor classification accuracy of either subtask at baseline and the relatively high accuracy of ROI measures. Taken together, these results complement previous research showing that parahippocampal gyrus atrophy is sensitive and specific to AD. However the detection of structural changes may not be sufficiently sensitive to detect the cellular dysfunction occurring in incipient AD which may manifest as deficits in metabolism (Khan *et al.*, 2014) or functional connectivity within the EC's disparate networks (Maass *et al.*, 2019). Whilst the addition of aIEC/pmEC volumes did not improve the classification accuracy of iVR performance in the present study, such measures may explain unique variance and thus aid in the detection of preclinical AD populations in future research.

This main limitation of this study was the small sample of patients in each group. This confounds the precision of the analysis of the EC's structure and function in prodromal AD as well as the classification analysis, both of which require replication in larger datasets. As such the classifications reported here require replication with larger sample sizes. The manual segmentation protocol exhibited very high inter- and intra-rater reliability, and was conducted blinded where possible, however manual segmentation in clinical populations could be biased by observable ventricular expansion/cortical degeneration. Whilst the partial segmentation protocol of aIEC and pmEC was predictive of OLT and PIT performance respectively, these results would be improved by applying a complete segmentation protocol for these subdivisions, but this is complicated by the absence of reliable landmarks marking the progressive aI/pm EC boundary. Manual segmentation of EC subdivision volumes more labour-intensive than automated approaches and is reliant on high-resolution imaging that is highly susceptible to motion artefacts. Finally VBM analysis, an approach that is not without criticism (see Bookstein (2001) but also Ashburner and Friston (2001)) enabled a hypothesis-free approach to assessing between group differences in macroscopic tissue morphometry and relating such differences to performance on iVR tasks. This approach revealed brain regions that were not part of the *a priori*

ROIs for this study, for example thalamic nuclei in PIT, and warrant further investigation with their own targeted approach.

In conclusion, this study demonstrated that the EC, its subdivisions and BA35 volumes are sensitive and specific for differentiating MCI and AD dementia patients from HCs but their sensitivity and specificity for prodromal AD could not be sufficiently evaluated with the limited sample size. Atrophy in the posteromedial EC was associated with deficits in path integration, whereas anterolateral EC and hippocampal atrophy were predictive of performance across object-location subtasks. Specifically, smaller hippocampal and anterolateral EC volumes were predictive of impaired object recognition and object-context memory, respectively, whereas no ROI predicted object replacement accuracy. This work supports the claims that the iVR tasks outlined in chapters two and three are dependent on the disparate functions of EC subdivisions and that greater volume loss is associated with worse performance in both tasks.

Chapter 5 - Discussion

The aim of this study was to test the hypothesis that tests based on the functions of the entorhinal cortex (EC) may aid in the detection of early Alzheimer's disease (AD). Immersive virtual reality tests were used to examine performance in path integration (PIT) and object location (OLT), as respective functions of the posteromedial and anterolateral EC, with the association between task performance and the volumetry of each EC subdivision additionally evaluated. Consistent with the postulated roles of EC subdivisions in navigation and object-oriented processing, larger performance errors across the PIT and OLT were associated with smaller pmEC and aLEC volumes, respectively. MCI patients were impaired in both the PIT and OLT compared to healthy controls, performance on each of these tasks outperformed individual and composite comparator cognitive tests in the classification of MCI. Critically, the PIT differentiated MCI patients at increased risk of developing AD dementia with greater sensitivity and specificity than a composite of gold standard neuropsychological tests currently used in clinical and research practice. Lastly, PIT performance was predicted by both amyloid and tau CSF levels, whereas neither pathological hallmark predicted performance across OLT subtasks.

This work indicates that tests based around theories of EC function have potential diagnostic value for the detection of MCI and prodromal AD. The spatial tasks used in this study were not only better classifiers of prodromal AD (PIT) and MCI (OLT) than 'traditional' neuropsychological tests but fulfil the unmet need for more ecologically valid cognitive assessments in patient screening and as potential outcome measures in prospective clinical trials (see Harvey *et al* (2017) for review). Path integration and object location are phylogenetically conserved behaviours that can be operationalised to causatively evaluate the effect of pathology on cell physiology with direct application to behaviour. The mechanistic insight offered by such an approach has important implications for resolving the current discontinuity in outcome measures between preclinical animal and human clinical trials. This lack of translational continuity may partially explain the

large disparity in treatment efficacy across species; a plethora of preclinical trials have demonstrated significant reduction in pathological hallmarks and improved cognition only, however no such effects have been replicated in humans to date (Cummings, 2018). Given that the PIT not only differentiates MCI due to prodromal AD, but is associated with EC subfield volumetry and with CSF measures of pathology, similar tasks may eventually be used as part of a wider neuropsychological battery to track the spread of pathology and consequent neuronal impairment in the earliest stages of AD. Immersive virtual reality systems (iVR) are a candidate modality for such translational research given their increasing use in spatial tasks across both animals (Thurley and Ayaz, 2016; see Tennant *et al* (2018) or Minderer *et al* (2016) for reviews) and humans (Diersch and Wolbers, 2019). This work therefore adds to the growing literature that demonstrates the diagnostic value of spatial cognitive tasks, this is of particular importance given that spatial behaviours may be overlooked in the clinical assessment of early AD (Coughlan. *et al.*, 2018). This cross-sectional work should therefore be considered preliminary and requires replication in larger cohorts across cultures before robust recommendations for clinical practice can be made.

This work is not without limitations. The samples used in all experiments were small and not representative of the population as a whole. On average participants spent more years in education and had higher socioeconomic status than is representative of their demographic, this limits the generalisation of these results as patients may have higher 'cognitive reserve' than would be representative (Cabeza *et al.*, 2018). Furthermore, patients were recruited from an academic memory clinic with more resources than non-specialist services, as such these patients likely exhibit less severe symptoms than would be captured by random sampling. This is particularly important given that a significant percentage of MCI patients revert back to normal cognition after one year (Koepsell and Monsell, 2012) and this reversion rate is far greater in community-based studies compared to clinic-based studies (Malek-Ahmadi, 2016). CSF biomarkers have been demonstrated to be highly sensitive and specific in aiding the detection of prodromal AD (Jack *et al.*, 2013), however the current study is unable to

differentiate patients with mixed dementia or posterior variants from 'typical' AD. For the purposes of this thesis patients with a diagnosis of mild cognitive impairment with negative AD biomarkers were categorised as AD negative, however these patients do not represent a homogeneous group and may encompass a range of aetiologies and varying degrees of amyloid/tau pathology, each likely to explain variance in iVR tasks and MRI measures. The present study was unable to control for such effects within the MCI- cohort. Whilst efforts were made to blind the researcher to the CSF status of the patient this was not always possible, as such we cannot completely exclude the impact of bias in either testing or recruiting patients. Future research should therefore seek to replicate this work in a double-blind manner.

The application of iVR enabled experimental manipulations that would not otherwise be experimentally viable, for example real world movement, 3D environments and control of local/global environmental cues was crucial for both tasks. However, whilst iVR accommodated these prerequisites and controlled problematic confounding variables, it also created other unforeseen difficulties such as the exclusion of frail or disabled participants. The development of desktop versions of these tasks would overcome such exclusions and have greater scalability as a clinical tool, furthermore this would permit the examination of the neural correlates of these tasks using fMRI. Such an approach is further supported by the mounting evidence indicating that spatial cells are recruited in spatial tasks even in the absence of active movement (Kunz *et al.*, 2015; Qasim *et al.*, 2018; Stangl *et al.*, 2018a). Indeed non-iVR spatial tests based around the function of the EC have demonstrated sensitivity to the presence of abnormal AD biomarkers (Kunz *et al.*, 2015; Moodley *et al.*, 2015; Allison *et al.*, 2016; Berron *et al.*, 2018a; Maass *et al.*, 2018a, 2019). However these practical limitations of iVR may be resolved with the next generation of VR technologies, a prediction that is reflected in the increasing integration of VR devices into the research milieu (Diersch and Wolbers, 2019; Clay *et al.* (submitted)) including: 'gamified' epidemiology of spatial cognition (Sea Hero quest; Coutrot *et al.*, 2019), cognitive training (Doniger *et al.*, 2018), 'daily living' tasks (Seo *et al.*, 2017), quality of life enrichment (Hodge *et al.*, 2018), and public engagement (<https://www.awalkthroughdementia.org/>,

Alzheimer's Research UK). However iVR may be superseded with the advent of augmented reality offering similar advantages without the limitations of iVR equipment (Vovk *et al.*, 2019) and has already demonstrated value in understanding the calibration of path integration in rodents (Jayakumar *et al.*, 2019).

This work provides evidence and proof of concept for the utility of the spatial-clinical approach, future research should therefore seek to preserve and extend such translational research. Such an approach will aid our understanding of the effect of pathology on cell physiology and its manifestation in cognitive and behavioural impairments that may manifest in the very earliest stages of AD. Going forwards, the PIT will be evaluated in a longitudinal study examining individuals at high risk of dementia (PREVENT, Ritchie and Ritchie (2012)), performance will be related to both EC atrophy (7T MRI) and the topographical distribution of pathology ($a\beta$ /tau PET). Such comparisons are vital to better inform the relationship between disease staging, the spatiotemporal deposition of pathology and PIT performance, as well as the PIT's predictive value. As such this on-going research will serve as the litmus test for the PIT's sensitivity to the presence of preclinical AD in asymptomatic individuals.

This thesis sought to examine the function and structure of the entorhinal cortex (EC) in mild cognitive impairment. Immersive virtual reality tasks based around the disparate function of the EC's subdivisions demonstrated considerable value in aiding the detection of MCI and prodromal AD above 'gold standard' neuropsychological tests. Performance in the PIT and OLT was related to the posteromedial and anterolateral EC, these findings support the central role of the EC in spatial cognition that are compromised in cognitive impairment. The findings presented here have implications not just for early diagnosis but also for translational AD research aimed at understanding mechanistic links between impaired cell activity and behaviour in AD. The tasks used in this study, combined with analogous navigation tasks in animal models of AD, would help address the need for outcome measures capable of comparing treatment effects across

preclinical and clinical phases of future treatment trials aimed at delaying or preventing the onset of dementia.

References

- Adamo DE, Briceño EM, Sindone JA, Alexander NB, Moffat SD. Age differences in virtual environment and real world path integration [Internet]. *Front. Aging Neurosci.* 2012; 4
- Aggleton JP, Pralus A, Nelson AJD, Hornberger M. Thalamic pathology and memory loss in early Alzheimer's disease: Moving the focus from the medial temporal lobe to Papez circuit. *Brain* 2016; 139: 1877–1890.
- Aghajan Z, Schuette P, Fields TA, Tran ME, Siddiqui SM, Hasulak NR, et al. Theta Oscillations in the Human Medial Temporal Lobe during Real-World Ambulatory Movement. *Curr. Biol.* 2017; 27: 3743-3751.e3.
- Agrawal Y. Editorial: Age-related vestibular loss: Current understanding and future research directions. *Front. Neurol.* 2017; 8: 231.
- Agster KL, Fortin NJ, Eichenbaum H. The hippocampus and disambiguation of overlapping sequences. *J. Neurosci.* 2002; 22: 5760–5768.
- Ahmed Z, Cooper J, Murray TK, Garn K, McNaughton E, Clarke H, et al. A novel in vivo model of tau propagation with rapid and progressive neurofibrillary tangle pathology: The pattern of spread is determined by connectivity, not proximity. *Acta Neuropathol.* 2014; 127: 667–683.
- Albasser MM, Davies M, Futter JE, Aggleton JP. Magnitude of the object recognition deficit associated with perirhinal cortex damage in rats: Effects of varying the lesion extent and the duration of the sample period. *Behav. Neurosci.* 2009; 123: 115.
- Albert MS, Dekosky ST, Dickson D, Dubois B, Feldman HH, Fox NC, et al. The diagnosis of mild cognitive impairment due to Alzheimer's disease: Recommendations from the National Institute on Aging-Alzheimer's Association workgroups on diagnostic guidelines for Alzheimer's disease. *Alzheimer's Dement.* 2011; 7: 270–279.
- Allen G, Barnard H, McColl R, Hester AL, Fields JA, Weiner MF, et al. Reduced hippocampal functional connectivity in Alzheimer disease. *Arch. Neurol.* 2007; 64: 1482–1487.
- Allen GL, Kirasic KC, Rashotte MA. Aging and path integration skill : Kinesthetic

and vestibular contributions to wayfinding. 2004; 66: 170–179.

Allison SL, Fagan AM, Morris JC, Head D. Spatial Navigation in Preclinical Alzheimer's Disease. *J. Alzheimer's Dis.* 2016; 52: 77–90.

Andreasen NC, Arndt S, Cohen G, Alliger R, Swayze VW. Correction for head size. *Psychiatry Res. Neuroimaging* 1993; 50: 283.

Andrews-Hanna JR, Reidler JS, Sepulcre J, Poulin R, Buckner RL. Functional-Anatomic Fractionation of the Brain's Default Network. *Neuron* 2010; 65: 550–562.

Apostolova LG, Hwang KS, Medina LD, Green AE, Braskie MN, Dutton RA, et al. Cortical and hippocampal atrophy in patients with autosomal dominant familial Alzheimer's disease. *Dement. Geriatr. Cogn. Disord.* 2011; 32: 118–125.

Ashburner J, Friston KJ. Why Voxel-based morphometry should be used. *Neuroimage* 2001; 14: 1238–1243.

Association A. 2015 Alzheimer's disease facts and figures. *Alzheimer's Dement.* 2015; 11: 332–384.

Astur RS, Taylor LB, Mamelak AN, Philpott L, Sutherland RJ. Humans with hippocampus damage display severe spatial memory impairments in a virtual Morris water task. *Behav. Brain Res.* 2002; 132: 77–84.

Atienza M, Atalaia-Silva KC, Gonzalez-Escamilla G, Gil-Neciga E, Suarez-Gonzalez A, Cantero JL. Associative memory deficits in mild cognitive impairment: The role of hippocampal formation. *Neuroimage* 2011; 57: 1331–1342.

Augustinack JC, Van Der Kouwe AJW, Fischl B. Medial temporal cortices in ex vivo magnetic resonance imaging. *J. Comp. Neurol.* 2013; 521: 4177–4188.

Avila J, Lucas JJ, Perez M, Hernandez F. Role of tau protein in both physiological and pathological conditions. *Physiol. Rev.* 2004; 84: 361–384.

Awipi T, Davachi L. Content-Specific Source Encoding in the Human Medial Temporal Lobe. *J. Exp. Psychol. Learn. Mem. Cogn.* 2008; 34: 769–779.

Bäckman L, Small BJ, Fratiglioni L. Stability of the preclinical episodic memory deficit in Alzheimer's disease. *Brain* 2001; 124: 96–102.

Badhwar A, Tam A, Dansereau C, Orban P, Hoffstaedter F, Bellec P. Resting-state network dysfunction in Alzheimer's disease: A systematic review and meta-analysis. *Alzheimer's Dement. (Amsterdam, Netherlands)* 2017; 8: 73–85.

Banino A, Barry C, Uria B, Blundell C, Lillicrap T, Mirowski P, et al. Vector-based

navigation using grid-like representations in artificial agents [Internet]. *Nature* 2018; 26

Banta Lavenex PA, Colombo F, Lambert FR, Lavenex P. The human hippocampus beyond the cognitive map: Evidence from a densely amnesic patient *The human hippocampus beyond the cognitive map: Evidence from a densely amnesic patient*. *Front. Hum. Neurosci.* 2014; 8: 1–18.

Barbeau E, Didic M, Tramon E, Felician O, Joubert S, Sontheimer A, et al. Evaluation of visual recognition memory in MCI patients. 2004: 1317–1322.

Barber R, Ballard C, McKeith IG, Gholkar A, O'Brien JT. MRI volumetric study of dementia with Lewy bodies: a comparison with AD and vascular dementia. *Neurology* 2000; 54: 1304–1309.

Barese MD, Henson RNA, Lee ACH, Graham KS. Medial temporal lobe activity during complex discrimination of faces, objects, and scenes: Effects of viewpoint. *Hippocampus* 2010; 20: 389–401.

Barker GRI, Bird F, Alexander V, Warburton EC. Recognition memory for objects, place, and temporal order: A disconnection analysis of the role of the medial prefrontal cortex and perirhinal cortex. *J. Neurosci.* 2007; 27: 2948–2957.

Barker GRI, Warburton EC. When is the hippocampus involved in recognition memory? *J. Neurosci.* 2011a; 31: 10721–10731.

Barker GRI, Warburton EC. When is the hippocampus involved in recognition memory? *J. Neurosci.* 2011b; 31: 10721–10731.

Barnes CA, Suster MS, Shen J, McNaughton BL. Multistability of cognitive maps in the hippocampus of old rats. *Nature* 1997; 388: 272–275.

Barnes J, Bartlett JW, van de Pol LA, Loy CT, Scahill RI, Frost C, et al. A meta-analysis of hippocampal atrophy rates in Alzheimer's disease. *Neurobiol. Aging* 2009; 30: 1711–1723.

Barnes J, Ridgway GR, Bartlett J, Henley SMD, Lehmann M, Hobbs N, et al. Head size, age and gender adjustment in MRI studies: A necessary nuisance? *Neuroimage* 2010; 53: 1244–1255.

Bartsch T, Schönfeld R, Müller FJ, Alfke K, Leplow B, Aldenhoff J, et al. Focal Lesions of Human Hippocampal CA1 Neurons in Transient Global Amnesia Impair Place Memory. *Science (80-.)*. 2010; 328: 1412–1415.

Bartzokis G. Age-related myelin breakdown: A developmental model of cognitive

decline and Alzheimer's disease. *Neurobiol. Aging* 2004; 25: 5–18.

Bateman TM. Advantages and disadvantages of PET and SPECT in a busy clinical practice. *J. Nucl. Cardiol.* 2012; 19: 3–11.

Bejanin A, Schonhaut DR, La Joie R, Kramer JH, Baker SL, Sosa N, et al. Tau pathology and neurodegeneration contribute to cognitive impairment in Alzheimer's disease. *Brain* 2017; 140: 3286–3300.

Bellgowan PSF, Buffalo EA, Bodurka J, Martin A. Lateralized spatial and object memory encoding in entorhinal and perirhinal cortices. *Learn. Mem.* 2009a; 16: 433–438.

Bellgowan PSF, Buffalo EA, Bodurka J, Martin A. Lateralized spatial and object memory encoding in entorhinal and perirhinal cortices. *Learn. Mem.* 2009b; 16: 433–438.

Bengoetxea X, Rodriguez-Perdigon M, Ramirez MJ. Object recognition test for studying cognitive impairments in animal models of Alzheimer's disease. *Front. Biosci. - Sch.* 2015; 7S: 10–29.

Bennett EM, Alpert R, Goldstein AC. Communications Through Limited Response Questioning. *Public Opin. Q.* 1954; 18: 303.

Bennett IJ, Golob EJ, Parker ES, Starr A. Memory Evaluation in Mild Cognitive Impairment using Recall and Recognition Tests. 2006

Berron D, Cardenas-Blanco A, Bittner D, Metzger CD, Spottke A, Heneka M, et al. Effects of Age and Tau Measured in Csf on Mnemonic Discrimination of Objects and Scenes in Medial Temporal Lobe Pathways. *Alzheimer's Dement.* 2018a; 14: P207.

Berron D, Cardenas-Blanco A, Bittner D, Metzger CD, Spottke A, Heneka MT, et al. Higher CSF Tau Levels Are Related to Hippocampal Hyperactivity and Object Mnemonic Discrimination in Older Adults. *J. Neurosci.* 2019; 39: 8788–8797.

Berron D, Neumann K, Maass A, Schütze H, Fliessbach K, Kiven V, et al. Age-related functional changes in domain-specific medial temporal lobe pathways. *Neurobiol. Aging* 2018b; 65: 86–97.

Berron D, Schütze H, Cardenas-Blanco A, Fliessbach K, Wagner M, Spottke A, et al. Object and Scene Memory Are Differentially Associated With Csf Markers of Alzheimer'S Disease and Mri Volumetry. *Alzheimer's Dement.* 2017a; 13: P1553–P1554.

Berron D, Vieweg P, Hochkeppeler A, Pluta JB, Ding SL, Maass A, et al. A protocol for manual segmentation of medial temporal lobe subregions in 7 Tesla MRI. *NeuroImage Clin.* 2017b; 15: 466–482.

Beth EH, Budson AE, Waring JD, Ally BA. Response bias for picture recognition in patients with Alzheimer’s disease. 2010; 22: 229–235.

Binder JR, Desai RH, Graves WW, Conant LL. Where is the semantic system? A critical review and meta-analysis of 120 functional neuroimaging studies. *Cereb. Cortex* 2009; 19: 2767–2796.

Bird CM. The role of the hippocampus in recognition memory. *Cortex* 2017; 93: 155–165.

Bird CM, Burgess N. The hippocampus and memory: Insights from spatial processing. *Nat. Rev. Neurosci.* 2008; 9: 182–194.

Bird CM, Chan D, Hartley T, Pijnenburg Y a., Rossor MN, Burgess N. Topographical short-term memory differentiates Alzheimer’s disease from frontotemporal lobar degeneration. *Hippocampus* 2010; 20: 1154–1169.

Bohbot VD, Copara MS, Gotman J, Ekstrom AD. Low-frequency theta oscillations in the human hippocampus during real-world and virtual navigation. *Nat. Commun.* 2017; 8: 14415.

Bolker BM, Brooks ME, Clark CJ, Geange SW, Poulsen JR, Stevens MHH, et al. Generalized linear mixed models : a practical guide for ecology and evolution. 2008: 127–135.

Bookstein FL. ‘Voxel-Based Morphometry’ Should Not Be Used With Imperfectly Registered Images. *Neuroimage* 2001; 14: 1454–1462.

Braak H, Braak E. Neuropathological staging of Alzheimer-related changes. *Acta Neuropathol.* 1991; 82: 239–259.

Braak H, Braak E. Staging of Alzheimer’s disease-related neurofibrillary changes. *Neurobiol. Aging* 1995; 16: 271–278.

Braak H, Del Tredici K. The preclinical phase of the pathological process underlying sporadic Alzheimer’s disease. *Brain* 2015; 138: 2814–2833.

Brandt J, Shpritz B, Munro C a, Marsh L, Rosenblatt a. Differential impairment of spatial location memory in Huntington’s disease. *J. Neurol. Neurosurg. Psychiatry* 2005; 76: 1516–1519.

Bremner JD, Narayan M, Anderson ER, Staib LH, Miller HL, Charney DS.

Hippocampal volume reduction in major depression. *Am. J. Psychiatry* 2000; 157: 115–118.

Broadbent NJ, Gaskin S, Squire LR, Clark RE. 1991-12-XX-Tesis de Miguel Angel Solano-Discontinuidades en guias-v01.pdf. 2004: 5–11.

Brown MW, Barker GRI, Aggleton JP, Warburton EC. What pharmacological interventions indicate concerning the role of the perirhinal cortex in recognition memory. *Neuropsychologia* 2012; 50: 3122–3140.

Buckley MJ, Gaffan D. Perirhinal cortical contributions to object perception. *Trends Cogn. Sci.* 2006; 10: 100–107.

Bucks R, Willison J. Development and validation of the Location Learning Test (LLT): A test of visuo-spatial learning designed for use with older adults and in dementia. *Clin. Neuropsychol.* 1997; 11: 273–286.

Buffalo EA, Bellgowan PSF, Martin A. Distinct roles for medial temporal lobe structures in memory for objects and their locations. *Learn. Mem.* 2006; 13: 638–643.

Burgess N, Spiers HJ, Paleologou E. Orientational manoeuvres in the dark: Dissociating allocentric and egocentric influences on spatial memory. *Cognition* 2004; 94: 149–166.

Burwell RD, Amaral DG. Perirhinal and postrhinal cortices of the rat: Interconnectivity and connections with the entorhinal cortex. *J. Comp. Neurol.* 1998; 391: 293–321.

Bush D, Barry C, Burgess N, Bush D, Barry C, Manson D, et al. Using Grid Cells for Navigation. *Neuron* 2015; 87: 507–520.

Bush D, Bisby JA, Bird CM, Gollwitzer S, Rodionov R, Diehl B, et al. Human hippocampal theta power indicates movement onset and distance travelled. *Proc. Natl. Acad. Sci.* 2017; 114: 12297–12302.

Bussey TJ, Duck J, Muir JL, Aggleton JP. Distinct patterns of behavioural impairments resulting from fornix transection or neurotoxic lesions of the perirhinal and postrhinal cortices in the rat. *Behav. Brain Res.* 2000a; 111: 187–202.

Bussey TJ, Duck J, Muir JL, Aggleton JP. Distinct patterns of behavioural impairments resulting from fornix transection or neurotoxic lesions of the perirhinal and postrhinal cortices in the rat. *Behav. Brain Res.* 2000b; 111: 187–

202.

Bussey TJ, Saksida LM. Object memory and perception in the medial temporal lobe: An alternative approach. *Curr. Opin. Neurobiol.* 2005; 15: 730–737.

Bussey TJ, Saksida LM, Murray EA. Impairments in visual discrimination after perirhinal cortex lesions: Testing ‘declarative’ vs. ‘perceptual-mnemonic’ views of perirhinal cortex function. *Eur. J. Neurosci.* 2003; 17: 649–660.

Bussey TJ, Saksida LM, Murray EA. The perceptual-mnemonic/feature conjunction model of perirhinal cortex function. *Q. J. Exp. Psychol. Sect. B Comp. Physiol. Psychol.* 2005; 58: 269–282.

Buuren V, Kroes MCW, Wagner IC, Genzel L, Morris XGM. Initial Investigation of the Effects of an Experimentally Learned Schema on Spatial Associative Memory in Humans. 2014; 34: 16662–16670.

Cabeza R, Albert M, Belleville S, Craik FIM, Duarte A, Grady CL, et al. Maintenance, reserve and compensation: the cognitive neuroscience of healthy ageing. *Nat. Rev. Neurosci.* 2018; 19: 701–710.

Cacucci F, Yi M, Wills TJ, Chapman P, O’Keefe J. Place cell firing correlates with memory deficits and amyloid plaque burden in Tg2576 Alzheimer mouse model. *Proc. Natl. Acad. Sci. U. S. A.* 2008; 105: 7863–8.

Camicioli R, Moore MM, Kinney A, Corbridge E, Glassberg K, Kaye J a. Parkinson’s disease is associated with hippocampal atrophy. *Mov. Disord.* 2003; 18: 784–790.

Carvalho V, Guimarães H, Beato R, Lima da Silva TB, Yassuda M, Bahia V, et al. The Addenbrooke’s Cognitive Examination-Revised (ACE-R) battery in the diagnoses of mild cognitive impairment, Alzheimer’s disease and frontotemporal dementia. *Alzheimer’s Dement. J. Alzheimer’s Assoc.* 2013; 9: P462.

Van Cauter T, Camon J, Alvernhe A, Elduayen C, Sargolini F, Save E. Distinct roles of medial and lateral entorhinal cortex in spatial cognition. *Cereb. Cortex* 2013; 23: 451–459.

Chadwick MJ, Jolly AEJ, Amos DP, Hassabis D, Spiers HJ. Report A Goal Direction Signal in the Human Entorhinal/Subicular Region. *Curr. Biol.* 2015; 25: 87–92.

Chan D, Fox NC, Scahill RI, Crum WR, Whitwell JL, Leschziner G, et al. Patterns of temporal lobe atrophy in semantic dementia and Alzheimer’s disease. *Ann. Neurol.* 2001; 49: 433–442.

Chao OY, Huston JP, Li JS, Wang AL, de Souza Silva MA. The medial prefrontal

cortex-lateral entorhinal cortex circuit is essential for episodic-like memory and associative object-recognition. *Hippocampus* 2016; 26: 633–645.

Charles DP, Browning PGF, Gaffan D. Entorhinal cortex contributes to object-in-place scene memory. *Eur. J. Neurosci.* 2004; 20: 3157–3164.

Chen J, Duan X, Shu H, Wang Z, Long Z, Liu D, et al. Differential contributions of subregions of medial temporal lobe to memory system in amnesic mild cognitive impairment : insights from fMRI study. *Nat. Publ. Gr.* 2016: 1–14.

Chien DT, Szardenings AK, Bahri S, Walsh JC, Mu F, Xia C, et al. Early clinical PET imaging results with the novel PHF-tau radioligand [F18]-T808. *J. Alzheimer's Dis.* 2014; 38: 171–184.

Choo IH, Lee DY, Oh JS, Lee JS, Lee DS, Song IC, et al. Posterior cingulate cortex atrophy and regional cingulum disruption in mild cognitive impairment and Alzheimer's disease. *Neurobiol. Aging* 2010; 31: 772–779.

Chrastil ER, Sherrill KR, Aselcioglu I, Hasselmo ME, Stern CE. Individual Differences in Human Path Integration Abilities Correlate with Gray Matter Volume in Retrosplenial Cortex, Hippocampus, and Medial Prefrontal Cortex. *Eneuro* 2017; 4: ENEURO.0346-16.2017.

Chrastil ER, Sherrill KR, Hasselmo ME, Stern CE. There and Back Again: Hippocampus and Retrosplenial Cortex Track Homing Distance during Human Path Integration. *J. Neurosci.* 2015; 35: 15442–15452.

Ciavarro M, Ambrosini E, Tosoni A, Committeri G, Fattori P, Galletti C. Reorganization of Retinotopic Maps After Occipital Lobe Infarction. *J. Cogn. Neurosci.* 2013; 26: 1–10.

Cipolotti L, Bird C, Good T, Macmanus D, Rudge P, Shallice T. Recollection and familiarity in dense hippocampal amnesia: A case study. *Neuropsychologia* 2006; 44: 489–506.

Clark LR, Stricker NH, Libon DJ, Delano-Wood L, Salmon DP, Delis DC, et al. Yes/No versus forced-choice recognition memory in mild cognitive impairment and Alzheimer's disease: Patterns of impairment and associations with dementia severity. *Clin. Neuropsychol.* 2012; 26: 1201–1216.

Clarke A, Tyler LK. Object-Specific Semantic Coding in Human Perirhinal Cortex. *J. Neurosci.* 2014; 34: 4766–4775.

Clarke JR, Cammarota M, Gruart A, Izquierdo I, Delgado-García JM. Plastic

modifications induced by object recognition memory processing. *Proc. Natl. Acad. Sci.* 2010; 107: 2652–2657.

Cohen SJ, Stackman RW. Assessing rodent hippocampal involvement in the novel object recognition task. A review. *Behav. Brain Res.* 2015; 285: 105–117.

Connor CE, Knierim JJ. Integration of objects and space in perception and memory. *Nat. Neurosci.* 2017; 20: 1493–1503.

Conover WJ, Iman RL. Analysis of covariance using the rank transformation. *Biometrics* 1982; 38: 715–724.

Coughlan. G, Laczó J, Hort J, Minihane AM, Hornberger M. Spatial navigation deficits – the overlooked cognitive fingerprint for incipient Alzheimer pathophysiology? *Nat. Rev. Neurol.* 2018: In press.

Coutrot A, Schmidt S, Coutrot L, Pittman J, Hong L, Wiener JM, et al. Virtual navigation tested on a mobile app is predictive of real-world wayfinding navigation performance. *PLoS One* 2019; 14: e0213272.

Cowell RA, Bussey TJ, Saksida LM. Components of recognition memory: Dissociable cognitive processes or just differences in representational complexity? *Hippocampus* 2010; 20: 1245–1262.

Crane J, Milner B. What Went Where? Impaired Object-Location Learning in Patients With Right Hippocampal Lesions. 2005; 231: 216–231.

Creighton SD, Mendell AL, Palmer D, Kalisch BE, MacLusky NJ, Prado VF, et al. Dissociable cognitive impairments in two strains of transgenic Alzheimer’s disease mice revealed by a battery of object-based tests. *Sci. Rep.* 2019; 9: 1–12.

Cueva CJ, Wei X. OF GRID - LIKE REPRESENTATIONS BY. 2018: 1–19.

Cummings J. Lessons Learned from Alzheimer Disease: Clinical Trials with Negative Outcomes. *Clin. Transl. Sci.* 2018; 11: 147–152.

Cusack R, Vicente-Grabovetsky A, Mitchell DJ, Wild CJ, Auer T, Linke AC, et al. Automatic analysis (aa): Efficient neuroimaging workflows and parallel processing using Matlab and XML. *Front. Neuroinform.* 2015; 8: 90.

Darwin C. Origin of certain instincts. *Nature* 1873: 417–418.

Deshmukh SS, Knierim JJ. Representation of non-spatial and spatial information in the lateral entorhinal cortex. *Front. Behav. Neurosci.* 2011; 5: 69.

DeToledo-Morrell L, Stoub TR, Bulgakova M, Wilson RS, Bennett DA, Leurgans S, et al. MRI-derived entorhinal volume is a good predictor of conversion from MCI

to AD. *Neurobiol. Aging* 2004; 25: 1197–1203.

Devanand DP, Bansal R, Liu J, Hao X, Pradhaban G, Peterson BS. MRI hippocampal and entorhinal cortex mapping in predicting conversion to Alzheimer's disease. *Neuroimage* 2012; 60: 1622–1629.

Devanand DP, Pradhaban G, Liu X, Khandji A, Santi S De, Segal S, et al. Hippocampal and entorhinal atrophy in mild cognitive impairment Prediction of Alzheimer disease. 2007

Di J, Cohen LS, Corbo CP, Phillips GR, El Idrissi A, Alonso AD. Abnormal tau induces cognitive impairment through two different mechanisms: Synaptic dysfunction and neuronal loss. *Sci. Rep.* 2016; 6: 1–12.

Dickerson BC, Goncharova I, Sullivan MP, Forchetti C, Wilson RS, Bennett DA, et al. MRI-derived entorhinal and hippocampal atrophy in incipient and very mild Alzheimer's disease. *Neurobiol. Aging* 2001; 22: 747–754.

Dickerson BC, Wolk DA. Biomarker-based prediction of progression in MCI: Comparison of AD signature and hippocampal volume with spinal fluid amyloid- β and tau. *Front. Aging Neurosci.* 2013; 5: 1–9.

Diehl GW, Hon OJ, Leutgeb S, Leutgeb JK. Grid and Nongrid Cells in Medial Entorhinal Cortex Represent Spatial Location and Environmental Features with Complementary Coding Schemes. *Neuron* 2017; 94: 83-92.e6.

Diersch N, Wolbers T. The potential of virtual reality for spatial navigation research across the adult lifespan. *J. Exp. Biol.* 2019; 222

Ding SL, Van Hoesen GW. Organization and detailed parcellation of human hippocampal head and body regions based on a combined analysis of Cyto- and chemoarchitecture. *J. Comp. Neurol.* 2015; 523: 2233–2253.

Distler HK, Veen HAHC Van, S. J. Braun WH, Franz MO, Bilthoff HH. Navigation in Real and Virtual Environments: Judging Orientation and Distance in a Large-Scale Landscape. *Virtual Environ. '98, Proc. Eurographics Work. Stuttgart 1998*: 124–133.

Doeller CF, Barry C, Burgess N. Evidence for grid cells in a human memory network. *Nature* 2010; 463: 657–661.

Doeller CF, King JA, Burgess N. Parallel striatal and hippocampal systems for landmarks and boundaries in spatial memory. *Proc Natl Acad Sci U S A* 2008; 105: 5915–5920.

Doniger GM, Beeri MS, Bahar-Fuchs A, Gottlieb A, Tkachov A, Kenan H, et al. Virtual reality-based cognitive-motor training for middle-aged adults at high Alzheimer's disease risk: A randomized controlled trial. *Alzheimer's Dement. Transl. Res. Clin. Interv.* 2018; 4: 118–129.

Dubois B, Feldman HH, Jacova C, Cummings JL, DeKosky ST, Barberger-Gateau P, et al. Revising the definition of Alzheimer's disease: A new lexicon. *Lancet Neurol.* 2010; 9: 1118–1127.

Dubois B, Feldman HH, Jacova C, DeKosky ST, Barberger-Gateau P, Cummings J, et al. Research criteria for the diagnosis of Alzheimer's disease: revising the NINCDS-ADRDA criteria. *Lancet Neurol.* 2007; 6: 734–746.

Dubois B, Feldman HH, Jacova C, Hampel H, Molinuevo JL, Blennow K, et al. Advancing research diagnostic criteria for Alzheimer's disease: The IWG-2 criteria. *Lancet Neurol.* 2014; 13: 614–629.

Dubois B, Hampel H, Feldman HH, Scheltens P, Aisen P, Andrieu S, et al. Preclinical Alzheimer's disease: Definition, natural history, and diagnostic criteria. 2016.

Dudas RB, Clague F, Thompson SA, Graham KS, Hodges JR. Episodic and semantic memory in mild cognitive impairment. 2005; 43: 1266–1276.

Düzel E, Berron D, Schütze H, Cardenas-Blanco A, Metzger C, Betts M, et al. CSF total tau levels are associated with hippocampal novelty irrespective of hippocampal volume. *Alzheimer's Dement. Diagnosis, Assess. Dis. Monit.* 2018; 10: 782–790.

Ekstrom AD, Caplan JB, Ho E, Shattuck K, Fried I, Kahana MJ. Human hippocampal theta activity during virtual navigation. *Hippocampus* 2005; 15: 881–889.

Ekstrom AD, Kahana MJ, Caplan JB, Fields TA, Isham EA, Newman EL, et al. Cellular networks underlying human spatial navigation. *Nature* 2003; 425: 184–187.

Eradath MK, Mogami T, Wang G, Tanaka K. Time context of cue-outcome associations represented by neurons in perirhinal cortex. *J. Neurosci.* 2015; 35: 4350–4365.

Etienne AS, Jeffery KJ. Path integration in mammals. *Hippocampus* 2004; 14: 180–192.

Fagan AM, Mintun MA, Mach RH, Lee SY, Dence CS, Shah AR, et al. Inverse relation between in vivo amyloid imaging load and cerebrospinal fluid Abeta₄₂ in humans. *Ann. Neurol.* 2006; 59: 512–519.

Fagan AM, Xiong C, Jasiolec MS, Bateman RJ, Goate AM, Benzinger TLS, et al. Longitudinal change in CSF biomarkers in autosomal-dominant Alzheimer disease. *Sci. Transl. Med.* 2014; 6: 1–35.

Feigenbaum JD, Morris RG. Allocentric Versus Egocentric Spatial Memory After Unilateral Temporal Lobectomy in Humans. *Neuropsychology* 2004; 18: 462–472.

Fellgiebel A, Wille P, Müller MJ, Winterer G, Scheurich A, Vucurevic G, et al. Ultrastructural hippocampal and white matter alterations in mild cognitive impairment: a diffusion tensor imaging study. *Dement. Geriatr. Cogn. Disord.* 2004; 18: 101–108.

Fidalgo C, Martin CB. The Hippocampus Contributes to Allocentric Spatial Memory through Coherent Scene Representations. *J. Neurosci.* 2016; 36: 2555 LP – 2557.

Fidalgo CO, Changoor AT, Page-Gould E, Lee ACH, Barense MD. Early cognitive decline in older adults better predicts object than scene recognition performance. *Hippocampus* 2016; 26: 1579–1592.

Fischl B, Salat DH, Busa E, Albert M, Dieterich M, Haselgrove C, et al. Whole brain segmentation: Automated labeling of neuroanatomical structures in the human brain. *Neuron* 2002; 33: 341–355.

de Flores R, La Joie R, Chételat G. Structural imaging of hippocampal subfields in healthy aging and Alzheimer’s disease. *Neuroscience* 2015; 309: 29–50.

Fortin NJ, Agster KL, Eichenbaum HB. Critical role of the hippocampus in memory for sequences of events. *Nat. Neurosci.* 2002; 5: 458–462.

Fortin NJ, Wright SP, Eichenbaum H. Recollection-like memory retrieval in rats is dependent on the hippocampus. *Nature* 2004; 431: 188–191.

Fox NC, Freeborough PA. Brain atrophy progression measured from registered serial MRI: Validation and application to Alzheimer’s disease. *J. Magn. Reson. Imaging* 1997; 7: 1069–1075.

Frank D, Montaldi D, Wittmann B, Talmi D. Beneficial and detrimental effects of schema incongruence on memory for contextual events. 2018: 352–361.

Frohardt RJ, Bassett JP, Taube JS. Path integration and lesions within the head direction cell circuit: Comparison between the roles of the anterodorsal thalamus and dorsal tegmental nucleus. *Behav. Neurosci.* 2006; 120: 135–149.

Fu H, Rodriguez GA, Herman M, Emrani S, Nahmani E, Barrett G, et al. Tau Pathology Induces Excitatory Neuron Loss, Grid Cell Dysfunction, and Spatial

Memory Deficits Reminiscent of Early Alzheimer's Disease. *Neuron* 2017; 93: 533-541.e5.

Gallagher M, Koh MT. Episodic memory on the path to Alzheimer's disease. *Curr. Opin. Neurobiol.* 2011; 21: 929–934.

Gaser C, Kurth F. *Manual Computational Anatomy Toolbox-CAT12.* Uni Jena 2016

Gil M, Ancau M, Schlesiger MI, Neitz A, Allen K, De Marco RJ, et al. Impaired path integration in mice with disrupted grid cell firing. *Nat. Neurosci.* 2018; 21: 81–93.

Gillis MM, Garcia S, Hampstead BM. Working memory contributes to the encoding of object location associations: Support for a 3-part model of object location memory. *Behav. Brain Res.* 2016; 311: 192–200.

Glasauer S, Amorim MA, Viaud-Delmon I, Berthoz A. Differential effects of labyrinthine dysfunction on distance and direction during blindfolded walking of a triangular path. *Exp. Brain Res.* 2002; 145: 489–497.

Goh JOS, Soon CS, Park D, Gutchess A, Hebrank A, Chee MWL. Cortical areas involved in object, background, and object-background processing revealed with functional magnetic resonance adaptation. *J. Neurosci.* 2004; 24: 10223–10228.

Gold CA, Budson AE. Memory loss in Alzheimer's disease: Implications for development of therapeutics. *Expert Rev. Neurother.* 2008; 8: 1879–1891.

Gomar JJ, Ragland JD, Ulu AM, Sousa A, Huey ED, Conejero-goldberg C, et al. Differential medial temporal lobe morphometric predictors of item- and relational-encoded memories in healthy individuals and in individuals with mild cognitive impairment and Alzheimer's disease. 2017; 3: 238–246.

Good MA, Barnes P, Staal V, McGregor A, Honey RC. Context- but not familiarity-dependent forms of object recognition are impaired following excitotoxic hippocampal lesions in rats. *Behav. Neurosci.* 2007; 121: 218–223.

Goodale MA, Milner AD. Separate visual pathways for perception and action. *Trends Neurosci.* 1992; 15: 20–25.

Goodrich-Hunsaker NJ, Livingstone SA, Skelton RW, Hopkins RO. Spatial deficits in a virtual water maze in amnesic participants with hippocampal damage. *Hippocampus* 2010; 20: 481–491.

Greicius MD, Srivastava G, Reiss AL, Menon V. Default-mode network activity distinguishes Alzheimer's disease from healthy aging: evidence from functional MRI. *Proc. Natl. Acad. Sci. U. S. A.* 2004; 101: 4637–42.

Greve A, Cooper E, Kaula A, Anderson MC, Henson R. Does prediction error drive one-shot declarative learning? *J. Mem. Lang.* 2017; 94: 149–165.

Greve A, Cooper E, Tibon R, Henson RN. Knowledge is power: Prior knowledge aids memory for both congruent and incongruent events, but in different ways. *J. Exp. Psychol. Gen.* 2019; 148: 325–341.

Grignion Y, Duyckaerts C, Bennech M, Hauw JJ. Cytoarchitectonic alterations in the supramarginal gyrus of late onset Alzheimer's disease. *Acta Neuropathol.* 1998; 95: 395–406.

Hafting T, Fyhn M, Bonnevie T, Moser MB, Moser EI. Hippocampus-independent phase precession in entorhinal grid cells. *Nature* 2008; 453: 1248–1252.

Hafting T, Fyhn M, Molden S, Moser MB, Moser EI. Microstructure of a spatial map in the entorhinal cortex. *Nature* 2005; 436: 801–806.

Hampstead BM, Stringer AY, Stilla RF, Amaraneni A, Sathian K. Where did I put that? Patients with amnesic mild cognitive impairment demonstrate widespread reductions in activity during the encoding of ecologically relevant object-location associations. *Neuropsychologia* 2011; 49: 2349–2361.

Hampstead BM, Towler S, Stringer AY, Sathian K. Continuous measurement of object location memory is sensitive to effects of age and mild cognitive impairment and related to medial temporal lobe volume. *Alzheimer's Dement. Diagnosis, Assess. Dis. Monit.* 2018; 10: 76–85.

Hanseeuw B, Dricot L, Kavac M, Grandin C, Seron X, Ivanoiu A. Associative encoding deficits in amnesic mild cognitive impairment: A volumetric and functional MRI study. *Neuroimage* 2011; 56: 1743–1748.

Hargreaves EL, Rao G, Lee I, Knierim JJ. Neuroscience: Major dissociation between medial and lateral entorhinal input to dorsal hippocampus. *Science* (80-.). 2005; 308: 1792–1794.

Harris J a, Devidze N, Verret L, Ho K, Halabisky B, Myo T, et al. Transsynaptic progression of amyloid- β -induced neuronal dysfunction within the entorhinal-hippocampal network. 2011; 68: 428–441.

Harris JA, Koyama A, Maeda S, Ho K, Devidze N, Dubal DB, et al. Human P301L-Mutant Tau Expression in Mouse Entorhinal-Hippocampal Network Causes Tau Aggregation and Presynaptic Pathology but No Cognitive Deficits. *PLoS One* 2012; 7: e45881.

Harris MA, Wolbers T. Ageing effects on path integration and landmark navigation. *Hippocampus* 2012; 22: 1770–1780.

Hartley T. The hippocampus is required for short-term topographical memory in humans. *Hippocampus* 2007; 000: 1–3.

Hartley T, Harlow R. An association between human hippocampal volume and topographical memory in healthy young adults. *Front. Hum. Neurosci.* 2012; 6: 338.

Harvey PD, Cosentino S, Curiel R, Goldberg TE, Kaye J, Loewenstein D, et al. Performance-based and observational assessments in clinical trials across the alzheimer's disease spectrum. *Innov. Clin. Neurosci.* 2017; 14: 30–39.

Hassabis D, Kumaran D, Maguire EA. Using imagination to understand the neural basis of episodic memory. *J. Neurosci.* 2007; 27: 14365–14374.

Hayes SM, Nadel L, Ryan L, Al HET. The Effect of Scene Context on Episodic Object Recognition : Parahippocampal Cortex Mediates Memory Encoding and Retrieval Success. 2007; 889: 873–889.

Hirata Y, Matsuda H, Nemoto K, Ohnishi T, Hirao K, Yamashita F, et al. Voxel-based morphometry to discriminate early Alzheimer's disease from controls. *Neurosci. Lett.* 2005; 382: 269–274.

Hodge J, Balaam M, Hastings S, Morrissey K. Exploring the design of tailored virtual reality experiences for people with dementia. In: *Conference on Human Factors in Computing Systems - Proceedings.* ACM; 2018. p. 514.

Hodges JR, Patterson K. Is semantic memory consistently impaired early in the course of Alzheimer's disease? Neuroanatomical and diagnostic implications. *Neuropsychologia* 1995; 33: 441–459.

Hojjati SH, Ebrahimzadeh A, Khazaee A, Babajani-Feremi A. Predicting conversion from MCI to AD by integrating rs-fMRI and structural MRI. *Comput. Biol. Med.* 2018; 102: 30–39.

Horner AJ, Bisby JA, Zotow E, Bush D, Burgess N. Grid-like Processing of Imagined Navigation. *Curr. Biol.* 2016; 26: 842–847.

Hort J, Hort J, Laczó J, Laczó J, Vyhnalek M, Vyhnalek M, et al. Spatial navigation deficit in amnesic mild cognitive impairment. *Proc. Natl. Acad. Sci.* 2007a; 104: 4042–4047.

Hort J, Laczó J, Vyhnalek M, Bojar M, Bures J, Vlcek K. Spatial navigation deficit in

amnesic mild cognitive impairment. *Proc. Natl. Acad. Sci.* 2007b; 104: 4042–4047.

Howard LR, Javadi AH, Yu Y, Mill RD, Morrison LC, Knight R, et al. Article The Hippocampus and Entorhinal Cortex Encode the Path and Euclidean Distances to Goals during Navigation. *Curr. Biol.* 2014; 24: 1331–1340.

Høydal ØA, Skytøen ER, Andersson SO, Moser MB, Moser EI. Object-vector coding in the medial entorhinal cortex. *Nature* 2019; 568: 400–404.

Hoydal OA, Skytoen ER, Moser M-B, Moser EI. Object-vector coding in the medial entorhinal cortex. *bioRxiv* 2018: 286286.

Huang P, Carlin JD, Alink A, Kriegeskorte N, Henson RN, Correia MM. Prospective motion correction improves the sensitivity of fMRI pattern decoding. *Hum. Brain Mapp.* 2018; 39: 4018–4031.

Hudon C, Belleville S, Souchay C, Gély-Nargeot MC, Chertkow H, Gauthier S. Memory for gist and detail information in Alzheimer’s disease and mild cognitive impairment. *Neuropsychology* 2006; 20: 566–577.

Hunsaker MR, Chen V, Tran GT, Kesner RP. The medial and lateral entorhinal cortex both contribute to contextual and item recognition memory: A test of the binding of items and context model. *Hippocampus* 2013; 23: 380–391.

Hunsaker MR, Kesner RP. The operation of pattern separation and pattern completion processes associated with different attributes or domains of memory. *Neurosci. Biobehav. Rev.* 2013; 37: 36–58.

Hunsaker MR, Mooy GG, Swift JS, Kesner RP. Dissociations of the medial and lateral perforant path projections into dorsal DG, CA3, and CA1 for spatial and nonspatial (visual object) information processing. *Behav. Neurosci.* 2007; 121: 742–750.

Hutchinson AD, Mathias JL. Neuropsychological deficits in frontotemporal dementia and Alzheimer’s disease: a meta-analytic review. *J. Neurol. Neurosurg. Psychiatry* 2007; 78: 917–928.

Hyman BT, Hoesen GW Van, Damasio AR, Barnes CL. Alzheimer’s Disease : Cell-Specific Pathology Isolates the Hippocampal Formation Alzheimer’s Disease: Cell-Specific Pathology Isolates the Hippocampal Formation. *Science* (80-.). 1984; 225: 1168–1170.

Iglesias JE, Augustinack JC, Nguyen K, Player CM, Player A, Wright M, et al. A computational atlas of the hippocampal formation using ex vivo, ultra-high resolution MRI: Application to adaptive segmentation of in vivo MRI. *Neuroimage*

2015; 115: 117–137.

Insausti R, Juottonen K, Soininen H, Insausti a M, Partanen K, Vainio P, et al. MR volumetric analysis of the human entorhinal, perirhinal, and tempopolar cortices. 1998; 19: 659–671.

Irish M, Halena S, Kamminga J, Tu S, Hornberger M, Hodges JR. Scene construction impairments in Alzheimer's disease - A unique role for the posterior cingulate cortex. *Cortex* 2015; 73: 10–23.

Irish M, Lawlor BA, Mara SMO, Coen RF. Impaired capacity for auto-noetic reliving during autobiographical event recall in mild Alzheimer's disease. *CORTEX* 2011; 47: 236–249.

Jack C, Knopman DS, Jagust WJ, Petersen RC, Weiner MW, Aisen PS, et al. Update on hypothetical model of Alzheimer's disease biomarkers. *Lancet Neurol.* 2013; 12: 207–216.

Jack CR, Petersen RC, Xu YC, Waring SC, O'Brien PC, Tangalos EG, et al. Medial temporal atrophy on MRI in normal aging and very mild Alzheimer's disease. *Neurology* 1997; 49: 786–794.

Jacobs J, Kahana MJ, Ekstrom AD, Mollison M V, Fried I. A sense of direction in human entorhinal cortex. *Proc. Natl. Acad. Sci.* 2010; 107: 6487–6492.

Jacobs J, Weidemann CT, Miller JF, Solway A, Burke JF, Wei XX, et al. Direct recordings of grid-like neuronal activity in human spatial navigation. *Nat. Neurosci.* 2013; 16: 1188–1190.

Jayakumar RP, Madhav MS, Savelli F, Blair HT, Cowan NJ, Knierim JJ. Recalibration of path integration in hippocampal place cells. *Nature* 2019; 566: 533–537.

Jessen F, Feyen L, Freymann K, Tepest R, Maier W, Heun R, et al. Volume reduction of the entorhinal cortex in subjective memory impairment. *Neurobiol. Aging* 2006; 27: 1751–1756.

Jo YS, Lee I. Disconnection of the hippocampal-perirhinal cortical circuits severely disrupts object-place paired associative memory. *J. Neurosci.* 2010; 30: 9850–9858.

De Jong LW, Van Der Hiele K, Veer IM, Houwing JJ, Westendorp RGJ, Bollen ELEM, et al. Strongly reduced volumes of putamen and thalamus in Alzheimer's disease: An MRI study. *Brain* 2008; 131: 3277–3285.

Joubert S, Felician O, Barbeau EJ, Didic M, Poncet M. Patterns of semantic memory

impairment in Mild Cognitive Impairment. 2008; 19: 35–40.

Juottonen K, Lehtovirta M, Helisalmi S, Sr PJR, Soininen H. Major decrease in the volume of the entorhinal cortex in patients with Alzheimer's disease carrying the apolipoprotein E ϵ 4 allele. *J. Neurol. Neurosurg. Psychiatry* 1998; 65: 322–327.

Kalová E, Vlček K, Jarolímová E, Bureš J. Allothetic orientation and sequential ordering of places is impaired in early stages of Alzheimer's disease: Corresponding results in real space tests and computer tests. *Behav. Brain Res.* 2005; 159: 175–186.

Kaufman SK, Del K, Talitha T, Heiko LT, Marc B. Tau seeding activity begins in the transentorhinal / entorhinal regions and anticipates phospho - tau pathology in Alzheimer ' s disease and PART . *Acta Neuropathol.* 2018; 136: 57–67.

Kavcic V, Fernandez R, Logan D, Duffy CJ. Neurophysiological and perceptual correlates of navigational impairment in Alzheimer's disease. *Brain* 2006; 129: 736–46.

Kearns MJ, Warren WH, Duchon AP, Tarr MJ. Path integration from optic flow and body senses in a homing task. *Perception* 2002; 31: 349–374.

Keene CS, Bladon J, McKenzie S, Liu CD, O'Keefe J, Eichenbaum H. Complementary functional organization of neuronal activity patterns in the perirhinal, lateral entorhinal, and medial entorhinal cortices. *J. Neurosci.* 2016; 36: 3660–3675.

Kessels RPC, Hendriks M, Schouten J, Van Asselen M, Postma A. Spatial memory deficits in patients after unilateral selective amygdalohippocampectomy. *J. Int. Neuropsychol. Soc.* 2004; 10: 907–12.

Kessels RPC, Jaap Kappelle L, De Haan EHF, Postma A. Lateralization of spatial-memory processes: Evidence on spatial span, maze learning, and memory for object locations. *Neuropsychologia* 2002; 40: 1465–1473.

Kessels RPC, Meulenbroek O, Fernández G, Olde MGM. Spatial Working Memory in Aging and Mild Cognitive Impairment : Effects of Task Load and Contextual Cueing
Spatial Working Memory in Aging and Mild Cognitive Impairment : Effects of Task Load and Contextual Cueing. 2010a; 5585

Kessels RPC, Rijken S, Joosten-Weyn Banningh LW a, Van Schuylenborgh-VAN Es N, Olde Rikkert MGM. Categorical spatial memory in patients with mild cognitive impairment and Alzheimer dementia: positional versus object-location recall. *J. Int. Neuropsychol. Soc.* 2010b; 16: 200–204.

KF T, JC C, HW H, SS W, TY K. Cognitive tests to detect dementia: A systematic review and meta-analysis. *JAMA Intern. Med.* 2015; 175: 1450–1458.

Khan UA, Liu L, Provenzano FA, Berman DE, Profaci CP, Sloan R, et al. Molecular drivers and cortical spread of lateral entorhinal cortex dysfunction in preclinical Alzheimer's disease. *Nat. Publ. Gr.* 2013; 17: 304–311.

Khan UA, Liu L, Provenzano FA, Berman DE, Profaci CP, Sloan R, et al. Molecular drivers and cortical spread of lateral entorhinal cortex dysfunction in preclinical Alzheimer's disease. *Nat. Neurosci.* 2014; 17: 304–311.

Killian NJ, Jutras MJ, Buffalo E a. A map of visual space in the primate entorhinal cortex. *Nature* 2012; 491: 761–764.

Killiany RJ, Hyman BT, Gomez-Isla T, Moss MB, Kikinis R, Jolesz F, et al. MRI measures of entorhinal cortex vs hippocampus in preclinical AD. *Neurology* 2002; 58: 1188–1196.

Kim M, Maguire EA. Encoding of 3D head direction information in the human brain. *Hippocampus* 2019; 29: 619–629.

Kivisaari SL, Tyler LK, Monsch AU, Taylor KI. Medial perirhinal cortex disambiguates confusable objects. *Brain* 2012; 135: 3757–3769.

Klatzky RL, Loomis JM, Beall AC, Chance SS, Golledge RG. Spatial Updating of Self-Position and Orientation During Real, Imagined, and Virtual Locomotion. *Psychol. Sci.* 1998; 9: 293–298.

Knierim JJ, Neunuebel JP, Deshmukh SS, Knierim JJ. Functional correlates of the lateral and medial entorhinal cortex : objects , path integration and local – global reference frames. 2014

Koepsell TD, Monsell SE. Reversion from mild cognitive impairment to normal or near-Normal cognition; Risk factors and prognosis. *Neurology* 2012; 79: 1591–1598.

Komorowski RW, Manns JR, Eichenbaum H. Robust Conjunctive Item-Place Coding by Hippocampal Neurons Parallels Learning What Happens Where. *J. Neurosci.* 2009; 29: 9918–9929.

Koo TK, Li MY. A Guideline of Selecting and Reporting Intraclass Correlation Coefficients for Reliability Research. *J. Chiropr. Med.* 2016; 15: 155–163.

Korolev IO, Symonds LL, Bozoki AC. Predicting Progression from Mild Cognitive Impairment to Alzheimer's Dementia Using Clinical, MRI, and Plasma Biomarkers

via Probabilistic Pattern Classification. *PLoS One* 2016; 11: e0138866.

KRAL VA. Senescent forgetfulness: benign and malignant. *Can. Med. Assoc. J.* 1962; 86: 257–260.

Krimer L. The entorhinal cortex: an examination of cyto- and myeloarchitectonic organization in humans. *Cereb. Cortex* 1997; 7: 722–731.

Kropff E, Carmichael JE, Moser MB, Moser EI. Speed cells in the medial entorhinal cortex. *Nature* 2015; 523: 419–424.

Krumm S, Kivisaari SL, Probst A, Monsch AU, Reinhardt J, Ulmer S, et al. Cortical thinning of parahippocampal subregions in very early Alzheimer’s disease. *Neurobiol. Aging* 2016; 38: 188–196.

Kulason S, Tward DJ, Brown T, Sicat CS, Liu C, Ratnanather JT, et al. NeuroImage : Clinical Cortical thickness atrophy in the transentorhinal cortex in mild cognitive impairment. *NeuroImage Clin.* 2019a; 21: 101617.

Kulason S, Tward DJ, Brown T, Sicat CS, Liu CF, Ratnanather JT, et al. Cortical thickness atrophy in the transentorhinal cortex in mild cognitive impairment. *NeuroImage Clin.* 2019b; 21: 101617.

Külzow N, Kerti L, Witte VA, Kopp U, Breitenstein C, Flöel A. An object location memory paradigm for older adults with and without mild cognitive impairment. *J. Neurosci. Methods* 2014; 237: 16–25.

Kunz L, Schroder TN, Lee H, Montag C, Lachmann B, Sariyska R, et al. Reduced grid-cell-like representations in adults at genetic risk for Alzheimer’s disease. *Science* (80-.). 2015; 350: 430–433.

Kuruvilla M V., Ainge JA. Lateral Entorhinal Cortex Lesions Impair Local Spatial Frameworks. *Front. Syst. Neurosci.* 2017a; 11: 1–12.

Kuruvilla M V, Ainge JA. Lateral Entorhinal Cortex Lesions Impair Local Spatial Frameworks. *Front. Syst. Neurosci.* 2017b; 11: 30.

De La Torre JC. Is Alzheimer’s disease a neurodegenerative or a vascular disorder? Data, dogma, and dialectics. *Lancet Neurol.* 2004; 3: 184–190.

Labash A, Majoral D, Valgur M. Towards Emergence of Grid Cells by Deep Reinforcement Learning. 2018.

Laczó J, Andel R, Vyhnalek M, Vlcek K, Nedelska Z, Matoska V, et al. APOE and spatial navigation in amnesic MCI: Results from a computer-based test. *Neuropsychology* 2014; 28: 676–684.

Lambon Ralph MA, Patterson K. Generalization and differentiation in semantic memory. *Ann. N. Y. Acad. Sci.* 2008; 1124: 61–76.

Langston RF, Wood ER. Associative recognition and the hippocampus: Differential effects of hippocampal lesions on object-place, object-context and object-place-context memory. *Hippocampus* 2010; 20: 1139–1153.

Lavenex P, Suzuki WA, Amaral DG. Perirhinal and Parahippocampal Cortices of the Macaque Monkey: Intrinsic Projections and Interconnections. *J. Comp. Neurol.* 2004; 472: 371–394.

Lee I, Hunsaker MR, Kesner RP. The role of hippocampal subregions in detecting spatial novelty. *Behav. Neurosci.* 2005; 119: 145–153.

Lenoble Q, Corveleyn X. ScienceDirect Attentional capture by incongruent object / background scenes in patients with Alzheimer disease. 2018; 7: 4–12.

Lever C, Burton S, Jeewajee A, O'Keefe J, Burgess N. Boundary Vector Cells in the Subiculum of the Hippocampal Formation. *J. Neurosci.* 2009; 29: 9771–9777.

Leyhe T, Müller S, Milian M, Eschweiler GW, Saur R. Neuropsychologia Impairment of episodic and semantic autobiographical memory in patients with mild cognitive impairment and early Alzheimer ' s disease. 2009; 47: 2464–2469.

Li B, Shi J, Gutman BA, Baxter LC, Thompson PM, Caselli RJ, et al. Influence of APOE Genotype on Hippocampal Atrophy over Time - An N=1925 Surface-Based ADNI Study. *PLoS One* 2016a; 11: e0152901.

Li S-J, Li Z, Wu G, Zhang M-J, Franczak M, Antuono PG. Alzheimer Disease: evaluation of a functional MR imaging index as a marker. *Radiology* 2002; 225: 253–259.

Li Y, Wang X, Li Y, Sun Y, Sheng C, Li H, et al. Abnormal Resting-State Functional Connectivity Strength in Mild Cognitive Impairment and Its Conversion to Alzheimer ' s Disease. 2016b; 2016

Liang Y, Pertzov Y, Nicholas JM, Henley SMD, Crutch S, Woodward F, et al. Visual short-term memory binding deficit in familial Alzheimer's disease. *Cortex* 2016; 78: 150–164.

Lister JP, Barnes CA. Neurobiological changes in the hippocampus during normative aging. *Arch. Neurol.* 2009; 66: 829–833.

Lo S, Andrews S. To transform or not to transform: using generalized linear mixed models to analyse reaction time data. *Front. Psychol.* 2015; 6: 1–16.

Long X, Chen L, Jiang C, Zhang L. Prediction and classification of Alzheimer disease based on quantification of MRI deformation. *PLoS One* 2017; 12: e0173372.

Lyketsos CG, Carrillo MC, Ryan JM, Khachaturian AS, Trzepacz P, Amatniek J, et al. Neuropsychiatric symptoms in Alzheimer's disease. *Alzheimer's Dement.* 2011; 7: 532–539.

Maass A, Berron D, Harrison T, Baker S, Mellinger T, Swinnerton K, et al. Effects of Tau and Amyloid Deposition Measured By Pet on Domain-Specific Memory Function in Old Age. *Alzheimer's Dement.* 2018a; 14: P87.

Maass A, Berron D, Harrison TM, Adams JN, La Joie R, Baker S, et al. Alzheimer's pathology targets distinct memory networks in the ageing brain. *Brain* 2019; 142: 2492–2509.

Maass A, Berron D, Libby L, Ranganath C, Düzel E. Functional subregions of the human entorhinal cortex. *Elife* 2015; 4: 1–20.

Maass A, Lockhart SN, Harrison TM, Bell RK, Mellinger T, Swinnerton K, et al. Entorhinal tau pathology, episodic memory decline, and neurodegeneration in aging. *J. Neurosci.* 2018b; 38: 530–543.

Machado SEDC, Cunha M, Minc D, Portella CE, Velasques B, Basile LF, et al. Alzheimer's disease and implicit memory. *Arq. Neuropsiquiatr.* 2009; 67: 334–342.

Maguire E a, Burgess N, Donnett JG, Frackowiak RS, Frith CD, O'Keefe J. Knowing where and getting there: a human navigation network. *Science* 1998; 280: 921–924.

Mahmood O, Adamo D, Briceno E, Moffat SD. Age differences in visual path integration. 2009; 205: 88–95.

Malek-Ahmadi M. Reversion from Mild Cognitive Impairment to Normal Cognition: A Meta-Analysis. *Alzheimer Dis. Assoc. Disord.* 2016; 30: 324–330.

Mankin EA, Sparks FT, Slayyeh B, Sutherland RJ, Leutgeb S, Leutgeb JK. Neuronal code for extended time in the hippocampus. *Proc. Natl. Acad. Sci. U. S. A.* 2012; 109: 19462–19467.

Manns JR, Eichenbaum H. A cognitive map for object memory in the hippocampus — *Learning & Memory.* 2009: 616–624.

Mapstone M, Dickerson K, Duffy CJ. Distinct mechanisms of impairment in cognitive ageing and Alzheimer ' s disease. 2008: 1618–1629.

Mathias JL, Burke J. Cognitive Functioning in Alzheimer's and Vascular Dementia : A Meta-Analysis. 2009; 23: 411–423.

Mayes AR, Holdstock JS, Isaac CL, Hunkin NM, Roberts N. Relative sparing of item recognition memory in a patient with adult-onset damage limited to the Hippocampus. *Hippocampus* 2002; 12: 325–340.

McGraw KO, Wong SP. Forming Inferences about Some Intraclass Correlation Coefficients. *Psychol. Methods* 1996; 1: 30–46.

McKhann GM, Knopman DS, Chertkow H, Hyman BT, Jack CR, Kawas CH, et al. The diagnosis of dementia due to Alzheimer's disease: Recommendations from the National Institute on Aging-Alzheimer's Association workgroups on diagnostic guidelines for Alzheimer's disease. *Alzheimer's Dement.* 2011; 7: 263–269.

McNaughton BL, Battaglia FP, Jensen O, Moser EI, Moser M-B. Path integration and the neural basis of the 'cognitive map'. *Nat. Rev. Neurosci.* 2006; 7: 663–678.

McNicol D. A primer of signal detection theory. Mahwah, NJ, US: Lawrence Erlbaum Associates Publishers; 2005.

Meiran N, Jelicic M. Implicit Memory in Alzheimer's Disease: A Meta-Analysis. *Neuropsychology* 1995; 9: 291–303.

Miller JF, Neufang M, Solway A, Brandt A, Trippel M, Mader I, et al. Neural activity in human hippocampal formation reveals the spatial context of retrieved memories. *Science* 2013; 342: 1111–4.

Miller MI, Ratnanather JT, Tward DJ, Brown T, Lee DS, Ketcha M, et al. Network neurodegeneration in Alzheimer's disease via MRI based shape diffeomorphometry and high-field atlas. *Front. Bioeng. Biotechnol.* 2015; 3: 54.

Minderer M, Harvey CD, Donato F, Moser EI. Neuroscience: Virtual reality explored. *Nature* 2016; 533: 324–325.

Mitchell AJ. A meta-analysis of the accuracy of the mini-mental state examination in the detection of dementia and mild cognitive impairment. *J. Psychiatr. Res.* 2009; 43: 411–431.

Moen EL, Fricano-Kugler CJ, Luikart BW, O'Malley AJ. Analyzing clustered data: Why and how to account for multiple observations nested within a study participant? *PLoS One* 2016; 11: 1–17.

Mokrisova I, Laczó J, Andel R, Gazova I, Vyhnalek M, Nedelska Z, et al. Real-space path integration is impaired in Alzheimer's disease and mild cognitive

impairment. *Behav. Brain Res.* 2016; 307: 150–158.

Montez T, Poil S-S, Jones BF, Manshanden I, Verbunt JPA, van Dijk BW, et al. Altered temporal correlations in parietal alpha and prefrontal theta oscillations in early-stage Alzheimer disease. *Proc. Natl. Acad. Sci.* 2009; 106: 1614 LP – 1619.

Moodley K, Minati L, Contarino V, Prioni S, Wood R, Cooper R, et al. Diagnostic differentiation of mild cognitive impairment due to Alzheimer's disease using a hippocampus-dependent test of spatial memory. *Hippocampus* 2015; 25: 939–51.

Moretti D V, Fracassi C, Pievani M, Geroldi C, Binetti G, Zanetti O, et al. Increase of theta/gamma ratio is associated with memory impairment. *Clin. Neurophysiol.* 2009; 120: 295–303.

Morris E, Chalkidou A, Hammers A, Peacock J, Summers J, Keevil S. Diagnostic accuracy of 18F amyloid PET tracers for the diagnosis of Alzheimer's disease: a systematic review and meta-analysis. *Eur. J. Nucl. Med. Mol. Imaging* 2016; 43: 374–385.

Morris GP, Clark IA, Vissel B. Inconsistencies and Controversies Surrounding the Amyloid Hypothesis of Alzheimer's Disease. *Acta Neuropathol. Commun.* 2014; 2: 1–21.

Morris JC. Clinical Dementia Rating: A reliable and valid diagnostic and staging measure for dementia of the Alzheimer type. In: *International Psychogeriatrics*. 1997. p. 173–176.

Morris R. Developments of a water-maze procedure for studying spatial learning in the rat. *J. Neurosci. Methods* 1984; 11: 47–60.

Mortamais M, Ash JA, Harrison J, Kaye J, Kramer J, Randolph C, et al. Detecting cognitive changes in preclinical Alzheimer's disease: A review of its feasibility. *Alzheimer's Dement.* 2017; 13: 468–492.

Mudher A, Colin M, Dujardin S, Medina M, Dewachter I, Alavi Naini SM, et al. What is the evidence that tau pathology spreads through prion-like propagation? *Acta Neuropathol. Commun.* 2017; 5: 99.

Mumby DG, Gaskin S, Glenn MJ, Schramek TE, Lehmann H. Hippocampal damage and exploratory preferences in rats: memory for objects, places, and contexts. *Learn. Mem.* 2002; 9: 49–57.

Murphy MP, Iii HL. Alzheimer's Disease and the β -Amyloid Peptide. *J. Alzheimer's Dis.* 2010; 19: 1–17.

Murray EA, Bussey TJ, Saksida LM. Visual Perception and Memory: A New View of Medial Temporal Lobe Function in Primates and Rodents. *Annu. Rev. Neurosci.* 2007; 30: 99–122.

Murray EA, Richmond BJ. Role of perirhinal cortex in object perception, memory, and associations Elisabeth A Murray* and Barry J Richmond. *Curr. Opin. Neurobiol.* 2001: 188–193.

Nadasdy Z, Nguyen TP, Török Á, Shen JY, Briggs DE, Modur PN, et al. Context-dependent spatially periodic activity in the human entorhinal cortex. *Proc. Natl. Acad. Sci.* 2017; 114: E3516–E3525.

Nardini M, Jones P, Bedford R, Braddick O. Development of Cue Integration in Human Navigation. *Curr. Biol.* 2008; 18: 689–693.

Naumann RK, Preston-Ferrer P, Brecht M, Burgalossi A. Structural modularity and grid activity in the medial entorhinal cortex. *J. Neurophysiol.* 2018; 119: 2129–2144.

Naumann RK, Ray S, Prokop S, Las L, Heppner FL, Brecht M. Conserved size and periodicity of pyramidal patches in layer 2 of medial/caudal entorhinal cortex. *J. Comp. Neurol.* 2016; 524: 783–806.

Navarro Schröder T, Haak K V, Zaragoza Jimenez NI, Beckmann CF, Doeller CF. Functional topography of the human entorhinal cortex. *Elife* 2015; 4: 1–17.

Nelson P. T. et al. Correlation of Alzheimer Disease Neuropathologic Changes With Cognitive Status: A Review of the Literature. *J Neuropathol Exp Neurol.* 2012 May ; 71(5) 362–381. doi10.1097/NEN.0b013e31825018f7 2013; 71: 362–381.

Norman G, Eacott MJ. Impaired object recognition with increasing levels of feature ambiguity in rats with perirhinal cortex lesions. *Behav. Brain Res.* 2004; 148: 79–91.

O’Brien N, Lehmann H, Lecluse V, Mumby DG. Enhanced context-dependency of object recognition in rats with hippocampal lesions. *Behav. Brain Res.* 2006; 170: 156–162.

O’Keefe J, Dostrovsky J. The hippocampus as a spatial map. Preliminary evidence from unit activity in the freely-moving rat. *Brain Res.* 1971; 34: 171–175.

O’Keefe J, Nadel L. *The Hippocampus As A Cognitive Map* [Internet]. 1978.

Okamura N, Furumoto S, Fodero-Tavoletti MT, Mulligan RS, Harada R, Yates P, et al. Non-invasive assessment of Alzheimer’s disease neurofibrillary pathology

using 18F-THK5105 PET. *Brain* 2014; 137: 1762–1771.

Okello A, Koivunen J, Edison P, Archer HA, Turkheimer FE, Någren K, et al. Conversion of amyloid positive and negative MCI to AD over 3 years: An 11C-PIB PET study. *Neurol.* 2009; 73: 754–760.

Ólafsdóttir HF, Barry C. Spatial cognition: Grid cell firing depends on self-motion cues. *Curr. Biol.* 2015; 25: R827–R829.

Oliveira AMM, Hawk JD, Abel T, Havekes R. Post-training reversible inactivation of the hippocampus enhances novel object recognition memory. *Learn. Mem.* 2010; 17: 155–160.

Olsen RK, Yeung LK, Noly-Gandon A, D’Angelo MC, Kacollja A, Smith VM, et al. Human anterolateral entorhinal cortex volumes are associated with cognitive decline in aging prior to clinical diagnosis. *Neurobiol. Aging* 2017; 57: 195–205.

Olsson B, Lautner R, Andreasson U, Öhrfelt A, Portelius E, Bjerke M, et al. CSF and blood biomarkers for the diagnosis of Alzheimer’s disease: a systematic review and meta-analysis. *Lancet Neurol.* 2016; 15: 673–684.

Ossenkoppele R, Schonhaut DR, Schöll M, Lockhart SN, Ayakta N, Baker SL, et al. Tau PET patterns mirror clinical and neuroanatomical variability in Alzheimer’s disease. *Brain* 2016: 1551–1567.

Palmer K, Bäckman L, Winblad B, Fratiglioni L. Mild Cognitive Impairment in the General Population: Occurrence and Progression to Alzheimer Disease. *Am. J. Geriatr. Psychiatry* 2008; 16: 603–611.

Palmqvist S, Schöll M, Strandberg O, Mattsson N, Stomrud E, Zetterberg H, et al. Earliest accumulation of β -amyloid occurs within the default-mode network and concurrently affects brain connectivity [Internet]. *Nat. Commun.* 2017; 8

Di Paola M, Macaluso E, Carlesimo GA, Tomaiuolo F, Worsley KJ, Fadda L, et al. Episodic memory impairment in patients with Alzheimer’s disease is correlated with entorhinal cortex atrophy: A voxel-based morphometry study. *J. Neurol.* 2007; 254: 774–781.

Papp K V, Rentz DM, Orlovsky I, Sperling RA, Mormino EC. Optimizing the preclinical Alzheimer’s cognitive composite with semantic processing: The PACC5. *Alzheimer’s Dement. (New York, N. Y.)* 2017; 3: 668–677.

Parslow DM, Morris RG, Fleminger S, Rahman Q, Abrahams S, Recce M. Allocentric spatial memory in humans with hippocampal lesions. *Acta Psychol. (Amst).* 2005;

118: 123–147.

Parslow DM, Rose D, Brooks B, Fleminger S, Gray JA, Giampietro V, et al. Allocentric spatial memory activation of the hippocampal formation measured with fMRI. *Neuropsychology* 2004a; 18: 450–461.

Parslow DM, Rose D, Brooks B, Fleminger S, Gray JA, Giampietro V, et al. Allocentric spatial memory activation of the hippocampal formation measured with fMRI. *Neuropsychology* 2004b; 18: 450–461.

Pedro T, Weiler M, Yasuda CL, D’Abreu A, Damasceno BP, Cendes F, et al. Volumetric brain changes in thalamus, corpus callosum and medial temporal structures: Mild alzheimer’s disease compared with amnesic mild cognitive impairment. *Dement. Geriatr. Cogn. Disord.* 2012; 34: 149–155.

Pengas G, Patterson K, Arnold RJ, Bird CM, Burgess N, Nestor PJ. Lost and found: Bespoke memory testing for Alzheimer’s disease and semantic dementia. *J. Alzheimer’s Dis.* 2010; 21: 1347–1365.

Pennanen C, Kivipelto M, Tuomainen S, Hartikainen P, Hänninen T, Laakso MP, et al. Hippocampus and entorhinal cortex in mild cognitive impairment and early AD. *Neurobiol. Aging* 2004; 25: 303–310.

Perl DP. Neuropathology of Alzheimer’s Disease. *Mt Sinai J Med* 2010; 77: 32–42.

Pertzov Y, Dong MY, Peich MC, Husain M. Forgetting What Was Where: The Fragility of Object-Location Binding. *PLoS One* 2012; 7

Pertzov Y, Miller TD, Gorgoraptis N, Caine D, Schott JM, Butler C, et al. Binding deficits in memory following medial temporal lobe damage in patients with voltage-gated potassium channel complex antibody-associated limbic encephalitis. *Brain* 2013; 136: 2474–2485.

Peter J, Sandkamp R, Minkova L, Schumacher L V., Kaller CP, Abdulkadir A, et al. Real-world navigation in amnesic mild cognitive impairment: The relation to visuospatial memory and volume of hippocampal subregions. *Neuropsychologia* 2018; 109: 86–94.

Petersen RC. Mild cognitive impairment as a diagnostic entity. *J. Intern. Med.* 2004; 256: 183–194.

Petersen RC. Mild cognitive impairment. *Continuum (N. Y.)*. 2016; 22: 404–418.

Petersen RC. How early can we diagnose Alzheimer disease (and is it sufficient)? *Neurology* 2018; 91: 395–402.

Petersen RC, Lopez O, Armstrong MJ, Getchius TSD, Ganguli M, Gloss D, et al. Practice guideline update summary: Mild cognitive impairment report of the guideline development, dissemination, and implementation. *Neurology* 2018; 90: 126–135.

Pflueger MO, Stieglitz R-D, Lemoine P, Leyhe T. Ecologically relevant episodic memory assessment indicates an attenuated age-related memory loss - A virtual reality study. *Neuropsychology* 2018; 32: 680–689.

Philbeck JW, O’Leary S. Remembered landmarks enhance the precision of path integration. *Psicologica* 2005; 26: 7–24.

Philippi N, Noblet V, Botzung A, Després O, Renard F, Sfikas G, et al. MRI-Based Volumetry Correlates of Autobiographical Memory in Alzheimer’s Disease. *PLoS One* 2012; 7

Pike KE, Savage G, Villemagne VL, Ng S, Moss SA, Maruff P, et al. β -amyloid imaging and memory in non-demented individuals: Evidence for preclinical Alzheimer’s disease. *Brain* 2007; 130: 2837–2844.

Pitkerkin P, Cole E, Cossette M-P, Gaskin S, Mumby DG. A limited role for the hippocampus in the modulation of novel-object preference by contextual cues. *Learn. Mem.* 2008; 15: 785–791.

Postma A, Kessels RPC, van Asselen M. How the brain remembers and forgets where things are: The neurocognition of object-location memory. *Neurosci. Biobehav. Rev.* 2008; 32: 1339–1345.

Qasim SE, Miller J, Inman CS, Gross RE, Willie JT, Lega B, et al. Single neurons in the human entorhinal cortex remap to distinguish individual spatial memories. *bioRxiv* 2018: 433862.

Qiu C, Kivipelto M, Von Strauss E. Epidemiology of Alzheimer’s disease: Occurrence, determinants, and strategies toward intervention. *Dialogues Clin. Neurosci.* 2009; 11: 111–128.

Ranganath C. A unified framework for the functional organization of the medial temporal lobes and the phenomenology of episodic memory. *Hippocampus* 2010; 20: 1263–1290.

Ranganath C, Ritchey M. Two cortical systems for memory-guided behaviour. *Nat. Rev. Neurosci.* 2012; 13: 713–726.

Raz N, Rodrigue KM, Head D, Kennedy KM, Acker JD. Differential aging of the

medial temporal lobe: a study of a five-year change. *Neurology* 2004; 62: 433–438.

Reagh Z, Noche J, Tustison NJ, Delisle D, Murray EA, Yassa MA. Anterolateral entorhinal-hippocampal imbalance in older adults disrupts object pattern separation. 2017: 1–31.

Reagh ZM, Ho HD, Leal SL, Noche JA, Chun A, Murray EA, et al. Greater loss of object than spatial mnemonic discrimination in aged adults. *Hippocampus* 2016; 26: 417–422.

Reagh ZM, Noche JA, Tustison NJ, Delisle D, Murray EA, Yassa MA. Functional Imbalance of Anterolateral Entorhinal Cortex and Hippocampal Dentate/CA3 Underlies Age-Related Object Pattern Separation Deficits. *Neuron* 2018; 97: 1187-1198.e4.

Reagh ZM, Yassa MA. Object and spatial mnemonic interference differentially engage lateral and medial entorhinal cortex in humans. *Proc. Natl. Acad. Sci. U. S. A.* 2014; 111: E4264-73.

Reger ML, Hovda DA, Giza CC. Ontogeny of Rat Recognition Memory measured by the novel object recognition task. *Dev. Psychobiol.* 2009; 51: 672–678.

Rempel-Clover NL, Zola SM, Squire LR, Amaral DG. Three cases of enduring memory impairment after bilateral damage limited to the hippocampal formation. *J. Neurosci.* 1996; 16: 5233–5255.

Ribeiro JA, Diógenes MJ, Sebastião AM. Influence of Age on BDNF Modulation of Hippocampal Synaptic Transmission. *Hippocampus* 2007; 17: 577–585.

Ritchie CW, Ritchie K. The PREVENT study: A prospective cohort study to identify mid-life biomarkers of late-onset Alzheimer’s disease. *BMJ Open* 2012; 2: 1–6.

Ritchie K, Carrière I, Howett D, Su L, Hornberger M, O’Brien JT, et al. Allocentric and Egocentric Spatial Processing in Middle-Aged Adults at High Risk of Late-Onset Alzheimer’s Disease: The PREVENT Dementia Study. *J. Alzheimer’s Dis.* 2018: 1–1.

Roberts R KD. Classification and Epidemiology of MCI. *Clin Geriatr Med.* 2013 Novemb. ; 29(4) . doi10.1016/j.cger.2013.07.003. NIH 2013; 29: 1–19.

Rodo C, Sargolini F, Save E. Processing of spatial and non-spatial information in rats with lesions of the medial and lateral entorhinal cortex: environmental complexity matters. *Behav. Brain Res.* 2017; 320: 200–209.

Rose SE, McMahon KL, Janke a L, O’Dowd B, de Zubicaray G, Strudwick MW, et al.

Diffusion indices on magnetic resonance imaging and neuropsychological performance in amnesic mild cognitive impairment. *J. Neurol. Neurosurg. Psychiatry* 2006; 77: 1122–1128.

Russo M, Cohen G, Campos J, Martin ME, Sabe L, Barcelo E, et al. Usefulness of Discriminability and Response Bias Indices for the Evaluation of Recognition Memory in Mild Cognitive Impairment and Alzheimer Disease. 2017: 1–14.

Ryan L, Cardoza JA, Barense MD, Kawa KH, Wallentin-Flores J, Arnold WT, et al. Age-related impairment in a complex object discrimination task that engages perirhinal cortex. *Hippocampus* 2012; 22: 1978–1989.

Salat DH, Tuch DS, van der Kouwe AJW, Greve DN, Pappu V, Lee SY, et al. White matter pathology isolates the hippocampal formation in Alzheimer's disease. *Neurobiol. Aging* 2010; 31: 244–256.

Sanfilipo MP, Benedict RHB, Zivadinov R, Bakshi R. Correction for intracranial volume in analysis of whole brain atrophy in multiple sclerosis: The proportion vs. residual method. *Neuroimage* 2004; 22: 1732–1743.

Sargolini F, Fyhn M, Hafting T, McNaughton BL, Witter MP, Moser M-B, et al. Conjunctive representation of position, direction, and velocity in entorhinal cortex. *Science* 2006; 312: 758–762.

Savić A, Jukić V. Neurobiology of aggression and violence. *Soc. Psihijatr.* 2014; 42: 109–113.

Schuff N, Woerner N, Boreta L, Kornfield T, Shaw LM, Trojanowski JQ, et al. MRI of hippocampal volume loss in early Alzheimers disease in relation to ApoE genotype and biomarkers. *Brain* 2009; 132: 1067–1077.

Schultz H, Sommer T, Peters J. Direct Evidence for Domain-Sensitive Functional Subregions in Human Entorhinal Cortex. *J. Neurosci.* 2012; 32: 4716–4723.

Schultz H, Sommer T, Peters J. The Role of the Human Entorhinal Cortex in a Representational Account of Memory. *Front. Hum. Neurosci.* 2015; 9: 628.

Schwarz AJ, Yu P, Miller BB, Shcherbinin S, Dickson J, Navitsky M, et al. Regional profiles of the candidate tau PET ligand ¹⁸F-AV-1451 recapitulate key features of Braak histopathological stages. *Brain* 2016: aww023.

Scoville W, Milner B. Loss of recent memory after bilateral hippocampal lesions. *J. Neurol. Neurosurg. Psychiatry* 1957; 20: 11–21.

Selkoe DJ, Hardy J. The amyloid hypothesis of Alzheimer's disease at 25 years.

EMBO Mol. Med. 2016; 8: 1–14.

Seo K, Kim J kwan, Oh DH, Ryu H, Choi H. Virtual daily living test to screen for mild cognitive impairment using kinematic movement analysis. PLoS One 2017; 12: 1–11.

Serino S, Cipresso P, Morganti F, Riva G. The role of egocentric and allocentric abilities in Alzheimer’s disease: A systematic review. Ageing Res. Rev. 2014; 16: 32–44.

Serino S, Repetto C. New Trends in Episodic Memory Assessment: Immersive 360° Ecological Videos . Front. Psychol. 2018; 9: 1878.

Serino S, Riva G. Getting lost in Alzheimer’s disease: a break in the mental frame syncing. Med. Hypotheses 2013; 80: 416–21.

Shcherbinin S, Schwarz AJ, Joshi AD, Navitsky M, Flitter M, Shankle WR, et al. Kinetics of the tau PET tracer 18F-AV-1451 (T807) in subjects with normal cognitive function, mild cognitive impairment and Alzheimers disease [Internet]. J. Nucl. Med. 2016; 1451

Sheline YI, Wang PW, Gado MH, Csernansky JG, Vannier MW. Hippocampal atrophy in recurrent major depression. Proc. Natl. Acad. Sci. U. S. A. 1996; 93: 3908–13.

Shi F, Liu B, Zhou Y, Yu C, Jiang T. Hippocampal volume and asymmetry in mild cognitive impairment and Alzheimer’s disease: Meta-analyses of MRI studies. Hippocampus 2009; 19: 1055–1064.

Sinai, Krebs, Darken W, Rp, Rowland, Mccarley J. Egocentric Distance Perception in a Virutal Environment Using a Perceptual Matching Task [Internet]. Proc. Hum. Factors Ergonormics Soc. 1999

Sjöbeck M, Haglund M, Englund E. Decreasing myelin density reflected increasing white matter pathology in azheimer’s disease - A neuropathological study. Int. J. Geriatr. Psychiatry 2005; 20: 919–926.

Sjöbeck M, Haglund M, Englund E. White matter mapping in Alzheimer’s disease: A neuropathological study. Neurobiol. Aging 2006; 27: 673–680.

Small G, Kepe V, Ercoli L. PET of brain amyloid and tau in mild cognitive impairment. ... Engl. J. ... 2006

Song Z, Insel PS, Buckley S, Yohannes S, Mezher A, Simonson A, et al. Brain Amyloid- Burden Is Associated with Disruption of Intrinsic Functional Connectivity within the Medial Temporal Lobe in Cognitively Normal Elderly. J.

Neurosci. 2015; 35: 3240–3247.

Spanwick SC, Sutherland RJ. Object/context-specific memory deficits associated with loss of hippocampal granule cells after adrenalectomy in rats. *Learn. Mem.* 2010; 17: 241–245.

Sperling R. Potential of functional MRI as a biomarker in early Alzheimer’s disease. *Neurobiol. Aging* 2011; 32 Suppl 1: S37–S43.

Sperling RA, Bates JF, Chua EF, Cocchiarella AJ, Rentz DM, Rosen BR, et al. fMRI studies of associative encoding in young and elderly controls and mild Alzheimer’s disease. 2003: 44–50.

Spiers HJ, Maguire EA. A navigational guidance system in the human brain. *Hippocampus* 2007; 17: 618–626.

Stahl R, Dietrich O, Teipel SJ, Hampel H, Reiser MF, Schoenberg SO. White matter damage in Alzheimer disease and mild cognitive impairment: assessment with diffusion-tensor MR imaging and parallel imaging techniques. *Radiology* 2007; 243: 483–492.

Stangl M, Achtzehn J, Huber K, Dietrich C, Tempelmann C, Wolbers T, et al. Compromised Grid-Cell-like Representations in Old Age as a Key Mechanism to Explain Age-Related Report Compromised Grid-Cell-like Representations in Old Age as a Key Mechanism to Explain Age-Related Navigational Deficits. *Curr. Biol.* 2018a: 1–8.

Stangl M, Kanitscheider I, Riemer M, Fiete I, Wolbers T. Sources of path integration error in young and aging humans. *bioRxiv* 2018b: 466870.

Staresina BP, Davachi L. Selective and shared contributions of the hippocampus and perirhinal cortex to episodic item and associative encoding. *J. Cogn. Neurosci.* 2008; 20: 1478–1489.

Staresina BP, Davachi L. Object unitization and associative memory formation are supported by distinct brain regions. *J. Neurosci.* 2010; 30: 9890–9897.

Staresina BP, Duncan KD, Davachi L. Perirhinal and parahippocampal cortices differentially contribute to later recollection of object- and scene-related event details. *J. Neurosci.* 2011; 31: 8739–8747.

Van Strien NM, Cappaert NLM, Witter MP. The anatomy of memory: An interactive overview of the parahippocampal- hippocampal network. *Nat. Rev. Neurosci.* 2009; 10: 272–282.

Supekar K, Menon V, Rubin D, Musen M, Greicius MD. Network analysis of intrinsic functional brain connectivity in Alzheimer's disease. *PLoS Comput. Biol.* 2008; 4

Tam SKE, Bonardi C, Robinson J. Relative recency influences object-in-context memory. *Behav. Brain Res.* 2015; 281: 250–257.

Taragano FE, Allegri RF, Krupitzki H, Sarasola DR, Serrano CM, Loñ L, et al. Mild behavioral impairment and risk of dementia: A prospective cohort study of 358 patients. *J. Clin. Psychiatry* 2009; 70: 584–592.

Taube JS. Head direction cells recorded in the anterior thalamic nuclei of freely moving rats. *J. Neurosci.* 1995; 15: 70–86.

Taube JS, Muller RU, Ranck JBJ. Head-direction cells recorded from the postsubiculum in freely moving rats. I. Description and quantitative analysis. *J. Neurosci.* 1990; 10: 420–435.

Taylor KI, Devereux BJ, Tyler LK. Conceptual structure: Towards an integrated neurocognitive account. *Lang. Cogn. Process.* 2011; 26: 1368–1401.

Tennant SA, Fischer L, Garden DLF, Gerlei KZ, Martinez-Gonzalez C, McClure C, et al. Stellate Cells in the Medial Entorhinal Cortex Are Required for Spatial Learning. *Cell Rep.* 2018; 22: 1313–1324.

Thal DR, Holzer M, Rüb U, Waldmann G, Günzel S, Zedlick D, et al. Alzheimer-related τ -pathology in the perforant path target zone and in the hippocampal stratum oriens and radiatum correlates with onset and degree of dementia. *Exp. Neurol.* 2000; 163: 98–110.

Thal DR, Rüb U, Orantes M, Braak H. Phases of A β -deposition in the human brain and its relevance for the development of AD. *Neurology* 2002; 58: 1791 LP – 1800.

Thorne CSE. *The SAGE Encyclopedia of Social Science Research Methods Secondary Analysis of Qualitative Data.* 2015: 618–624.

Thurley K, Ayaz A. Virtual reality systems for rodents. *Curr. Zool.* 2017; 63: 109–119.

de Toledo-Morrell L, Goncharova I, Dickerson B, Wilson RS, Bennett DA. From healthy aging to early Alzheimer's disease: in vivo detection of entorhinal cortex atrophy. *Ann. N. Y. Acad. Sci.* 2000; 911: 240–53.

Tromp D, Dufour A, Lithfous S, Pebayle T, Després O. Episodic memory in normal aging and Alzheimer disease: Insights from imaging and behavioral studies. *Ageing Res. Rev.* 2015; 24: 232–262.

Troyer AK, Murphy KJ, Anderson ND, Moscovitch M, Craik FIM. Changing everyday memory behaviour in amnesic mild cognitive impairment: A randomised controlled trial. *Neuropsychol. Rehabil.* 2008; 18: 65–88.

Tsao A, Moser MB, Moser EI. Traces of experience in the lateral entorhinal cortex. *Curr. Biol.* 2013; 23: 399–405.

Tu S, Wong S, Hodges JR, Irish M, Piguet O, Hornberger M. Lost in spatial translation - A novel tool to objectively assess spatial disorientation in Alzheimer's disease and frontotemporal dementia. *Cortex* 2015; 67: 83–94.

Tward DJ, Sicat CS, Brown T, Bakker A, Gallagher M, Albert M, et al. Entorhinal and transentorhinal atrophy in mild cognitive impairment using longitudinal diffeomorphometry. *Alzheimer's Dement. Diagnosis, Assess. Dis. Monit.* 2017a; 9: 41–50.

Tward DJ, Sicat CS, Brown T, Bakker A, Gallagher M, Albert M, et al. Entorhinal and transentorhinal atrophy in mild cognitive impairment using longitudinal diffeomorphometry. *Alzheimer's Dement. Diagnosis, Assess. Dis. Monit.* 2017b; 9: 41–50.

Tyler LK, Stamatakis EA, Bright P, Acres K, Abdallah S, Rodd JM, et al. Processing objects at different levels of specificity. *J. Cogn. Neurosci.* 2004; 16: 351–362.

Vacante M, Wilcock GK, De Jager CA. Computerized adaptation of the Placing Test for early detection of both mild cognitive impairment and Alzheimers disease. *J. Clin. Exp. Neuropsychol.* 2013; 35: 846–856.

Vago DR, Kesner RP. Disruption of the direct perforant path input to the CA1 subregion of the dorsal hippocampus interferes with spatial working memory and novelty detection. *Behav. Brain Res.* 2008; 189: 273–283.

Valerio S, Taube JS. Path integration: How the head direction signal maintains and corrects spatial orientation. *Nat. Neurosci.* 2012; 15: 1445–1453.

Vandenberghe R, Van Laere K, Ivanoiu A, Salmon E, Bastin C, Triau E, et al. 18F-flutemetamol amyloid imaging in Alzheimer disease and mild cognitive impairment a phase 2 trial. *Ann. Neurol.* 2010; 68: 319–329.

Velayudhan L, Ryu S-H, Raczek M, Philpot M, Lindesay J, Critchfield M, et al. Review of brief cognitive tests for patients with suspected dementia. *Int. Psychogeriatr.* 2014; 26: 1247–62.

Vemuri P, Jones DT, Jack CR. Resting state functional MRI in Alzheimer's disease.

Alzheimer's Res. Ther. 2012; 4: 1–9.

Voevodskaya O. The effects of intracranial volume adjustment approaches on multiple regional MRI volumes in healthy aging and Alzheimer's disease. *Front. Aging Neurosci.* 2014; 6: 264.

de Vos F, Koini M, Schouten TM, Seiler S, van der Grond J, Lechner A, et al. A comprehensive analysis of resting state fMRI measures to classify individual patients with Alzheimer's disease. *Neuroimage* 2018; 167: 62–72.

Vovk A, Chan D, Patel A. Augmented reality for early Alzheimer's disease diagnosis [Internet]. *Conf. Hum. Factors Comput. Syst. - Proc.* 2019

Wang C, Chen X, Lee H, Deshmukh SS, Yoganarasimha D, Savelli F, et al. Egocentric coding of external items in the lateral entorhinal cortex. *Science (80-.).* 2018; 362: 945–949.

Wang DS, Bennett DA, Mufson EJ, Mattila P, Cochran E, Dickson DW. Contribution of changes in ubiquitin and myelin basic protein to age-related cognitive decline. *Neurosci. Res.* 2004; 48: 93–100.

Wang HM, Yang CM, Kuo WC, Huang CC, Kuo HC. Use of a Modified Spatial-Context Memory Test to Detect Amnesic Mild Cognitive Impairment. *PLoS One* 2013; 8: 1–8.

Wang L, Zang Y, He Y, Liang M, Zhang X, Tian L, et al. Changes in hippocampal connectivity in the early stages of Alzheimer ' s disease : Evidence from resting state fMRI. 2006; 31: 496–504.

Wang P, Zhou B, Yao H, Zhan Y, Zhang Z, Cui Y, et al. Aberrant intra- and inter-network connectivity architectures in Alzheimer's disease and mild cognitive impairment. *Sci. Rep.* 2015; 5: 14824.

Watson HC, Wilding EL, Graham KS. A role for perirhinal cortex in memory for novel object-context associations. *J. Neurosci.* 2012; 32: 4473–4481.

Weniger G, Ruhleder M, Lange C, Wolf S, Irle E. Egocentric and allocentric memory as assessed by virtual reality in individuals with amnesic mild cognitive impairment. *Neuropsychologia* 2011; 49: 518–527.

Wiebe SP, Stäubli U V. Dynamic filtering of recognition memory codes in the hippocampus. *J. Neurosci.* 1999; 19: 10562–10574.

Wilson DIG, Langston RF, Schlesinger MI, Wagner M, Watanabe S, Ainge JA. Lateral entorhinal cortex is critical for novel object-context recognition. *Hippocampus*

2013a; 23: 352–366.

Wilson DIG, Watanabe S, Milner H, Ainge JA. Lateral entorhinal cortex is necessary for associative but not nonassociative recognition memory. *Hippocampus* 2013b; 23: 1280–1290.

Winter SS, Mehlman ML, Clark BJ, Taube JS. Passive Transport Disrupts Grid Signals in the Parahippocampal Cortex. *Curr. Biol.* 2015; 25: 2493–2502.

Winters BD, Bussey TJ. Glutamate receptors in perirhinal cortex mediate encoding, retrieval, and consolidation of object recognition memory. *J. Neurosci.* 2005; 25: 4243–4251.

Winters BD, Forwood SE, Cowell RA, Saksida LM, Bussey TJ. Double dissociation between the effects of peri-postrhinal cortex and hippocampal lesions on tests of object recognition and spatial memory: Heterogeneity of function within the temporal lobe. *J. Neurosci.* 2004; 24: 5901–5908.

Wisse LEM, Daugherty AM, Olsen RK, Berron D, Carr VA, Stark CEL, et al. A harmonized segmentation protocol for hippocampal and parahippocampal subregions: Why do we need one and what are the key goals? *Hippocampus* 2017; 27: 3–11.

Witter MP, Groenewegen HJ, Lopes da Silva FH, Lohman AHM. Functional organization of the extrinsic and intrinsic circuitry of the parahippocampal region. *Prog. Neurobiol.* 1989; 33: 161–253.

Wolbers T, Wiener JM, Mallot HA, Büchel C. Differential recruitment of the hippocampus, medial prefrontal cortex, and the human motion complex during path integration in humans. *J. Neurosci.* 2007; 27: 9408–9416.

Wolk DA, Price JC, Saxton JA, Snitz BE, James JA, Lopez OL, et al. Amyloid imaging in mild cognitive impairment subtypes. *Ann. Neurol.* 2009; 65: 557–568.

Wood RA, Moodley KK, Lever C, Minati L, Chan D. Allocentric spatial memory testing predicts conversion from mild cognitive impairment to dementia: An initial proof-of-concept study [Internet]. *Front. Neurol.* 2016; 7

World Health Organization. *Dementia: A public health priority.* 2015

Worsley CL, Recce M, Spiers HJ, Marley J, Polkey CE, Morris RG. Path integration following temporal lobectomy in humans. *Neuropsychologia* 2001; 39: 452–464.

Xiang JZ, Brown MW. Differential neuronal encoding of novelty, familiarity and recency in regions of the anterior temporal lobe. *Neuropharmacology* 1998; 37:

657–676.

Xie Y, Bigelow RT, Frankenthaler SF, Studenski SA, Moffat SD, Agrawal Y. Vestibular loss in older adults is associated with impaired spatial navigation: Data from the triangle completion task. *Front. Neurol.* 2017; 8: 173.

Yamada K, Arai M, Suenaga T, Ichitani Y. Involvement of hippocampal NMDA receptors in encoding and consolidation, but not retrieval, processes of spontaneous object location memory in rats. *Behav. Brain Res.* 2017; 331: 14–19.

Yang X, Tan MZ, Qiu A. CSF and Brain Structural Imaging Markers of the Alzheimer's Pathological Cascade. *PLoS One* 2012; 7

Yartsev MM, Witter MP, Ulanovsky N. Grid cells without theta oscillations in the entorhinal cortex of bats. *Nature* 2011; 479: 103–107.

Yeung L-K, Olsen RK, Bild-Enkin HEP, D'Angelo MC, Kacollja A, McQuiggan DA, et al. Anterolateral Entorhinal Cortex Volume Predicted by Altered Intra-Item Configural Processing. *J. Neurosci.* 2017; 37: 5527–5538.

Yeung L-K, Olsen RK, Hong B, Mihajlovic V, D'Angelo MC, Kacollja A, et al. Object-in-Place Memory Predicted by Anterolateral Entorhinal Cortex and Parahippocampal Cortex Volume in Older Adults. *bioRxiv* 2018: 409607.

Yeung LK, Olsen RK, Hong B, Mihajlovic V, D'angelo MC, Kacollja A, et al. Object-in-place memory predicted by anterolateral entorhinal cortex and parahippocampal cortex volume in older adults. *J. Cogn. Neurosci.* 2019; 31: 711–729.

Yi HA, Möller C, Dieleman N, Bouwman FH, Barkhof F, Scheltens P, et al. Relation between subcortical grey matter atrophy and conversion from mild cognitive impairment to Alzheimer's disease. *J. Neurol. Neurosurg. Psychiatry* 2016; 87: 425–432.

Yoganarasimha D, Rao G, Knierim JJ. Lateral entorhinal neurons are not spatially selective in cue-rich environments. *Hippocampus* 2011; 21: 1363–1374.

Yonelinas AP, Ranganath C, Ekstrom AD, Wiltgen BJ. A contextual binding theory of episodic memory: systems consolidation reconsidered. *Nat. Rev. Neurosci.* 2019; 20: 364–375.

Yoo SW, Lee I. Functional double dissociation within the entorhinal cortex for visual scenedependent choice behavior. *Elife* 2017; 6: 1–16.

Yuan Y, Gu ZX, Wei WS. Fluorodeoxyglucose-positron-emission tomography, single-photon emission tomography, and structural MR imaging for prediction of

rapid conversion to alzheimer disease in patients with mild cognitive impairment: A meta-analysis. *Am. J. Neuroradiol.* 2009; 30: 404–410.

Yushkevich PA, Piven J, Hazlett HC, Smith RG, Ho S, Gee JC, et al. User-guided 3D active contour segmentation of anatomical structures: Significantly improved efficiency and reliability. *Neuroimage* 2006; 31: 1116–1128.

Zhao M, Warren WH. Environmental stability modulates the role of path integration in human navigation. *Cognition* 2015; 142: 96–109.

Zhou Y, Dougherty JHJ, Hubner KF, Bai B, Cannon RL, Hutson RK. Abnormal connectivity in the posterior cingulate and hippocampus in early Alzheimer's disease and mild cognitive impairment. *Alzheimers. Dement.* 2008; 4: 265–270.